Mechanisms of β-Cell Compensation for Age and Obesity

By

Trillian Gregg

A dissertation submitted in partial fulfillment of the

requirements for the degree of

Doctor of Philosophy
(Biophysics)

at the

University of Wisconsin-Madison

2017

Date of final oral examination: 06-27-2017

The dissertation is approved by the following members of the Final Oral Committee:

Matthew J. Merrins, Professor, Endocrinology
Alan D Attie, Professor, Biochemistry
Tomas F J Martin, Professor, Biochemistry
Kevin Eliceiri, Professor, Biomedical Engineering
Randall H Goldsmith Professor, Chemistry

Table of Contents

Acknowledgments

I spent the first four years of my graduate career bouncing among various labs and projects. Although often enjoyable and always educational, working without a permanent scientific home and primary adviser was also incredibly challenging. If Matt Merrins hadn't come to the University of Wisconsin-Madison to start his lab, I might still be wandering in the desert. Matt took a chance on a 4th-year graduate student, giving me the scientific direction and mentorship that I needed. I could never have succeeded without being a part of the Merrins Lab.

I would also like to thank my committee: Kevin Eliceiri, Alan Attie, Randy Goldsmith, and Tom Martin for their guidance and support. I'm especially grateful to Kevin for offering me a desk at LOCI, giving me the freedom to explore new microscopy techniques, and providing valuable mentorship while I found my scientific path. I learned the vast majority of my imaging expertise and discovered some of my core scientific interests while at LOCI. Alan Attie, meanwhile, took me under his wing as an honorary lab member during my free-floating days and presented me with a biological question to which I could apply my passion for microscopy. As an especially insightful mentor, Alan also recognized that I could not achieve everything I hoped to in his lab. It was Alan who introduced me to Matt and facilitated my joining the Merrins lab. I will always be grateful for Alan's guidance, compassion, and scientific wisdom.

The other members of the Merrins Lab were also enormously supportive as I completed this work. Helena VanDeusen in particular held my hand throughout the entire dissertation-writing process and has been a tremendous help with all of my research.

Adam Mandelman was a top-notch editor, helping me get this manuscript into shape while also being a supportive partner. Finally, my mother, Linda Gregg, deserves the largest thanks of all. Her insight and understanding has helped me to achieve more than anyone ever thought possible. It means so much to make her proud.

Abstract

Type 2 diabetes is a disease of glucose dysregulation that increases the risk of developing several secondary conditions, including cardiovascular disease, peripheral neuropathy, and blindness. Affecting 9.3% of the U.S. population with nearly 2 million new cases diagnosed each year, type 2 diabetes is an undisputed national public health crisis. Aging and obesity both substantially increase the risk of acquiring type 2 diabetes. The physiological response to these two challenges involves increased demand for insulin release from pancreatic islet β-cells, which in turn compensate with changes in β-cell function (i.e. insulin secretion) and expansion of β-cell mass. Through the novel application of NAD(P)H fluorescent lifetime imaging (FLIM) to pancreatic islets, we determined that impaired mitochondrial activity underlies an age-dependent reduction in insulin secretion in human islets. However, we also found that insulin secretion and glucose tolerance are preserved in aged mice through heightened β-cell glucose sensitivity due to a compensatory decrease in K_{ATP} channel conductance. In the context of obesity and adaptive proliferation, we identified the cell cycle regulator cyclin-dependent kinase 1 (Cdk1) as an enhancer of mitochondrial electron transport chain flux at Complex I. In so doing, we demonstrated that electron transport chain flux is inversely proportional to insulin secretion. Finally, we suggest future studies that focus on the spatiotemporal dynamics of this relationship and its impact on pancreatic islet metabolism.

Chapter 1

Introduction

Type 2 Diabetes

Type 2 diabetes (T2D) is the most common metabolic disorder worldwide. The number of Americans diagnosed with diabetes has soared from 5.6 million in 1980 to 29.1 million in 2014, or 1 out of every 11 adults (1). T2D is a disease of glucose dysregulation that increases the risk of developing cardiovascular disease, peripheral neuropathy, hypertension, blindness, and nephropathy (2). In addition to the negative health impacts of this disease, the economic repercussions are significant. In 2012, diabetes and its related complications accounted for $245 billion in total medical costs, lost work, and missed wages in the United States—a staggering 1.4% of GDP. If current trends continue, the CDC estimates that 1 in 3 adults in the US will be diagnosed with diabetes by 2050. In addition, the incidence of T2D in the United States is correlated with socioeconomic status, race, and educational attainment (Figure 1.1). This reveals that T2D is a crisis of not only health and economics, but also of social and racial inequality.

Glucose homeostasis is critical for cell survival and organismal well-being. As such, glucose uptake, metabolism, and production are all tightly controlled to maintain proper blood glucose levels. Dysregulation of glucose homeostasis in T2D is characterized by insulin deficiency in response to increased insulin demand due to insulin inefficacy at its target tissues, termed insulin resistance. Insulin resistance can result from several factors including obesity and advanced age. The question of whether insulin resistance precedes islet dysfunction or vice versa remains controversial (3). Regardless, to meet increasing insulin demands, the pancreas must increase insulin production either by increasing the efficiency with which each β-cell secretes insulin (increased β-cell function), or by increasing the total number of cells secreting insulin (increased β-cell mass). Not all obese or elderly individuals will develop T2D. Rather, the majority of individuals who develop insulin resistance will compensate for the increased demand and never develop overt T2D. Failure of the β cell to meet the demands of compensation is central to the development of this disease.

Susceptibility to T2D is determined by a combination of genetic factors, fetal environment, and nutrient environment over the course of an individual's life (4–6). Individuals whose islets fail to compensate for increased demand will ultimately develop hyperglycemia and T2D. The arc of T2D pathophysiology, as proposed in Ralph DeFronzo's 1987 Lilly Lecture, is known as the arc of compensation/decompensation (7,8) (Figure 1.2). As plasma insulin levels rise in response to increased demand, the rate of insulin-mediated glucose uptake begins to fall, a hallmark of insulin resistance. This feed-forward loop begets more insulin secretion in order to maintain normal glucose homeostasis, further increasing demands on the pancreatic islets. This stage is known as the phase of compensation. Eventually, in susceptible individuals, the β-cell is no longer capable of meeting the increased demand and begins to fail either through progressive loss of mature β cells and/or deterioration of function (9,10). β-cell failure coincides with rising plasma glucose levels and continued insulin resistance. This marks the beginning of decompensation, soon followed by overt T2D (11).

Pancreatic islets make up only 1-2% of total pancreatic mass yet are responsible for secreting all the necessary insulin to maintain euglycemia. Islets themselves are composed of multiple cell types, predominantly insulin-producing β cells and glucagon-producing α cells, but also δ and γ cells (producing somatostatin and ghrelin, respectively), and polypeptide-producing PP cells (12). α and β cells are the most significant contributors to organismal glucose homeostasis comprising 15-20% and 60-80%, respectively, of islet cells in rodents and 40% and 50%, respectively, in human islets (13).

β-cell function is dedicated to glucose sensing and insulin secretion in the effort to maintain glucose homeostasis. Approximately 30% of the mRNA content of a β cell is proinsulin mRNA and that, following glucose stimulation, insulin can account for up to 50% of total β-cell protein content

(14,15). However, the process underlying fuel-induced insulin secretion is nuanced and still not completely understood.

In the current consensus model, insulin secretion is triggered when glucose enters the β cell through a bidirectional glucose transporter, predominantly GLUT2 in rodents and GLUT1 and GLUT3 in humans (16). Subsequent phosphorylation of glucose by glucokinase initiates glucose metabolism through glycolysis and the tricarboxylic acid (TCA) cycle (17). Glucose oxidation raises cellular levels of the metabolic co-enzymes and substrates necessary to produce mitochondrial ATP via the electron transport chain (ETC), such as NADH, $FADH_2$, and succinate (18). ATP produced by glycolysis and the ETC binds to K_{ATP} channel subunit Kir6.2, inducing K_{ATP} channel closure and cellular depolarization (19). Plasma membrane depolarization opens L-type voltage gated Ca^{2+} channels leading to Ca^{2+} influx which directly triggers exocytosis via SNARE mediated membrane fusion (20). This pathway is known as the "triggering" pathway of insulin secretion and functions as the on/off switch of insulin secretion (Figure 1.3). The magnitude of the response to stimulation of the triggering pathway is set by the "amplifying" pathways and can be likened to a dimmer switch controlling the amplitude of secretion (21,22). In this pathway, metabolic intermediates such as NADPH, Malonyl CoA (MalCoA), Acetyl CoA (AcCoA), phosphoenolpyruvate (PEP), and amino acids—to name a few—interact with the insulin granule secretory pathway to enhance the magnitude of secretion (23). A more detailed mechanistic treatment of several amplifying pathways will be addressed in chapters 4 and 5. It is essential to understand the cellular and mechanistic details underpinning a decline in these pathways in order to identify new potential targets for T2D prevention and treatment.

Age Associated Changes in β Cells

The percentage of the human population over the age of 65 is projected to increase at a rate of 0.2% every year (24). Over one quarter of the world's population is expected to be elderly by 2026. Aging itself is a risk factor for metabolic diseases including obesity, impaired glucose tolerance, and type 2 diabetes (25–27). Elderly adults are twice as likely to be diagnosed with type 2 diabetes as younger adults, with 20% of the elderly population suffering from overt T2D, compared with just 9% percent of the general adult population (1,28) (Figure 1.1C). As such, it is important to understand which aspects of T2D pathophysiology are associated with aging. Current understanding of the link between aging and T2D relies on changes in multiple aspects of islet biology and glucose homeostasis, including changes in insulin resistance, β-cell function, and pancreatic β-cell mass.

One of the first hypothesized causes for age-related glucose intolerance was increased peripheral insulin resistance (28–33). Increased circulating insulin levels and decreased responsiveness in insulin target tissues in the elderly is likely due to increased adiposity, decreased physical activity, and decreased lean muscle mass connected with aging (34). To maintain normoglycemia in the context of insulin resistance, islets must compensate with increased insulin secretion to match elevated insulin demand. A series of experiments conducted in the latter 20th century employed hyperglycemic and euglycemic clamp to measure both insulin secretion and insulin sensitivity in young (20-60 years) and aged (60-90 years) human patients (29,30,32,35). These studies concluded that although glycemic control declines with age, it is not due to defects in insulin secretion, but rather to decreased sensitivity of peripheral tissue to insulin action. Iozzo et al. and Rafaie et al., however, have suggested otherwise. Although these studies similarly found that insulin sensitivity declines with age, they both also demonstrated a concomitant decline in islet function (28,33). Although there is consensus around the role of insulin resistance in the susceptibility of

aging populations to T2D, these contradictory results regarding islet function in the aged necessitated further, more mechanistic studies of β-cell function.

Several specific mechanisms have been suggested in recent years that point to decreasing islet function with age in both human and animal models. The degenerative effects of aging on β-cell function span the full range of the β-cell stimulant-secretion coupling pathway. Numerous groups have found age-associated defects in translocation of glucose across the β-cell plasma membrane, the first step in glucose-stimulated insulin secretion (GSIS) (36–40). Glucose, along with other dietary sugars are transported into the cell via GLUT transporters GLUT1, GLUT2, and GLUT3 (41). GLUT2, the primary isoform in rodent β cells, is a dynamically regulated protein whose presence on the plasma membrane is directly affected by plasma glucose concentration (42,43). Loss of GLUT2 results in glucose dysregulation and hyperglycemia. Several studies have established a link between decreased GLUT2 expression and age, thus highlighting the feed-forward loop between elevated blood glucose and impaired glucose sensitivity in the elderly.

Once glucose has entered the β cell, it is metabolized and the energy—as carbon—is distributed among different cellular processes. This allocation of glucose affects downstream metabolic signaling pathways. One possible pathway is through mitochondrial anaplerotic-cataplerotic shuttling (23). Mitochondrial shuttles and cycles, such as the malate-aspartate shuttle, the glycerol-phosphate shuttle, the isocitrate α-ketoglutarate shuttle, and pyruvate cycles effectively carry reducing equivalents across the mitochondrial membrane either to replenish cytosolic NAD^+ for glycolysis or to produce GSIS amplifying factors like NADPH or malonyl-CoA in the cytosol (21–23,44–49). The glycerol-phosphate shuttle, specifically mitochondrial glycerol-3-phosphate dehydrogenase (mGPDH), in concert with cytosolic GPDH (cGPDH), plays a critical role in regenerating cytosolic NAD^+ for β-cell glycolysis through an electron exchange between NADH,

FAD, and coenzyme Q (50). mGPDH may also be implicated in age-related decline in β-cell function. A study by Azhar et al. found that mGPDH decreased by 53.5%±6.5% in 12-month-old rats compared to 2-month-old rats suggesting a role for mGPDH in decreased glucose oxidation in aged β cells (51). Similarly, Reaven and Reaven observed decreased glucose oxidation based on radio-labeled carbon oxidation in aged rat islets (52).

Further defects in aged islet function have been observed just distal to glycolysis in the mitochondria. Decreased mitochondrial function is a hallmark of many aging cell types (53). Restoration of mitochondrial metabolism through supplementation with mitochondrial substrates has recently become a leading strategy for anti-aging interventions (54,55). Because mitochondrial energy production is so tightly linked to insulin secretion, it seems likely that an age-associated decline in mitochondrial metabolism would predispose β cells to secretory dysfunction. Several studies have reported decreased rates of oxidative phosphorylation (up to 40%) as well as abrogate mitochondrial membrane potential and Ca^{2+} signaling in aged β-cells (53,56–59).

One of the final steps in glucose-stimulated insulin secretion is the closure of ATP-sensitive K^+ channels (K_{ATP}) (60). One potential explanation for decreased exocytosis in aged islets is improper closure or functioning of K_{ATP} channels. Work by Ammon et al. suggests precisely this in aged rat islets (61). In this study, based on liquid scintillation counting, the authors examined the rate of K^+ efflux (proxied by Rb^+) and Ca^{2+} uptake in adult and aged rat islets in response to basal and stimulatory glucose levels. Inhibition of Rb^+ efflux after glucose stimulation was found to be insufficient for both maximal Ca^{2+} influx and insulin secretion in aged islets compared to controls. These results suggest that impaired ATP generation or insensitivity of K_{ATP} channels may be responsible for the decreased insulin secretion observed in aged islets.

There is significant literature showing a link between aging and impaired β-cell function. It is reasonable to hypothesize, then, that the widely accepted age-associated cellular degeneration observed in many organisms and tissue types is applicable to pancreatic islets as well, and that this degeneration in function is responsible for both the impaired glucose tolerance and susceptibility to T2D observed in the elderly. There are, however, several studies that suggest otherwise. Research in both human and rodent models has concluded that aged β cells do not suffer from functional impairment and are as competent at insulin secretion as their young counterparts (29,32,62). Additional studies have even found improved β-cell function with age (63,64).

Improved islet function in the aged has been shown to result from changes in gene expression and DNA methylation. Aging is associated with a wide range of genetic and epigenetic changes (65,66). This phenomenon also applies to aging β cells. Changes in the methylome and transcriptome of genes related to two major categories have been identified in aging islets. First, demethylation changes to promoters and enhancers controlling expression of genes related to mitochondrial activity, protein transport, MAPKinase, and glucose metabolism have all be shown to be upregulated in aged islets, enhancing function (63). Concomitant inhibitory methylation associated with β-cell specific transcription factors such as Pdx1, FoxA2, and NeuroD1 has also been observed in aged islets. Further changes in gene expression related to the age-related decrease in cellular proliferation are associated with β-cell function as well. Increased expression of the cellular senescence effector p16INK4a has been linked to aging (67,68). Interestingly, increased p16INK4a expression has been found to enhance β-cell glucose uptake, mitochondrial activity, and GSIS (64). Since decreased proliferative signaling is a hallmark of aging, the resulting increase in β-cell function is a valuable mechanism of compensation for insulin insensitivity in the elderly when β-cell mass expansion is in decline.

Other age-related changes contribute to decreased proliferative signaling in islets. In the young, hyperglycemia and hyperinsulinemia are known to trigger a compensatory increase in β-cell mass (69,70). Substrate-induced β-cell mass expansion, or adaptive proliferation, in adult islets can derive from multiple potential mechanisms of β-cell generation and will be addressed in detail later in this chapter (73). Self-regeneration through proliferation, however, is the most likely source of new β cells in the adult islet (74). In recent years, the ability of aged islets to undergo adaptive proliferation has been called into question and this impairment has been suggested as the mechanism responsible for glucose dysregulation in the elderly, independent of β-cell function (75–78).

β-cell proliferation in the elderly is linked to restricted transcription factor expression. Two transcription factors are downregulated with age: the more general, pro-proliferative FoxM1 transcription factor, and the islet β-cell specific Pdx1 transcription factor. FoxM1 facilitates cell-cycle progression at both the G1/S and G2/M transitions through a series of positive feedback loops involving several cyclin-dependent kinases as well as other transcription factors (79). FoxM1 expression decreases with age, thereby limiting adaptive proliferation in aging islets (80). Consistently, activation of FoxM1 effectively restores islet replicative potential (81). Decreased Pdx1, a β-cell specific transcription factor, is implicated in both decreased proliferation and β-cell dedifferentiation in aged islets (82–84). In addition to transcription factors, age is accompanied by increased expression of cell cycle inhibitors such as p16INK4a (67,68,77,85). As a cellular senescence effector, p16INK4a binds to cyclin-dependent kinases 4 and 6, inhibiting their interaction with D-type cyclins and therefore blocking cell-cycle progression at the G0/G1 transition. This topic will be addressed in more detail in subsequent sections in this chapter. This inhibition is inopportune considering the increases in insulin resistance associated with age. Adaptive

β-cell proliferation is a major mode of compensation in response to metabolic stress in young humans and animal models. Accordingly, Krishnamurthy et al. have shown that the decline in replicative potential associated with age is restored in p16INK4a knock-out mice, indicating a critical role for this cell-cycle inhibitor in age-related susceptibility to T2D (67). Recent work from the Ben-Porath laboratory has suggested an alternative, compensatory role for p16INK4a in insulin secretion. They found that although general proliferative capacity was decreased in aged islets, individual β-cell function and secretory capacity was increased and this increase was directly related to p16INK4a expression (64). Mirroring several studies mentioned earlier that showed increased β-cell function in aged islets, they also discovered increases in GSIS and mitochondrial activity with heightened p16INK4a expression, suggesting that β-cell proliferation and secretory function appear to be at mutual expense (63).

While there is still some controversy in the field as to the effect of age on β-cell function, a new consensus is emerging. It is clear that age-related insulin resistance is the driving factor leading to T2D susceptibility in the elderly. What is only now becoming evident, however, is that age-associated proliferative failure is likely the major mechanism preventing compensation and resulting in the high incidence of overt T2D. The role played by changes in β-cell function is likely species-specific, with more β-cell functional compensation being observed in rodent models compared to humans, but changes in function are ultimately overshadowed by replicative failure. Based on these new discoveries, developing age-specific T2D therapeutics that increase β-cell proliferation or prevent senescence may prove fruitful.

β-Cell Proliferation and the Cell Cycle

Under normal physiological conditions, β cells are quiescent, residing in the G0 stage of the cell cycle (86) (Figure 1.4). In the setting of obesity, however, cell-cycle gene expression has been shown to correlate with compensation for over-nutrition (87). Compensatory β-cell growth is a hallmark of prediabetes and is a mitogenic response to the deviation from normoglycemia (3,11,88,89). Obese mice able to maintain a compensatory increase in insulin secretion have been shown to increase pancreatic β-cell mass at a rate of 10% over the course of 2 weeks (87). Mouse models known to succumb to overt T2D lack both cell-cycle gene expression or adaptive β-cell proliferation (87). The compensatory increase in cell-cycle protein expression is in keeping with observations regarding the origin of new β cells in the context of obesity. Several studies have found that the primary mechanism of postnatal β-cell mass expansion is through proliferation of existing β cells and not through neogenesis (74,90).

Stimulation of adaptive proliferation can be derived from several extrinsic factors including growth factor signaling, incretin stimulation, elevated glucose, and—as a consequence of GSIS (and indirectly, insulin resistance)—autocrine signaling by insulin (70,91–100). Several insulin-receptor initiated proliferative signaling cascades have been established. Most work examining insulin induction of cellular proliferation has been carried out in the βIRKO mouse model (93). βIRKO mice have a pancreatic β-cell specific knock out of the insulin receptor which results in decreased islet size and impaired glucose homeostasis. This phenotype is likely due to loss of insulin-receptor signaling cascades through Forkhead box transcription regulator proteins, FoxO1 and FoxM1. FoxO1 and FoxM1 are nuclear/cytoplasmic transcription regulators whose nuclear translocation coincides with their activity. FoxO1 and FoxM1 have opposing actions when located in the nucleus (101). Accordingly, insulin signaling has the opposite effect on the two regulators. Increased

autocrine signaling through the insulin receptor has been shown to induce translocation of FoxO1 from the nucleus to the cytoplasm (96). Once FoxO1 is excluded from the nucleus, repression of β-cell specific transcription regulator Pdx1 is relieved, allowing progression through the cell cycle and compensatory β-cell mass increase (98,99,102). Conversely, insulin receptor signaling induces nuclear localization of FoxM1. Nuclear FoxM1 is a positive regulator of cell-cycle progression, stimulating expression of a wide range of cell-cycle genes (103). Recently, Shirakawa et al. (100) showed that insulin receptor stimulation increases β-cell proliferation by activating FoxM1, which in turn translocates to the nucleus with help from ERK, an extracellular signal-related kinase. Once in the nucleus, FoxM1, bolstered by AKT-mediated Cdk1/2 activity, activates M-phase proteins, polo-like Kinase 1 (PLK1), and centromere protein A (CENP-A). CENP-A and PLK1 together promote β-cell mitosis (100).

Incretin signaling can also stimulate β-cell mass expansion. Incretins are metabolic hormones secreted postprandial by endocrine cells in the epithelium of the small intestine (104). The two most studied incretins are glucagon-like peptide-1 (GLP-1) and glucose-dependent insulinotropic peptide (GIP). Several mimetics have also been discovered including exendin-4, a GLP-1 receptor agonist originally isolated from the salivary glands of lizards (105). Like exendin-4, GLP-1 and GIP are insulinotropic, acting through a G-protein coupled receptor/cAMP-mediated pathway, as well as through modulations in KATP channel activity via PKA (106,107). Their roles in compensation for hyperglycemia, however, are believed to differ (106,108). In addition to increasing insulin secretion in response to food intake, incretins also stimulate adaptive proliferation and β-cell neogenesis (95,97,109). GLP-1 receptor signaling has been shown to facilitate β-cell mass expansion by upregulating Pdx1 expression and nuclear translocation as well as through an ERK/MAPKinase pro-proliferative pathway (110,111). Several studies report that GLP-1 receptor sensitivity is

impervious to hyperglycemia, making GLP-1 signaling an extremely attractive target for T2D treatment (104). This result is still controversial in the literature, however (112). GIP signaling, on the other hand, declines with prolonged blood-glucose elevation (113). Furthermore, recent work indicates that GLP-1, but not GIP, is responsible for the compensatory increase of β-cell mass, at least in the context of pregnancy (114). It is important to recognize that despite both incretin receptors GIPR and GLP-1R being G-protein coupled receptors which have similar effects on cellular cAMP levels, their long-term impacts on β-cell function are significantly different (104). These results highlight the deep level of understanding necessary to appropriately manipulate β-cell function as part of type 2 diabetes treatment.

Finally, glucose itself, as well as several other extrinsic circulatory factors such as free fatty acids, have been implicated in stimulating β-cell mass expansion. It is important to note, however, that the effects of elevated glucose on proliferation may in fact be secondary to increased insulin. Elevated blood glucose and free fatty acids have been shown to increase β-cell mass by 80% and 54% respectively (70,92). Elevated glucose has been shown to increase Cyclin D2 expression in islets initiating cellular proliferation cascades (91). This effect is likely due to glucose-dependent stimulation of insulin receptor substrate 2 activity, leading to elevated ERK and mTOR signaling but not elevated AKT activity; it is not yet clear how these mitogenic effects interact with insulin autocrine signaling (100,115).

Regardless of which mitogenic factor stimulates adaptive proliferation, increasing β-cell mass is a critical compensatory mechanism for prolonged hyperglycemia and insulin resistance. Progression through the cell cycle is a highly regulated and complex process involving many proteins. Some of the most indispensable regulators are cyclin-dependent kinases (Cdks) and their associated, activating cyclins (Table 1.1). Appropriate action and functional maintenance of

Cyclin/Cdk pairs is essential for movement through cell-cycle checkpoints, which is well studied, but their function appears relevant to non-proliferating cells. Each of these Cyclin/Cdk functions are discussed in turn.

There are two main control check points in the cell cycle: G1/S and G2/M, both of which are regulated by Cyclin/Cdk pairs (Table 1.1 and Figure 1.4). Most β cells are quiescent, residing in the cell-cycle gap phase known as G0. Mitogenic signals, like those discussed above, push β cells from non-dividing G0 into G1 to begin the cell-division process (86). During G1 phase, the first phase of the cell cycle, the β cell grows in size and synthesizes the mRNA and proteins required to facilitate subsequent DNA replication. The Cyclin/Cdk pair responsible for mediating the G0/G1 transition and for G1 control is Cyclin D and Cdk4 (Cdk6 in humans) (94,116). While Cdk levels remain relatively constant over the course of a cell cycle, cyclin protein levels are dynamically regulated and Cdk activity is strongly correlated with cyclin expression levels (117). As mentioned earlier, mitogenic stimulation induces Cyclin D expression, activating Cdk4/6-Cyclin D signaling cascades (118). Upon synthesis, Cyclin D binding activates and directs Cdk4/6 to its target substrates (119). Cyclin D/Cdk4/6 provide the initial phosphorylation events necessary to pass the G1/S checkpoint (120).

The G1/S checkpoint is controlled by retinoblastoma protein, Rb (121). In its hypo-phosphorylated state, Rb is a negative regulator of G1/S through inhibition of the transcription factor family E2F (122). Recruitment of chromatin remodeling enzymes by Rb represses E2F responsive promoters limiting expression of other cell-cycle regulators, as well as S-phase genes necessary for DNA replication (123–128). Without E2F activation, the cell cannot proceed into the next phase. Following activation by Cyclin D, Cdk4/6 phosphorylates Rb, decreasing its E2F repression (129–131). While Cdk4/6 is responsible for initiating the cell cycle in response to mitogenic signals, Cdk2 is responsible for carrying the cell through the next stages, namely the G1/S

transition and S phase. Briefly, Cyclin E, a tightly controlled cyclin that interacts with Cdk2 at the beginning of S phase, assists in further phosphorylating Rb (132). Expression of Cdk2 and its activating cyclins are themselves directly controlled by E2F activity, thus creating a positive feedback loop mediated by Cyclin E expression. E2F then drives Cyclin A expression and Cyclin A/Cdk2 complexes take over, phosphorylating proteins for DNA replication in S phase.

There are two major families of Cdk inhibitors in β cells. Cdk4/6 is affected by the INK family of inhibitors which includes p15, p16, p18, and p19 (133,134) (Table 1.1). INK family inhibitors bind directly to the Cdk, preventing interaction with their appropriate cyclin. As mentioned previously, Cdk4/6 inhibitors, specifically p16INK4a play an important role in β-cell adaptation (64,67). There is some argument as to how crucial Cdk4/6 and Cdk2 are to proper cell-cycle progression as there may be a considerable amount of redundancy between Cdks (135–138). However, this redundancy may be tissue or species-specific. In β cells, modulations in Cdk4/6 activity have been shown to play an important role in β-cell function. Furthermore, increased Cyclin D expression levels are associated with T2D in human islets (139). In 1999, Rane and colleagues reported that Cdk4 knockout mice develop insulin deficiency due to a 14-fold decrease in β-cell number (140). Furthermore, mice expressing constitutively active Cdk4 were shown to have β-cell hyperplasia, resulting in an 8-fold increase of β-cell area. Additionally, a more recent study by Miyawaki et al. found that obese mice missing their leptin receptor—*db*/*db* mice—which usually become diabetic with age, never progress to overt diabetes if also expressing constitutively active Cdk4 ($Cdk4^{R24C}$) (141). These results clearly demonstrate the importance of Cdk4 in postnatal β-cell proliferation. Cdk4 also directly impacts insulin secretion because of E2F regulation of the KATP channel subunit Kir6.2 (142). In addition, Helman et al. recently reported that increased expression of Cdk4 inhibitor p16INK4a enhanced insulin secretion (64). This result is further supported by

data demonstrating decreased insulin secretion in islets from p16 null and $Cdk4^{R24C}$ overexpressing mice. Further work will be necessary to fully understand the effects of Cdk4 activity on insulin secretion.

Cdk2 is inhibited by the Cip/Kip family of Cdk inhibitors comprised of p21, p27, and p57 (133). Unlike the INK family Cdk inhibitors, Cip/Kip inhibitors bind to the Cyclin/Cdk complex, directly inhibiting the catalytic cleft (143). It has also been suggested that the Cip/Kip inhibitors interact with Cdk4/6 in addition to Cdk2 (144). Much like Cdk4, Cdk2 knock out has been shown to affect both insulin secretion and compensatory mass expansion through cell-cycle arrest (145).

The next critical checkpoint in cell-cycle progression, is the G2/M transition, marking the beginning of mitosis. This transition is regulated by Cyclin B1/Cdk1 and is essential for cell division (146,147). Cdk1 was the first cyclin-dependent kinase identified and is highly conserved (148). Knock out of Cdk1 in mice is embryonic lethal (149). Expression of Cdk1 begins in G1/S and is regulated by E2F, whereas Cyclin B1 expression is associated with M phase and is regulated by FoxM1 (150–152). Regulation of Cyclin B1 by FoxM1 creates a positive feed-forward loop between Cyclin A/Cdk2 and Cyclin B1/Cdk1 (153,154). This feed-forward signaling is partially responsible for the rapid upregulation in Cyclin B1 expression at the onset of the G2/M transition. Regulation of Cdk1 is quite different from that of Cdk4/6 and Cdk2. Cdk1 is regulated by a series of phosphorylations and dephosphorylations by specific Cdk1 regulatory phosphatases and kinases. Specifically, Cdk1 is inhibited via phosphorylation at Thr14 and Tyr15 by kinases Myt1 and Wee1, respectively (155–157). The family of Cdc25 phosphatases, specifically Cdc25c, is responsible for Cdk1 activation through dephosphorylation (158,159). Cdk1 itself can further activate Cdc25c, creating yet another positive feedback loop, pushing the cell into M phase (160,161) .

Cdk1 localization is a topic of particular interest for determining its functions. To date, active Cyclin B1/Cdk1 has been identified in the nucleus, cytoplasm, and mitochondria of dividing

cells. Cyclin B1/Cdk1 is predominantly cytosolic at the onset of G2 (162–164). Although nuclear/cytoplasmic shuttling has been observed, the predominant cytosolic localization is due to a high rate of nuclear export compared to nuclear import (165,166). Phosphorylation of nuclear export sequence of Cyclin B1 by Plk1 decreases the rate of nuclear export, trapping active Cyclin B1/Cdk1 in the nucleus. Nuclear accumulation of Cdk1 is required for the initiation of mitosis. Once in the nucleus, Cyclin B1/Cdk1 has been shown to phosphorylate, among other things, Lamin A, triggering its disassembly and facilitating nuclear envelope breakdown (167).

A portion of Cdk1 had also be shown to localize to the mitochondrial matrix (168). From inside the mitochondria, Cdk1 carries out additional functions that facilitate cell division. Although many of the mitochondrial actions of Cdk1 have yet to be fully explored, a number of Cdk1 substrates have been identified including Mn superoxide dismutase (MnSOD), nicotinamide nucleotide transhydrogenase (NNT), aldehyde dehydrogenase 2 (ALDH2), Complex I of the electron transport chain (CI), NAD-dependent deacetylase SIRT3, anti-apoptotic protein p53, and pro-apoptotic protein Bcl-xL (168,169). There is some understanding of the role of Cdk1 phosphorylation in MnSOD, Bcl-xL, SIRT3, p53, and Complex I, while the function of the other mitochondrial Cdk1 targets remain undiscovered (168–172). Of particular interest, Wang et al. reported that in the lead-up to mitosis, during the G2/M transition, mitochondrial Cyclin B1/Cdk1 phosphorylates 8 of the 44 subunits of Complex I of the electron transport chain. These phosphorylation events activate Complex I, increasing the rate of NADH consumption and its proton pumping capacity. Increased flux through Complex I increases the overall rate of ATP generation by the ETC. This increased metabolic activity helps provide the cell with the necessary energy resources to undergo division.

So far, very little work has been conducted examining the effects of Cdk1 in pancreatic islets, especially in the context of T2D. As mentioned previously, Shirakawa et al. has shown that insulin

receptor (IR) stimulation induces Cdk1-mediated FoxM1 activity, leading to increased CENP-A and PLK1 expression and β-cell mass (100).

There are several other Cyclin/Cdk pairs that regulate other cyclins, activate transcription factors, and control RNA splicing (173,174). Those most relevant to adaptive β-cell proliferation and subsequent work described here, however, are Cdk4, Cdk6, Cdk2, and Cdk1. It is also important to point out the growing body of work recognizing the link between cell-cycle regulation and metabolic activity (175). This link is particularly relevant for understanding β-cell function. β cells are metabolic sensors, focusing our work on islet metabolic regulation and activity will provide the greatest insight into the pathophysiology of our time's most relevant disease, type 2 diabetes.

There are many ways to assess cellular metabolism. Traditionally, experiments have hinged upon traditional biochemical methods. However, an ideal metabolic assay would produce real-time data from live, intact cells while simultaneously being non-invasive and highly reproducible. Fluorescence lifetime imaging of NAD(P)H, a technique described in Chapter 2, fulfills many of these requirements and is therefore ideally suited to investigating β-cell function and its impact on type 2 diabetes progression.

Summary and Hypotheses

Diabetes is an enormous public-health crisis. β-cell mass expansion and functional compensation point to some of the most promising avenues for effective treatment and prevention of the disease. It is therefore crucial to understand the detailed mechanisms that alternately regulate β-cell compensation and contribute to β-cell dysfunction. Age and obesity-associated glucose dysregulation are multifaceted processes that stem from a combination of insulin resistance, β-cell functional failure, and β-cell loss. Compensation is an equally complex process and can be achieved

with increased insulin secretion through either enhanced β-cell function or increased β-cell mass. In β cells, cell-cycle regulation and metabolism are deeply intertwined. Using techniques novel to the β-cell field we can probe this relationship in intact islets and expand our understanding of the impact of β-cell compensation on metabolic function and vice versa.

Chapter 2 of this dissertation outlines our current use of NAD(P)H Fluorescent Lifetime Imaging (FLIM) in the pancreatic islet. This method is new to the β-cell field and harnesses the power of multiphoton imaging and time-correlated single photon counting to assess changes in the TCA cycle and ETC in intact islets.

Using NAD(P)H FLIM in addition to other more classic biochemistry and microscopy techniques, Chapter 3 characterizes the effects of aging on β-cell mitochondrial function and insulin secretion. This chapter also examines the differences between mouse and human β cells, and the species-specific differences in β-cell compensation.

Chapter 4 examines the impact of β-cell adaptive proliferation on metabolic function and the implications for insulin secretion. In so doing, it highlights emerging evidence regarding the relationship between Cdk1/Cyclin B1, electron transport chain flux, and the amplitude of GSIS.

Finally, Chapter 5 summarizes our current understanding of the interplay between metabolic flux and insulin secretion in β cells. This section also suggests future work necessary to improve our grasp on the effects of glucose utilization by the cell as it relates to insulin secretion.

Figure 1.1

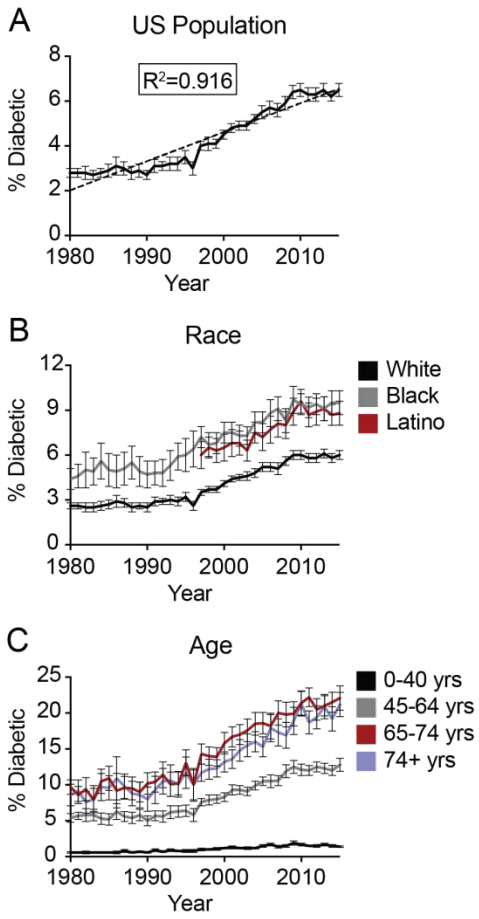

Figure 1.1. Increasing incidence of type 1 and type 2 diabetes in the US population from 1980 to 2014. (**A**) The age-adjusted percent of the US population diagnosed with type 1 or type 2 diabetes increases over time, R^2=0.916. (**B**) Percent of US population diagnosed with diabetes by race for White (black), Black (grey), and Latino (red) populations. (**C**) Percent of US population diagnosed with diabetes by age group: 0-44 years (black), 45-64 years (grey), 65-74 years (red), and 74+ years (periwinkle). Data are mean ± SEM and are taken from the CDC's National Health Interview Survey.

Figure 1.2

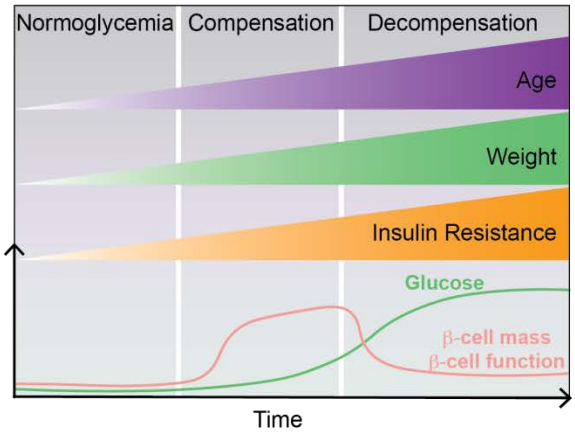

Figure 1.2. Timeline of β-cell adaptation to age, insulin resistance, and obesity. As metabolic demand increases, normoglycemia is maintained through increased pancreatic β-cell mass and function, a phenomenon known as compensation. In susceptible individuals, compensation is followed by a period of decompensation marked by a decline in islet size and function. Decompensation leads to the development of hyperglycemia and overt type 2 diabetes. Adapted from (Alejandro et al. 2015).

Figure 1.3

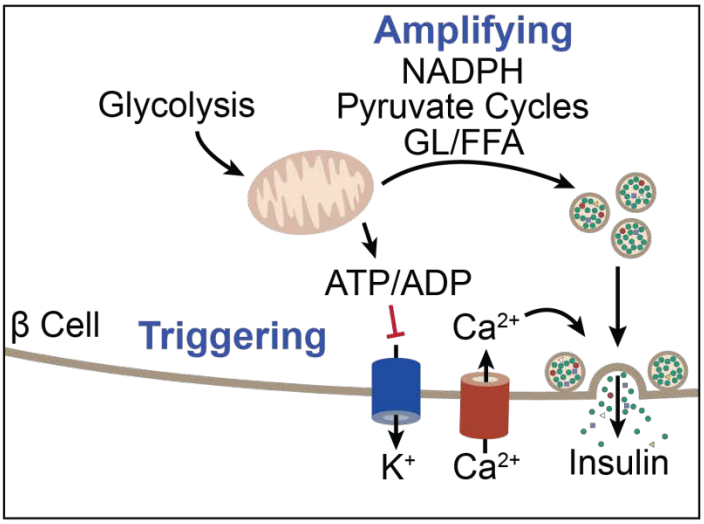

Figure 1.3. Triggering and amplifying pathways of glucose-stimulated insulin secretion. Glucose stimulates ATP production, increasing the cellular ATP/ADP ratio. Increased cellular levels of ATP inhibit ATP-dependent K+ channels, depolarizing the cell, inducing Ca2+ influx, and triggering insulin secretion. The amplifying pathways are also enhanced via glucose metabolism and are comprised of, among others, cytosolic NADPH generation, glycerolipid/free fatty acid production, and mitochondrial pyruvate cycles. The amplifying pathways then in turn enhance the magnitude of insulin secretion.

Figure 1.4

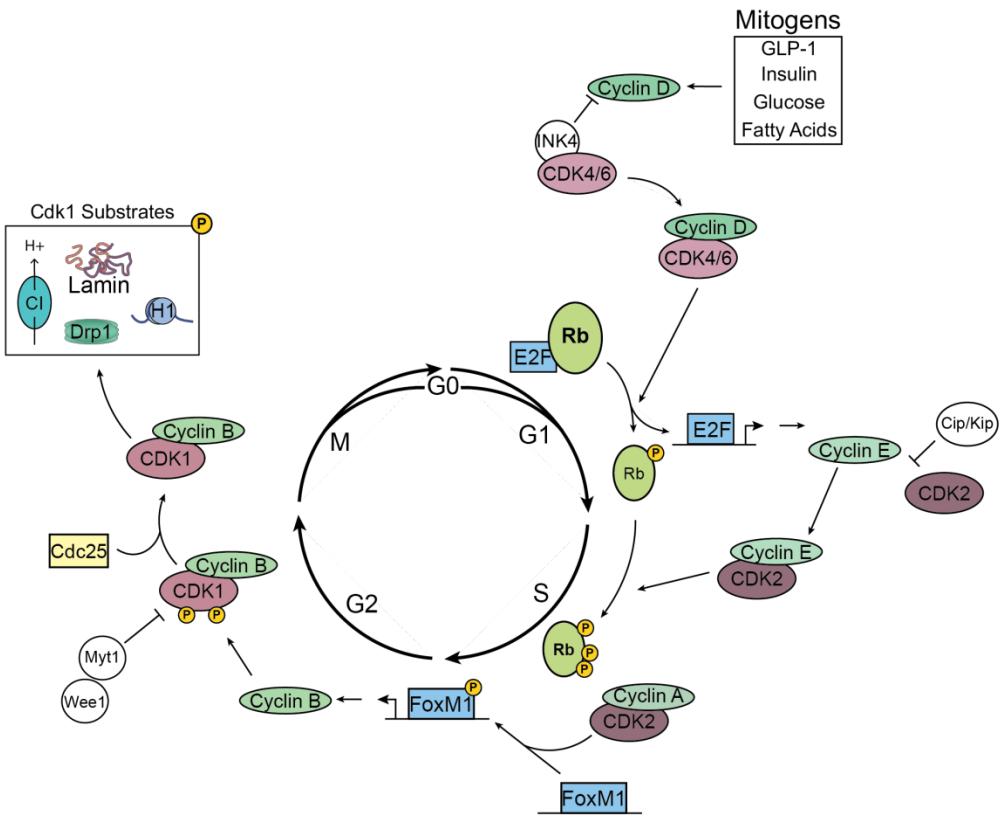

Figure 1.4. The β-cell cycle can be divided into four sequential phases, G1, S, G2, and M, with an additional reversible resting phase, G0. In G0, cellular levels of Cdk4/6 inhibitor p16INK4a are high. Mitogenic stimulation with insulin, glucose, incretins, or free fatty acids stimulates increased Cyclin D expression levels sufficient to overcome Cdk4/6 inhibition. CycD/Cdk4/6 complexes then initiate phosphorylation of Rb. Phosphorylation of Rb leads to de-repression of transcription factor E2F and increased expression of Cyclin E. Cyclin E pairs with Cdk2 to further phosphorylate Rb, pushing the cell into S phase. In S phase, activated FoxM1 leads to increased expression of Cyclin B1. Cyclin B1, paired with Cdk1, is inhibited by phosphorylation via Myt1 and Wee1. Activating phosphatase Cdc25c removes inhibitor phosphorylation, activating CycB1/Cdk1. Activated CycB1/Cdk1 phosphorylates numerous targets (including Complex I, Lamin, Histone H1, and Drp1), initiating mitosis and completing cell division.

Table 1.1

Cdk	Cyclin	Cell Cycle Stage	Function	Inhibitor
Cdk1	Cyclin B + Cyclin A	G2/M	Control mitotic entry and mitosis	Myt1, Wee1, p21
Cdk2	Cyclin E + Cyclin A	G1/S	Control G1/S transition and S phase and E2F expression	Cip/Kip — p21, p27, p57
Cdk4/6	Cyclin D	G1 and G0/G1 transition	Control G1 and E2F expression	INK — p15, p16, p18, p19, p27, p57

Table 1.1. Summary of cyclin-dependent kinase regulation and activity. Every Cdk has one or more corresponding cyclin activators and protein inhibitors, as well as its own role and timing in cell-cycle progression.

REFERENCES

1. Diabetes Report Card | Reports | Resource Library | Diabetes | CDC [Internet]. [cited 2017 May 12]. Available from: https://www.cdc.gov/diabetes/library/reports/reportcard.html

2. Jl S. [Type 2 diabetes complications]. Presse Medicale Paris Fr 1983. 2013 May;42(5):839–48.

3. Cerf ME. Beta Cell Dysfunction and Insulin Resistance. Front Endocrinol [Internet]. 2013 Mar 27 [cited 2017 May 5];4. Available from: http://www.ncbi.nlm.nih.gov/pmc/articles/PMC3608918/

4. Asif M. The prevention and control the type-2 diabetes by changing lifestyle and dietary pattern. J Educ Health Promot [Internet]. 2014 Feb 21 [cited 2017 May 25];3. Available from: http://www.ncbi.nlm.nih.gov/pmc/articles/PMC3977406/

5. Reusens B, Ozanne SE, Remacle C. Fetal determinants of type 2 diabetes. Curr Drug Targets. 2007 Aug;8(8):935–41.

6. Palmer ND, Langefeld CD, Campbell JK, Williams AH, Saad M, Norris JM, et al. Genetic Mapping of Disposition Index and Acute Insulin Response Loci on Chromosome 11q. Diabetes. 2006 Apr 1;55(4):911–8.

7. DeFronzo RA. The Triumvirate: β-Cell, Muscle, Liver: A Collusion Responsible for NIDDM. Diabetes. 1988 Jun 1;37(6):667–87.

8. Weir GC, Bonner-Weir S. Five Stages of Evolving Beta-Cell Dysfunction During Progression to Diabetes. Diabetes. 2004 Dec 1;53(suppl 3):S16–21.

9. Alejandro EU, Gregg B, Blandino-Rosano M, Cras-Méneur C, Bernal-Mizrachi E. Natural history of β-cell adaptation and failure in type 2 diabetes. Mol Aspects Med. 2015 Apr;42:19–41.

10. Swisa A, Glaser B, Dor Y. Metabolic Stress and Compromised Identity of Pancreatic Beta Cells. Front Genet [Internet]. 2017 [cited 2017 May 8];8. Available from: http://journal.frontiersin.org/article/10.3389/fgene.2017.00021/full

11. Weir GC, Laybutt DR, Kaneto H, Bonner-Weir S, Sharma A. Beta-cell adaptation and decompensation during the progression of diabetes. Diabetes. 2001 Feb 1;50(suppl 1):S154.

12. Elayat AA, el-Naggar MM, Tahir M. An immunocytochemical and morphometric study of the rat pancreatic islets. J Anat. 1995 Jun;186(Pt 3):629–37.

13. Steiner DJ, Kim A, Miller K, Hara M. Pancreatic islet plasticity: Interspecies comparison of islet architecture and composition. Islets. 2010 May;2(3):135–45.

14. Tillmar L, Carlsson C, Welsh N. Control of Insulin mRNA Stability in Rat Pancreatic Islets Regulatory Role Of A 3'-Untranslated Region Pyrimidine-Rich Sequence. J Biol Chem. 2002 Jan 11;277(2):1099–106.

15. Schuit FC, In't Veld PA, Pipeleers DG. Glucose stimulates proinsulin biosynthesis by a dose-dependent recruitment of pancreatic beta cells. Proc Natl Acad Sci U S A. 1988 Jun;85(11):3865–9.

16. De Vos A, Heimberg H, Quartier E, Huypens P, Bouwens L, Pipeleers D, et al. Human and rat beta cells differ in glucose transporter but not in glucokinase gene expression. J Clin Invest. 1995 Nov;96(5):2489–95.

17. Rutter GA, Pullen TJ, Hodson DJ, Martinez-Sanchez A. Pancreatic β-cell identity, glucose sensing and the control of insulin secretion. Biochem J. 2015 Mar 1;466(2):203–18.

18. Sugden MC, Holness MJ. The pyruvate carboxylase-pyruvate dehydrogenase axis in islet pyruvate metabolism. Islets. 2011 Nov 1;3(6):302–19.

19. Ashcroft FM. ATP-sensitive potassium channelopathies: focus on insulin secretion. J Clin Invest. 2005 Aug;115(8):2047–58.

20. Straub SG, Sharp GWG. Glucose-stimulated signaling pathways in biphasic insulin secretion. Diabetes Metab Res Rev. 2002 Dec;18(6):451–63.

21. Henquin JC. Triggering and amplifying pathways of regulation of insulin secretion by glucose. Diabetes. 2000 Nov 1;49(11):1751–60.

22. Henquin J-C. The dual control of insulin secretion by glucose involves triggering and amplifying pathways in β-cells. Diabetes Res Clin Pract. 2011 Aug 1;93:S27–31.

23. Prentki M, Matschinsky FM, Madiraju SRM. Metabolic Signaling in Fuel-Induced Insulin Secretion. Cell Metab. 2013 Aug 6;18(2):162–85.

24. Population ages 65 and above (% of total) | Data [Internet]. [cited 2017 May 30]. Available from: http://data.worldbank.org/indicator/SP.POP.65UP.TO.ZS

25. Gong Z, Muzumdar RH. Pancreatic Function, Type 2 Diabetes, and Metabolism in Aging. Int J Endocrinol. 2012 May 17;2012:e320482.

26. De Tata V. Age-Related Impairment of Pancreatic Beta-Cell Function: Pathophysiological and Cellular Mechanisms. Front Endocrinol [Internet]. 2014 Sep 3 [cited 2017 May 16];5. Available from: http://www.ncbi.nlm.nih.gov/pmc/articles/PMC4153315/

27. Kalyani RR, Egan JM. Diabetes and Altered Glucose Metabolism with Aging. Endocrinol Metab Clin North Am. 2013 Jun;42(2):333–47.

28. Iozzo P, Beck-Nielsen H, Laakso M, Smith U, Yki-Järvinen H, Ferrannini E. Independent Influence of Age on Basal Insulin Secretion in Nondiabetic Humans. J Clin Endocrinol Metab. 1999 Mar 1;84(3):863–8.

29. DeFronzo RA. Glucose Intolerance and Aging: Evidence for Tissue Insensitivity to Insulin. Diabetes. 1979 Dec 1;28(12):1095–101.

30. Elahi D, Muller DC, McAloon-Dyke M, Tobin JD, Andres R. The effect of age on insulin response and glucose utilization during four hyperglycemic plateaus. Exp Gerontol. 1993 Jul;28(4–5):393–409.

31. Novelli M, Tata VD, Bombara M, Lorenzini A, Masini M, Pollera M, et al. Insufficient adaptive capability of pancreatic endocrine function in dexamethasone-treated ageing rats. J Endocrinol. 1999 Sep 1;162(3):425–32.

32. Fink RI, Kolterman OG, Griffin J, Olefsky JM. Mechanisms of Insulin Resistance in Aging. J Clin Invest. 1983 Jun;71(6):1523–35.

33. Refaie MR, Sayed-Ahmed NA, Bakr AM, Abdel Aziz MY, El Kannishi MH, Abdel-Gawad SS. Aging is an Inevitable Risk Factor for Insulin Resistance. J Taibah Univ Med Sci. 2006;1(1):30–41.

34. Scheen AJ. Diabetes mellitus in the elderly: insulin resistance and/or impaired insulin secretion? Diabetes Metab. 2005 Dec;31 Spec No 2:5S27-25S34.

35. Stout RW. Glucose tolerance and ageing. J R Soc Med. 1994 Oct;87(10):608–9.

36. Ohneda M, Johnson JH, Inman LR, Chen L, Suzuki K-I, Goto Y, et al. GLUT2 Expression and Function in β-cells of GK rats with NIDDM: Dissociation Between Reductions in Glucose Transport and Glucose-Stimulated Insulin Secretion. Diabetes. 1993 Jul 1;42(7):1065–72.

37. Kramer J, Moeller EL, Hachey A, Mansfield KG, Wachtman LM. Differential expression of GLUT2 in pancreatic islets and kidneys of New and Old World nonhuman primates. Am J Physiol - Regul Integr Comp Physiol. 2009 Mar 1;296(3):R786–93.

38. Ihm S-H, Matsumoto I, Sawada T, Nakano M, Zhang HJ, Ansite JD, et al. Effect of Donor Age on Function of Isolated Human Islets. Diabetes. 2006 May 1;55(5):1361–8.

39. Novelli M, De Tata V, Bombara M, Bergamini E, Masiello P. Age-dependent reduction in GLUT-2 levels is correlated with the impairment of the insulin secretory response in isolated islets of Sprague–Dawley rats. Exp Gerontol. 2000 Aug 1;35(5):641–51.

40. Frese T, Bazwinsky I, Mühlbauer E, Peschke E. Circadian and Age-dependent Expression Patterns of GLUT2 and Glucokinase in the Pancreatic β-Cell of Diabetic and Nondiabetic Rats. Horm Metab Res. 2007 Aug;39(8):567–74.

41. McCulloch LJ, van de Bunt M, Braun M, Frayn KN, Clark A, Gloyn AL. GLUT2 (SLC2A2) is not the principal glucose transporter in human pancreatic beta cells: Implications for understanding genetic association signals at this locus. Mol Genet Metab. 2011 Dec;104(4):648–53.

42. Ohtsubo K, Takamatsu S, Minowa MT, Yoshida A, Takeuchi M, Marth JD. Dietary and Genetic Control of Glucose Transporter 2 Glycosylation Promotes Insulin Secretion in Suppressing Diabetes. Cell. 2005 Dec 29;123(7):1307–21.

43. Hou JC, Williams D, Vicogne J, Pessin JE. The Glucose Transporter 2 Undergoes Plasma Membrane Endocytosis and Lysosomal Degradation in a Secretagogue-Dependent Manner. Endocrinology. 2009 Sep 1;150(9):4056–64.

44. Jitrapakdee S, Wutthisathapornchai A, Wallace JC, MacDonald MJ. Regulation of insulin secretion: role of mitochondrial signalling. Diabetologia. 2010 Jun;53(6):1019–32.

45. Mourad NI, Nenquin M, Henquin J-C. Metabolic amplifying pathway increases both phases of insulin secretion independently of β-cell actin microfilaments. Am J Physiol - Cell Physiol. 2010 Aug 1;299(2):C389–98.

46. Ferdaoussi M, Dai X, Jensen MV, Wang R, Peterson BS, Huang C, et al. Isocitrate-to-SENP1 signaling amplifies insulin secretion and rescues dysfunctional β cells. J Clin Invest. 2015 Oct 1;125(10):3847–60.

47. Guay C, Joly É, Pepin É, Barbeau A, Hentsch L, Pineda M, et al. A Role for Cytosolic Isocitrate Dehydrogenase as a Negative Regulator of Glucose Signaling for Insulin Secretion in Pancreatic ß-Cells. PLoS ONE [Internet]. 2013 Oct 10 [cited 2017 May 8];8(10). Available from: http://www.ncbi.nlm.nih.gov/pmc/articles/PMC3795013/

48. Guay C, Madiraju SRM, Aumais A, Joly É, Prentki M. A Role for ATP-Citrate Lyase, Malic Enzyme, and Pyruvate/Citrate Cycling in Glucose-induced Insulin Secretion. J Biol Chem. 2007 Dec 7;282(49):35657–65.

49. Nolan CJ, Madiraju MSR, Delghingaro-Augusto V, Peyot M-L, Prentki M. Fatty Acid Signaling in the β-Cell and Insulin Secretion. Diabetes. 2006 Dec 1;55(Supplement 2):S16–23.

50. MacDonald MJ. High content of mitochondrial glycerol-3-phosphate dehydrogenase in pancreatic islets and its inhibition by diazoxide. J Biol Chem. 1981 Aug 25;256(16):8287–90.

51. Azhar S, Ho H, Reaven EP, Reaven GM. Evidence of an age-related decline in mitochondrial glycerophosphate dehydrogenase activity of isolated rat islets. Metabolism. 1983 Nov 1;32(11):1019–21.

52. Reaven GM, Reaven PD. Effect of age on glucose oxidation by isolated rat islets. Diabetologia. 1980 Jan 1;18(1):69–71.

53. Payne BAI, Chinnery PF. Mitochondrial dysfunction in aging: Much progress but many unresolved questions. Biochim Biophys Acta. 2015 Nov;1847(11):1347–53.

54. Mills KF, Yoshida S, Stein LR, Grozio A, Kubota S, Sasaki Y, et al. Long-Term Administration of Nicotinamide Mononucleotide Mitigates Age-Associated Physiological Decline in Mice. Cell Metab. 2016 Dec 13;24(6):795–806.

55. Zhang H, Ryu D, Wu Y, Gariani K, Wang X, Luan P, et al. NAD+ repletion improves mitochondrial and stem cell function and enhances life span in mice. Science. 2016 Jun 17;352(6292):1436–43.

56. Barzilai N, Huffman DM, Muzumdar RH, Bartke A. The Critical Role of Metabolic Pathways in Aging. Diabetes. 2012 Jun;61(6):1315–22.

57. Cree LM, Patel SK, Pyle A, Lynn S, Turnbull DM, Chinnery PF, et al. Age-related decline in mitochondrial DNA copy number in isolated human pancreatic islets. Diabetologia. 2008 Aug 1;51(8):1440–3.

58. Petersen KF, Befroy D, Dufour S, Dziura J, Ariyan C, Rothman DL, et al. Mitochondrial Dysfunction in the Elderly: Possible Role in Insulin Resistance. Science. 2003 May 16;300(5622):1140–2.

59. Lu H, Koshkin V, Allister EM, Gyulkhandanyan AV, Wheeler MB. Molecular and Metabolic Evidence for Mitochondrial Defects Associated With β-Cell Dysfunction in a Mouse Model of Type 2 Diabetes. Diabetes. 2010 Feb 1;59(2):448–59.

60. Koster JC, Permutt MA, Nichols CG. Diabetes and Insulin Secretion. Diabetes. 2005 Nov 1;54(11):3065–72.

61. Ammon HP, Fahmy A, Mark M, Wahl MA, Youssif N. The effect of glucose on insulin release and ion movements in isolated pancreatic islets of rats in old age. J Physiol. 1987 Mar;384:347–54.

62. Almaça J, Molina J, Drigo RA e, Abdulreda MH, Jeon WB, Berggren P-O, et al. Young capillary vessels rejuvenate aged pancreatic islets. Proc Natl Acad Sci. 2014 Dec 9;111(49):17612–7.

63. Avrahami D, Li C, Zhang J, Schug J, Avrahami R, Rao S, et al. Aging-Dependent Demethylation of Regulatory Elements Correlates with Chromatin State and Improved β Cell Function. Cell Metab. 2015 Oct 6;22(4):619–32.

64. Helman A, Klochendler A, Azazmeh N, Gabai Y, Horwitz E, Anzi S, et al. p16Ink4a-induced senescence of pancreatic beta cells enhances insulin secretion. Nat Med. 2016 Apr;22(4):412–20.

65. Yang J, Huang T, Petralia F, Long Q, Zhang B, Argmann C, et al. Synchronized age-related gene expression changes across multiple tissues in human and the link to complex diseases. Sci Rep. 2015 Oct 19;5:15145.

66. Glass D, Viñuela A, Davies MN, Ramasamy A, Parts L, Knowles D, et al. Gene expression changes with age in skin, adipose tissue, blood and brain. Genome Biol. 2013;14:R75.

67. Krishnamurthy J, Ramsey MR, Ligon KL, Torrice C, Koh A, Bonner-Weir S, et al. p16INK4a induces an age-dependent decline in islet regenerative potential. Nature. 2006 Sep 28;443(7110):453–7.

68. Krishnamurthy J, Torrice C, Ramsey MR, Kovalev GI, Al-Regaiey K, Su L, et al. *Ink4a/Arf* expression is a biomarker of aging. J Clin Invest. 2004 Nov 1;114(9):1299–307.

69. Malakar P, Chartarifsky L, Hija A, Leibowitz G, Glaser B, Dor Y, et al. Insulin receptor alternative splicing is regulated by insulin signaling and modulates beta cell survival. Sci Rep. 2016 Aug 16;6:31222.

70. Steil GM, Trivedi N, Jonas J-C, Hasenkamp WM, Sharma A, Bonner-Weir S, et al. Adaptation of β-cell mass to substrate oversupply: enhanced function with normal gene expression. Am J Physiol - Endocrinol Metab. 2001 May 1;280(5):E788–96.

71. Wang P, Fiaschi-Taesch NM, Vasavada RC, Scott DK, García-Ocaña A, Stewart AF. Diabetes mellitus—advances and challenges in human β-cell proliferation. Nat Rev Endocrinol. 2015 Apr;11(4):201–12.

72. Sullivan BA, Hollister-Lock J, Bonner-Weir S, Weir GC. Reduced Ki67 Staining in the Postmortem State Calls Into Question Past Conclusions About the Lack of Turnover of Adult Human β-Cells. Diabetes. 2015 May 1;64(5):1698–702.

73. Levine F, Itkin-Ansari P. β-cell regeneration: Neogenesis, replication or both? J Mol Med. 2008 Mar 1;86(3):247–58.

74. Dor Y, Brown J, Martinez OI, Melton DA. Adult pancreatic β-cells are formed by self-duplication rather than stem-cell differentiation. Nature. 2004 May 6;429(6987):41–6.

75. Teta M, Long SY, Wartschow LM, Rankin MM, Kushner JA. Very Slow Turnover of β-Cells in Aged Adult Mice. Diabetes. 2005 Sep 1;54(9):2557–67.

76. Perl S, Kushner JA, Buchholz BA, Meeker AK, Stein GM, Hsieh M, et al. Significant Human β-Cell Turnover Is Limited to the First Three Decades of Life as Determined by in Vivo Thymidine Analog Incorporation and Radiocarbon Dating. J Clin Endocrinol Metab. 2010 Oct;95(10):E234–9.

77. Tschen S-I, Dhawan S, Gurlo T, Bhushan A. Age-Dependent Decline in β-Cell Proliferation Restricts the Capacity of β-Cell Regeneration in Mice. Diabetes. 2009 Jun 1;58(6):1312–20.

78. Rankin MM, Kushner JA. Adaptive β-Cell Proliferation Is Severely Restricted With Advanced Age. Diabetes. 2009 Jun 1;58(6):1365–72.

79. Sullivan C, Liu Y, Shen J, Curtis A, Newman C, Hock JM, et al. Novel Interactions between FOXM1 and CDC25A Regulate the Cell Cycle. PLOS ONE. 2012 Dec 11;7(12):e51277.

80. Zhang H, Ackermann AM, Gusarova GA, Lowe D, Feng X, Kopsombut UG, et al. The FoxM1 Transcription Factor Is Required to Maintain Pancreatic β-Cell Mass. Mol Endocrinol. 2006 Aug 1;20(8):1853–66.

81. Golson ML, Dunn JC, Maulis MF, Dadi PK, Osipovich AB, Magnuson MA, et al. Activation of FoxM1 Revitalizes the Replicative Potential of Aged β-Cells in Male Mice and Enhances Insulin Secretion. Diabetes. 2015 Nov;64(11):3829–38.

82. Maedler K, Schumann DM, Schulthess F, Oberholzer J, Bosco D, Berney T, et al. Aging Correlates With Decreased β-Cell Proliferative Capacity and Enhanced Sensitivity to Apoptosis. Diabetes. 2006 Sep 1;55(9):2455–62.

83. Ihm S-H, Moon HJ, Kang JG, Park CY, Oh KW, Jeong IK, et al. Effect of aging on insulin secretory function and expression of beta cell function-related genes of islets. Diabetes Res Clin Pract. 2007 Sep;77(3, Supplement):S150–4.

84. Thomas MK, Devon ON, Lee JH, Peter A, Schlosser DA, Tenser MS, et al. Development of diabetes mellitus in aging transgenic mice following suppression of pancreatic homeoprotein IDX-1. J Clin Invest. 2001 Jul 15;108(2):319–29.

85. Salas E, Rabhi N, Froguel P, Annicotte J-S, bastien. Role of Ink4a/Arf Locus in Beta Cell Mass Expansion under Physiological and Pathological Conditions. J Diabetes Res. 2014 Feb 6;2014:e873679.

86. Hija A, Salpeter S, Klochendler A, Grimsby J, Brandeis M, Glaser B, et al. G0-G1 Transition and the Restriction Point in Pancreatic β-Cells In Vivo. Diabetes. 2014 Feb 1;63(2):578–84.

87. Keller MP, Choi Y, Wang P, Davis DB, Rabaglia ME, Oler AT, et al. A gene expression network model of type 2 diabetes links cell cycle regulation in islets with diabetes susceptibility. Genome Res. 2008 May 1;18(5):706–16.

88. Ohn JH, Kwak SH, Cho YM, Lim S, Jang HC, Park KS, et al. 10-year trajectory of β-cell function and insulin sensitivity in the development of type 2 diabetes: a community-based prospective cohort study. Lancet Diabetes Endocrinol. 2016 Jan 1;4(1):27–34.

89. Golson ML, Misfeldt AA, Kopsombut UG, Petersen CP, Gannon M. High Fat Diet Regulation of β-Cell Proliferation and β-Cell Mass. Open Endocrinol J [Internet]. 2010 [cited 2017 May 12];4. Available from: http://www.ncbi.nlm.nih.gov/pmc/articles/PMC3856766/

90. Hanley NA, Hanley KP, Miettinen PJ, Otonkoski T. Weighing up β-cell mass in mice and humans: Self-renewal, progenitors or stem cells? Mol Cell Endocrinol. 2008 Jun 25;288(1–2):79–85.

91. Alonso LC, Yokoe T, Zhang P, Scott DK, Kim SK, O'Donnell CP, et al. Glucose Infusion in Mice. Diabetes. 2007 Jul 1;56(7):1792–801.

92. Hull RL, Kodama K, Utzschneider KM, Carr DB, Prigeon RL, Kahn SE. Dietary-fat-induced obesity in mice results in beta cell hyperplasia but not increased insulin release: evidence for specificity of impaired beta cell adaptation. Diabetologia. 2005 Jul 1;48(7):1350–8.

93. Kulkarni RN, Brüning JC, Winnay JN, Postic C, Magnuson MA, Kahn CR. Tissue-Specific Knockout of the Insulin Receptor in Pancreatic β Cells Creates an Insulin Secretory Defect Similar to that in Type 2 Diabetes. Cell. 1999 Feb 5;96(3):329–39.

94. Cozar-Castellano I, Weinstock M, Haught M, Velázquez-Garcia S, Sipula D, Stewart AF. Evaluation of β-Cell Replication in Mice Transgenic for Hepatocyte Growth Factor and Placental Lactogen. Diabetes. 2006 Jan 1;55(1):70–7.

95. Bulotta A, Farilla L, Hui H, Perfetti R. The role of GLP-1 in the regulation of islet cell mass. Cell Biochem Biophys. 2004;40(3 Suppl):65–78.

96. Martinez SC, Cras-Méneur C, Bernal-Mizrachi E, Permutt MA. Glucose Regulates Foxo1 Through Insulin Receptor Signaling in the Pancreatic Islet β-cell. Diabetes. 2006 Jun 1;55(6):1581–91.

97. Mudaliar S, Henry RR. Effects of Incretin Hormones on β-Cell Mass and Function, Body Weight, and Hepatic and Myocardial Function. Am J Med. 2010 Mar;123(3, Supplement):S19–27.

98. Okada T, Liew CW, Hu J, Hinault C, Michael MD, Krtzfeldt J, et al. Insulin receptors in β-cells are critical for islet compensatory growth response to insulin resistance. Proc Natl Acad Sci. 2007 May 22;104(21):8977–82.

99. Otani K, Kulkarni RN, Baldwin AC, Krutzfeldt J, Ueki K, Stoffel M, et al. Reduced β-cell mass and altered glucose sensing impair insulin-secretory function in βIRKO mice. Am J Physiol - Endocrinol Metab. 2004 Jan 1;286(1):E41–9.

100. Shirakawa J, Fernandez M, Takatani T, El Ouaamari A, Jungtrakoon P, Okawa ER, et al. Insulin Signaling Regulates the FoxM1/PLK1/CENP-A Pathway to Promote Adaptive Pancreatic β Cell Proliferation. Cell Metab. 2017 Apr 4;25(4):868–882.e5.

101. Sengupta A, Kalinichenko VV, Yutzey KE. FoxO and FoxM1 Transcription Factors Have Antagonistic Functions in Neonatal Cardiomyocyte Cell Cycle Withdrawal and IGF1 Gene Regulation. Circ Res. 2013 Jan 18;112(2):267–77.

102. Kitamura T, Nakae J, Kitamura Y, Kido Y, Biggs WH, Wright CVE, et al. The forkhead transcription factor *Foxo1* links insulin signaling to *Pdx1* regulation of pancreatic β cell growth. J Clin Invest. 2002 Dec 15;110(12):1839–47.

103. Davis DB, Lavine JA, Suhonen JI, Krautkramer KA, Rabaglia ME, Sperger JM, et al. FoxM1 Is Up-Regulated by Obesity and Stimulates β-Cell Proliferation. Mol Endocrinol. 2010 Sep 1;24(9):1822–34.

104. Seino Y, Fukushima M, Yabe D. GIP and GLP-1, the two incretin hormones: Similarities and differences. J Diabetes Investig. 2010 Apr 22;1(1–2):8–23.

105. Nielsen LL, Young AA, Parkes DG. Pharmacology of exenatide (synthetic exendin-4): a potential therapeutic for improved glycemic control of type 2 diabetes. Regul Pept. 2004 Feb 15;117(2):77–88.

106. Meloni AR, DeYoung MB, Lowe C, Parkes DG. GLP-1 receptor activated insulin secretion from pancreatic β-cells: mechanism and glucose dependence. Diabetes Obes Metab. 2013 Jan 1;15(1):15–27.

107. MacDonald PE, El-kholy W, Riedel MJ, Salapatek AMF, Light PE, Wheeler MB. The Multiple Actions of GLP-1 on the Process of Glucose-Stimulated Insulin Secretion. Diabetes. 2002 Dec 1;51(suppl 3):S434–42.

108. Shigeto M, Ramracheya R, Tarasov AI, Cha CY, Chibalina MV, Hastoy B, et al. GLP-1 stimulates insulin secretion by PKC-dependent TRPM4 and TRPM5 activation. J Clin Invest. 2015 Dec 1;125(12):4714–28.

109. Vasu S, Moffett RC, Thorens B, Flatt PR. Role of Endogenous GLP-1 and GIP in Beta Cell Compensatory Responses to Insulin Resistance and Cellular Stress. PLOS ONE. 2014 Jun 26;9(6):e101005.

110. Perfetti R, Zhou J, Doyle ME, Egan JM. Glucagon-Like Peptide-1 Induces Cell Proliferation and Pancreatic-Duodenum Homeobox-1 Expression and Increases Endocrine Cell Mass in the Pancreas of Old, Glucose-Intolerant Rats. Endocrinology. 2000 Dec 1;141(12):4600–5.

111. Buteau J, Foisy S, Rhodes CJ, Carpenter L, Biden TJ, Prentki M. Protein Kinase Cζ Activation Mediates Glucagon-Like Peptide-1–Induced Pancreatic β-Cell Proliferation. Diabetes. 2001 Oct 1;50(10):2237–43.

112. Rajan S, Dickson LM, Mathew E, Orr CMO, Ellenbroek JH, Philipson LH, et al. Chronic hyperglycemia downregulates GLP-1 receptor signaling in pancreatic β-cells via protein kinase A. Mol Metab. 2015 Feb 3;4(4):265–76.

113. Nauck MA, Heimesaat MM, Orskov C, Holst JJ, Ebert R, Creutzfeldt W. Preserved incretin activity of glucagon-like peptide 1 [7-36 amide] but not of synthetic human gastric inhibitory polypeptide in patients with type-2 diabetes mellitus. J Clin Invest. 1993 Jan;91(1):301–7.

114. Moffett RC, Vasu S, Thorens B, Drucker DJ, Flatt PR. Incretin Receptor Null Mice Reveal Key Role of GLP-1 but Not GIP in Pancreatic Beta Cell Adaptation to Pregnancy. PLOS ONE. 2014 Jun 13;9(6):e96863.

115. Stamateris RE, Sharma RB, Kong Y, Ebrahimpour P, Panday D, Ranganath P, et al. Glucose induces mouse beta cell proliferation via IRS2, mTOR and cyclin D2 but not the insulin receptor. Diabetes. 2016 Jan 5;db150529.

116. Fiaschi-Taesch NM, Salim F, Kleinberger J, Troxell R, Cozar-Castellano I, Selk K, et al. Induction of Human β-Cell Proliferation and Engraftment Using a Single G1/S Regulatory Molecule, cdk6. Diabetes. 2010 Aug 1;59(8):1926–36.

117. Morgan DO. Principles of CDK regulation. Nat Lond. 1995 Mar 9;374(6518):131–4.

118. Duronio RJ, Xiong Y. Signaling Pathways that Control Cell Proliferation. Cold Spring Harb Perspect Biol [Internet]. 2013 Mar [cited 2017 May 26];5(3). Available from: http://www.ncbi.nlm.nih.gov/pmc/articles/PMC3578363/

119. Obaya AJ, Sedivy JM. Regulation of cyclin-Cdk activity in mammalian cells. Cell Mol Life Sci CMLS. 2002 Jan;59(1):126–42.

120. Lundberg AS, Weinberg RA. Functional Inactivation of the Retinoblastoma Protein Requires Sequential Modification by at Least Two Distinct Cyclin-cdk Complexes. Mol Cell Biol. 1998 Feb;18(2):753–61.

121. Yao G, Lee TJ, Mori S, Nevins JR, You L. A bistable Rb-E2F switch underlies the restriction point. Nat Cell Biol. 2008 Apr;10(4):476–82.

122. Chellappan SP, Hiebert S, Mudryj M, Horowitz JM, Nevins JR. The E2F transcription factor is a cellular target for the RB protein. Cell. 1991 Jun 14;65(6):1053–61.

123. Brehm A, Miska EA, McCance DJ, Reid JL, Bannister AJ, Kouzarides T. Retinoblastoma protein recruits histone deacetylase to repress transcription. Nature. 1998 Feb 5;391(6667):597–601.

124. Schulze A, Zerfass K, Spitkovsky D, Middendorp S, Bergès J, Helin K, et al. Cell cycle regulation of the cyclin A gene promoter is mediated by a variant E2F site. Proc Natl Acad Sci. 1995 Nov 21;92(24):11264–8.

125. Ohtani K, DeGregori J, Nevins JR. Regulation of the cyclin E gene by transcription factor E2F1. Proc Natl Acad Sci U S A. 1995 Dec 19;92(26):12146–50.

126. Dalton S. Cell cycle regulation of the human cdc2 gene. EMBO J. 1992 May;11(5):1797–804.

127. Pearson BE, Nasheuer HP, Wang TS. Human DNA polymerase alpha gene: sequences controlling expression in cycling and serum-stimulated cells. Mol Cell Biol. 1991 Apr;11(4):2081–95.

128. Ohtani K, DeGregori J, Leone G, Herendeen DR, Kelly TJ, Nevins JR. Expression of the HsOrc1 gene, a human ORC1 homolog, is regulated by cell proliferation via the E2F transcription factor. Mol Cell Biol. 1996 Dec 1;16(12):6977–84.

129. Weinberg RA. The retinoblastoma protein and cell cycle control. Cell. 1995 May 5;81(3):323–30.

130. Narasimha AM, Kaulich M, Shapiro GS, Choi YJ, Sicinski P, Dowdy SF. Cyclin D activates the Rb tumor suppressor by mono-phosphorylation. eLife [Internet]. 2014 Jun 4 [cited 2017 May 21];3. Available from: http://www.ncbi.nlm.nih.gov/pmc/articles/PMC4076869/

131. Hinds PW, Mittnacht S, Dulic V, Arnold A, Reed SI, Weinberg RA. Regulation of retinoblastoma protein functions by ectopic expression of human cyclins. Cell. 1992 Sep 18;70(6):993–1006.

132. Strohmaier H, Spruck CH, Kaiser P, Won KA, Sangfelt O, Reed SI. Human F-box protein hCdc4 targets cyclin E for proteolysis and is mutated in a breast cancer cell line. Nature. 2001 Sep 20;413(6853):316–22.

133. Sherr CJ, Roberts JM. CDK inhibitors: positive and negative regulators of G1-phase progression. Genes Dev. 1999 Jun 15;13(12):1501–12.

134. Serrano M, Hannon GJ, Beach D. A new regulatory motif in cell-cycle control causing specific inhibition of cyclin D/CDK4. Nature. 1993 Dec 16;366(6456):704–7.

135. Berthet C, Aleem E, Coppola V, Tessarollo L, Kaldis P. Cdk2 Knockout Mice Are Viable. Curr Biol. 2003 Oct 14;13(20):1775–85.

136. Malumbres M, Sotillo R, Santamaría D, Galán J, Cerezo A, Ortega S, et al. Mammalian Cells Cycle without the D-Type Cyclin-Dependent Kinases Cdk4 and Cdk6. Cell. 2004 Aug 20;118(4):493–504.

137. Ortega S, Prieto I, Odajima J, Martín A, Dubus P, Sotillo R, et al. Cyclin-dependent kinase 2 is essential for meiosis but not for mitotic cell division in mice. Nat Genet. 2003 Sep;35(1):25–31.

138. Tsutsui T, Hesabi B, Moons DS, Pandolfi PP, Hansel KS, Koff A, et al. Targeted Disruption of CDK4 Delays Cell Cycle Entry with Enhanced p27Kip1 Activity. Mol Cell Biol. 1999 Oct;19(10):7011–9.

139. Taneera J, Fadista J, Ahlqvist E, Zhang M, Wierup N, Renström E, et al. Expression profiling of cell cycle genes in human pancreatic islets with and without type 2 diabetes. Mol Cell Endocrinol. 2013 Aug 15;375(1–2):35–42.

140. Rane SG, Dubus P, Mettus RV, Galbreath EJ, Boden G, Reddy EP, et al. Loss of Cdk4 expression causes insulin-deficient diabetes and Cdk4 activation results in β-islet cell hyperplasia. Nat Genet. 1999 May;22(1):44–52.

141. Miyawaki K, Inoue H, Keshavarz P, Mizuta K, Sato A, Sakamoto Y, et al. Transgenic expression of a mutated cyclin-dependent kinase 4 (CDK4/R24C) in pancreatic β-cells prevents progression of diabetes in db/db mice. Diabetes Res Clin Pract. 2008 Oct;82(1):33–41.

142. Annicotte J-S, Blanchet E, Chavey C, Iankova I, Costes S, Assou S, et al. The CDK4–pRB–E2F1 pathway controls insulin secretion. Nat Cell Biol. 2009 Aug;11(8):1017–23.

143. Russo AA, Jeffrey PD, Patten AK, Massagué J, Pavletich NP. Crystal structure of the p27Kip1 cyclin-dependent-kinase inhibitor bound to the cyclin A-Cdk2 complex. Nature. 1996 Jul 25;382(6589):325–31.

144. Soos TJ, Kiyokawa H, Yan JS, Rubin MS, Giordano A, DeBlasio A, et al. Formation of p27-CDK complexes during the human mitotic cell cycle. Cell Growth Differ. 1996 Feb 1;7(2):135.

145. Kim SY, Lee J-H, Merrins MJ, Gavrilova O, Bisteau X, Kaldis P, et al. Loss of Cyclin Dependent Kinase 2 in the Pancreas Links Primary β-cell Dysfunction to Progressive Depletion of β-cell Mass and Diabetes. J Biol Chem. 2017 Jan 18;jbc.M116.754077.

146. Diril MK, Ratnacaram CK, Padmakumar VC, Du T, Wasser M, Coppola V, et al. Cyclin-dependent kinase 1 (Cdk1) is essential for cell division and suppression of DNA re-replication but not for liver regeneration. Proc Natl Acad Sci U S A. 2012 Mar 6;109(10):3826–31.

147. Santamaría D, Barrière C, Cerqueira A, Hunt S, Tardy C, Newton K, et al. Cdk1 is sufficient to drive the mammalian cell cycle. Nature. 2007 Aug 16;448(7155):811–5.

148. Nurse P, Thuriaux P. Regulatory Genes Controlling Mitosis in the Fission Yeast SCHIZOSACCHAROMYCES POMBE. Genetics. 1980 Nov;96(3):627–37.

149. Brandeis M, Rosewell I, Carrington M, Crompton T, Jacobs MA, Kirk J, et al. Cyclin B2-null mice develop normally and are fertile whereas cyclin B1-null mice die in utero. Proc Natl Acad Sci U S A. 1998 Apr 14;95(8):4344–9.

150. Lim S, Kaldis P. Cdks, cyclins and CKIs: roles beyond cell cycle regulation. Development. 2013 Aug 1;140(15):3079–93.

151. Alvarez B, Martínez-A C, Burgering BM, Carrera AC. Forkhead transcription factors contribute to execution of the mitotic programme in mammals. Nature. 2001 Oct 18;413(6857):744–7.

152. Laoukili J, Kooistra MRH, Brás A, Kauw J, Kerkhoven RM, Morrison A, et al. FoxM1 is required for execution of the mitotic programme and chromosome stability. Nat Cell Biol. 2005 Feb;7(2):126–36.

153. Laoukili J, Alvarez M, Meijer LAT, Stahl M, Mohammed S, Kleij L, et al. Activation of FoxM1 during G2 Requires Cyclin A/Cdk-Dependent Relief of Autorepression by the FoxM1 N-Terminal Domain. Mol Cell Biol. 2008 May 1;28(9):3076–87.

154. Major ML, Lepe R, Costa RH. Forkhead Box M1B Transcriptional Activity Requires Binding of Cdk-Cyclin Complexes for Phosphorylation-Dependent Recruitment of p300/CBP Coactivators. Mol Cell Biol. 2004 Apr;24(7):2649–61.

155. Ayeni JO, Varadarajan R, Mukherjee O, Stuart DT, Sprenger F, Srayko M, et al. Dual Phosphorylation of Cdk1 Coordinates Cell Proliferation with Key Developmental Processes in Drosophila. Genetics. 2014 Jan;196(1):197–210.

156. Chow JPH, Poon RYC, Ma HT. Inhibitory Phosphorylation of Cyclin-Dependent Kinase 1 as a Compensatory Mechanism for Mitosis Exit. Mol Cell Biol. 2011 Apr 1;31(7):1478–91.

157. Mueller PR, Coleman TR, Kumagai A, Dunphy WG. Myt1: A Membrane-Associated Inhibitory Kinase That Phosphorylates Cdc2 on Both Threonine-14 and Tyrosine-15. Science. 1995 Oct 6;270(5233):86–90.

158. Gould KL, Nurse P. Tyrosine phosphorylation of the fission yeast cdc2+ protein kinase regulates entry into mitosis. Nature. 1989 Nov 2;342(6245):39–45.

159. O'Farrell PH. Triggering the all-or-nothing switch into mitosis. Trends Cell Biol. 2001 Dec;11(12):512–9.

160. Lindqvist A, Rodríguez-Bravo V, Medema RH. The decision to enter mitosis: feedback and redundancy in the mitotic entry network. J Cell Biol. 2009 Apr 20;185(2):193–202.

161. Rhind N, Russell P. Signaling Pathways that Regulate Cell Division. Cold Spring Harb Perspect Biol. 2012 Oct 1;4(10):a005942.

162. Hagting A, Karlsson C, Clute P, Jackman M, Pines J. MPF localization is controlled by nuclear export. EMBO J. 1998 Jul 15;17(14):4127–38.

163. Toyoshima F, Moriguchi T, Wada A, Fukuda M, Nishida E. Nuclear export of cyclin B1 and its possible role in the DNA damage-induced G2 checkpoint. EMBO J. 1998 May 15;17(10):2728–35.

164. Yang J, Bardes ESG, Moore JD, Brennan J, Powers MA, Kornbluth S. Control of Cyclin B1 localization through regulated binding of the nuclear export factor CRM1. Genes Dev. 1998 Jul 15;12(14):2131–43.

165. Porter LA, Donoghue DJ. Cyclin B1 and CDK1: nuclear localization and upstream regulators. Prog Cell Cycle Res. 2003;5:335–47.

166. Gavet O, Pines J. Activation of cyclin B1–Cdk1 synchronizes events in the nucleus and the cytoplasm at mitosis. J Cell Biol. 2010 Apr 19;189(2):247–59.

167. Chen J-T, Ho C-W, Chi L-M, Chien K-Y, Hsieh Y-J, Lin S-J, et al. Identification of the lamin A/C phosphoepitope recognized by the antibody P-STM in mitotic HeLa S3 cells. BMC Biochem. 2013 Jul 19;14:18.

168. Terrano DT, Upreti M, Chambers TC. Cyclin-Dependent Kinase 1-Mediated Bcl-xL/Bcl-2 Phosphorylation Acts as a Functional Link Coupling Mitotic Arrest and Apoptosis. Mol Cell Biol. 2010 Feb 1;30(3):640–56.

169. Wang Z, Fan M, Candas D, Zhang T-Q, Qin L, Eldridge A, et al. Cyclin B1/Cdk1 Coordinates Mitochondrial Respiration for Cell-Cycle G2/M Progression. Dev Cell. 2014 Apr 28;29(2):217–32.

170. Candas D, Fan M, Nantajit D, Vaughan AT, Murley JS, Woloschak GE, et al. Cyclin B1/Cdk1 phosphorylates mitochondrial antioxidant MnSOD in cell adaptive response to radiation stress. J Mol Cell Biol. 2013 Jun 1;5(3):166–75.

171. Liu R, Fan M, Candas D, Qin L, Zhang X, Eldridge A, et al. CDK1-Mediated SIRT3 Activation Enhances Mitochondrial Function and Tumor Radioresistance. Mol Cancer Ther. 2015 Sep 1;14(9):2090–102.

172. Nantajit D, Fan M, Duru N, Wen Y, Reed JC, Li JJ. Cyclin B1/Cdk1 Phosphorylation of Mitochondrial p53 Induces Anti-Apoptotic Response. PLOS ONE. 2010 Aug 23;5(8):e12341.

173. Malumbres M, Barbacid M. Mammalian cyclin-dependent kinases. Trends Biochem Sci. 2005 Nov;30(11):630–41.

174. Loyer P, Trembley JH, Katona R, Kidd VJ, Lahti JM. Role of CDK/cyclin complexes in transcription and RNA splicing. Cell Signal. 2005 Sep;17(9):1033–51.

175. Fajas L. Re-thinking cell cycle regulators: the cross-talk with metabolism. Front Oncol [Internet]. 2013 Jan 25 [cited 2017 May 21];3. Available from: http://www.ncbi.nlm.nih.gov/pmc/articles/PMC3555080/

Chapter 2

NAD(P)H Fluorescence Lifetime Imaging of Pancreatic Islets

Quantifying metabolic activity in live, intact islets is essential to our understanding of islet biology. **F**luorescence **L**ifetime **Im**aging, or FLIM, is an old technique but new to T2D research and is capable of exactly that. Recent work—presented elsewhere in this dissertation—has pioneered the use of FLIM to quantify changes in metabolism associated with the progression of type 2 diabetes in islets. As a preface, this chapter provides an overview of the basic principles of fluorescence lifetime and FLIM and will discuss briefly the two most common acquisition and analysis techniques. This chapter will then detail the application of fluorescence lifetime imaging to the study of redox coenzymes and, in so doing, will review the state of metabolic FLIM analysis and recent developments in the technique as it pertains to islet biology.

Fluorescence and Fluorescence Lifetime

Fluorescence lifetime is an intrinsic property of the fluorophore, much like the excitation and emission spectrum, or quantum yield (1). Unlike intensity measurements, under non-quenching conditions, lifetime has a high degree of parametric independence, being relatively unaffected by photo-bleaching, excitation intensity, or fluorophore concentration. When a fluorophore is excited by a photon of appropriate energy, a valance electron is promoted from the ground state (S_0) to one of the higher energy singlet states (S_1, S_2, etc.) (2) (Figure 2.1). This process of absorption is rapid, occurring on the order of femtoseconds. After a period of vibrational relaxation, the electron returns to the lowest promoted state, S_1. From this point, the electron returns to the ground state via one of several pathways. When the electron returns to the ground state via radiative decay, which results in fluorescence, a photon of lower energy compared to the exciting photon is produced. This energy difference between the excitation light and the emission light is known as the Stokes Shift (2). The time scale for fluorescence emission, otherwise known as fluorescence lifetime, is on the order of 1 to 100 ns. Alternatively, the electron may return to the ground state via internal conversion, a non-

radiative process that does not produce a photon. Finally, the electron may proceed via intersystem crossing into the triplet state, where the electron can then interact with its environment to form reactive oxygen species or, in deoxygenated environments, emit a photon on a time scale of milliseconds to seconds. This latter phenomenon is known as phosphorescence. The probability of each of these possible reactions depends on the individual fluorophore and its environment, and this defines the fluorescence lifetime.

The fluorescence lifetime, τ, is a kinetic parameter and is inversely proportional to the sum of radiative (k_f) and non-radiative (k_{nr}) decay rates. More simply put, fluorescence lifetime is defined by the time it takes for an excited fluorophore to emit a photon and return to its ground state. Due to the stochastic nature of the photon emission rate, the lifetime of a fluorophore is actually made up of a distribution of photon arrival times, characterized by exponential decay. Fluorescence lifetime, therefore, is typically defined as the time required for the excited population to be reduced by a factor of 1/e (~37%) (Figure 2.2). This exponential decay curve is unique to the fluorophore and is the parameter measured in FLIM. Fluorescence excitation is an unstable energetic state and while lifetime enjoys a great deal of parametric independence, it is quite sensitive to temperature, pH, and the presence of quenchers (3). This environmental sensitivity is a critical aspect of FLIM and provides valuable information about the fluorophore's microenvironment.

Fluorescence Lifetime Acquisition and Analysis

Fluorescence lifetime data is generally acquired in one of two ways, time domain or frequency domain (4,5). While the two techniques produce roughly equivalent information, there are some distinct differences affecting their applications. For example, while time domain acquisition delivers the highest time resolution and accuracy, as well as photon efficiency (especially for dim

samples), frequency domain is significantly faster and more applicable for dynamic measurements (6,7).

Time domain is a digital technique using time-correlated, single-photon counting (TCSPC) electronics, which directly measure the photon flight time (4). Data recording is based on detecting a single photon and determining the photon's arrival time relative to the excitation pulse. Briefly, a TCSPC board is synchronized to a pulsed light source of short pulse width, commonly an 80 MHz multi-photon laser. The TCSPC board then uses voltage ramps in a time-to-amplitude converter (TAC) to quantify the time elapsed between excitation pulse and photon arrival at the detector. The collected data is built into a 3D array with the 2D x,y pixel orientation superimposed on a histogram of photon arrival times for each pixel. These histograms are then used in the calculation of the fluorophore's lifetime.

Frequency domain is related to time domain through a Fourier transform and is an analog technique often conducted in wide field rather than through point scanning. In frequency domain acquisition, the sample is excited by an intensity modulated light source and the emission is collected with a modulated detector (5). The phase of the detector modulation is shifted relative to the excitation modulation and the intensity of the image is acquired over the different detector frequency modulations. The sample will have a decreased modulation degree (or amplitude), as well as a phase shift, relative to the excitation source. The plot of image intensity across the detector modulation range will directly mirror the phase shift and demodulation of the fluorophore. These values—the frequency lag (φ) and the modulation depth (m)—are then used to determine the fluorescence lifetime. Longer lifetimes will give rise to larger phase shifts and smaller modulations (3).

There are also two distinct approaches for analysis: fitting and phasor. Classically, time-domain data has been analyzed using the fitting approach and frequency-domain data with phasor,

but Fourier transforms ensure that these two approaches are not mutually exclusive. Each analysis approach has its own benefits and shortcomings, and the choice of which approach to use depends on the type of information needed from the data.

The fitting approach applies a single or multi-exponential chi-squared best-fit curve directly to the lifetime decay curve (Figure 2.2). The lifetime (τ) is then calculated as the time is takes for the curve to decay to 1/e or ~37% of its initial peak at time = 0 (Equation 1).

$$I = I_0 e^{\frac{-t}{\tau}} \quad [1]$$

Although fitting might seem like a simple and straightforward approach, calculating an accurate exponential fit is a challenging mathematical process. This is further complicated when measuring complex biological samples that are often mixtures of several components, necessitating multi-exponential fits. As such, each pixel—or bin of pixels—must contain enough photons to allow for an accurate fit. The number of photons required can range from 10,000 to over 500,000, depending on the fitting parameters. Best practice is to achieve at least 400,000 photons per pixel bin when calculating a typical bi-exponential fit with 256 time bins (8). Current TCSPC boards tend to have a maximum count rate of 10^6 photons per second, leading to collection times in the minutes to satisfy the demands of fitting analysis. When necessary conditions are satisfied, however, the fitting approach can generate accurate and precise lifetime values (τ_n) and the fractional contribution (α_n) made by each to the mean lifetime (τ_m).

Phasor analysis, although typically used with frequency data, can also analyze time-domain data once it has gone through a Fourier transform. Unlike the fitting approach, phasor math relies on only two numbers per pixel—s and g—which correspond to a single point on the phasor plot and are equivalent to the real and imaginary components of a Fourier transform (Figure 2.3A). For

frequency domain data, (s,g) can be calculated with Equation 2, where φ represents the phase delay and m is the modulation ratio.

$$g(m) = mcos(\varphi) \qquad [2]$$
$$s(\mathrm{m}) = msin(\varphi)$$

Time-domain data is related to the phasor plot by the real (g) and imaginary (s) components of a Fourier transform.

On a phasor plot, also known as the universal circle, phase is the angle of the pointer and the modulation is the amplitude which defines the location of the pixel at (s,g). The phase angle, i.e. the location on the universal circle, is the fluorescence lifetime (τ). As such, single-component lifetimes lie on the edge of the universal circle; complicated, multi-exponential mixtures fall inside the circle; and convoluted signals such as FRET emissions fall outside the circle (9). Short lifetimes lie to the right on the circle with higher corresponding g values, while longer lifetimes reside on the left with smaller g values. One benefit to phasor analysis is that it does not require the assignment of an exponential to each molecular species, thus mitigating the need for a minimum number of photons as required by the fitting approach. Instead, a 3D phasor histogram is generated on the universal circle and changes in shape or location correspond to changes in sample lifetime. Different regions of the phasor histogram can then be labeled and highlighted in the original image generating a spatial map of lifetime distributions (Figure 2.3B). In phasor space, lifetime mixtures can be separated into their corresponding parts through vector analysis. By fitting a line to two-component data and extending this line until it intersects with the edge of the circle, one can identify the parent lifetime. The location on the universal circle where this intersection occurs is representative of the lifetime values that contribute to the mixed population. For mixed populations comprised of three separate

components, the system will be contained within a triangle rather than along a straight line. Accordingly, lifetime mixtures of more than 3 will be located within a polygon.

Work described in this dissertation uses time-domain data acquired via multi-photon TCSPC, which is then analyzed by custom built MATLAB scripts using the phasor approach. Within the script, the peaks of smoothed 3D phasor histograms are identified and (s,g) coordinates of the peak are recorded as (s_{max}, g_{max}). Changes in g_{max} roughly approximate changes in the mean lifetime, τ_m.

Metabolism and Fluorescence Lifetime

A great many fluorophores can be used in FLIM, but two species, NADH and NADPH, are of particular value for quantifying cellular metabolism. NADH and NADPH are metabolic co-enzymes that play a critical role in cellular redox metabolism. The reduced forms of NADH and NADPH are fluorescent and make up the majority of green cellular auto-fluorescence. The fluorescence signatures, both spectral and fluorescence lifetime, of NADH and NADPH are indistinguishable, absorbing around 350 nm with emission centering around 450 nm. A peculiar and useful property of NAD(P)H is that the fluorophore displays two distinct lifetimes: a short lifetime between 0.3 and 0.4 ns when the coenzyme is free and not bound to protein; and a second, long lifetime of 2.3-3 ns when protein-bound, allowing for the separation for free and bound populations (10,11). This is a distinct advantage of fluorescence lifetime measurements over traditional NAD(P)H intensity measurements. However, to complicate matters, each NAD(P)H binding partner corresponds to a different long fluorescence lifetime. These lifetime differences are due to the change in radiationless electron decay rates due to variations in the free rotation between pyridine and amide groups in protein-bound NAD(P)H (12). As expected, NAD(P)H lifetime signatures from biological samples are complex mixtures and fall within the universal circle (13).

Current understanding of changes in NAD(P)H FLIM signature is based almost entirely on work conducted in cancer cells (14). The present model likens changes in NAD(P)H to changes in glycolytic flux relative to changes in oxidative phosphorylation. In keeping with this hypothesis, treating cells with KCN, a Complex IV inhibitor, changes the shape of the phasor histogram, increasing the amount of free NADH in the system due to decreased electron-transport-chain flux (14). Additionally, cancer cells exposed to high glucose, stimulating glycolysis, display a similar shift towards free NADH. This is interpreted as an increase in glycolytic flux. Additionally, treatment of cancer cells with either oxidizing H_2O_2 or dichloroacetate, a pyruvate-dehydrogenase-kinase inhibitor and TCA-cycle enhancer, shifts the NAD(P)H phasor histogram to a more bound state, supporting the idea that more bound NADH is indicative of increased oxidative phosphorylation (15). It is important to point out, however, that treatment with KCN in cancer cells shifts the NAD(P)H phasor histogram along a trajectory in line with the lifetime of NADH bound to lactate dehydrogenase (LDH) (16). β cells are known to have unusually low levels of LDH activity, which raises the question: what is the behavior of NAD(P)H FLIM signatures in islets?

Dominant Factors Affecting FLIM Signatures

In islets, the majority of NAD(P)H fluorescence is localized to the mitochondria (18). Work by Blinova et al. explains that the mitochondrial NAD(P)H signal is dominated by Complex I-associated fluorescence (19). They show that NADH bound to Complex I displays a 10-fold fluorescence multiplication factor over free NADH, as well as a particularly long lifetime of ~5.7 ns. Within the mitochondria, there appear to be three distinct pools of NAD(P)H: a free NAD(P)H pool that comprises 63% of the mitochondrial NAD(P)H and displays the associated short lifetime of 0.4 ns; an intermediate-lifetime pool that accounts for 30% of mitochondrial NAD(P)H and is proposed to emanate from NAD(P)H bound to the many mitochondrial dehydrogenases; and a

Complex I-bound pool, with a lifetime of 5.7 ns, which accounts for only 7% of mitochondrial NADH. Despite the small fractional contribution to total NAD(P)H in the mitochondria, Complex I-bound NADH accounts for 30% of the mitochondrial fluorescence (10).

The dominance of the Complex I component of NAD(P)H FLIM signature appears to be especially true in islets. As islets have low flux through LDH, glycolytic products predominantly flow through the mitochondria (20). As such, shifts in NADH utilization in islets may not be representative of a balance between glycolysis and oxidative phosphorylation, as in cancer cells, but rather of the rate of NADH consumption by the electron transport chain. This is evidenced by the straight-line trajectory of islet phasor histograms on the universal circle for both basal and stimulatory glucose concentrations as well as a suite of ETC inhibitors, suggesting one dominant contributor to islet NAD(P)H lifetime (Figure 2.4).

Preliminary Results in Islets

In islets, the NAD(P)H FLIM signature is strongly impacted by the stressors of age and obesity (Figure 2.5). Islets challenged by obesity have significantly elevated and equivalent basal and stimulatory $1\text{-}g_{max}$ values, indicating enhanced ETC flux, especially under non-stimulatory conditions. Aged human islets, on the other hand, display decreased NAD(P)H utilization and an altered relationship between basal and stimulatory glucose. These data suggest that islet NAD(P)H utilization is affected differently by the stressors of age and obesity. This observation motivates a closer examination of islet mitochondrial metabolism as a potential mechanism for the changes associated with islet stress.

Figure 2.1

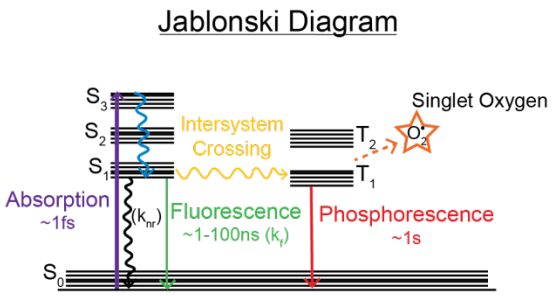

Figure 2.1. Jablonski Diagram representing energy levels (S) of a fluorescent molecule. Solid lines indicate the radiative transitions of absorption, fluorescence emission (k_f), and phosphorescence. Wiggly lines indicate the non-radiative transitions (k_{nr}) of intersystem crossing and internal conversion. Dashed lines indicate external interaction, photo bleaching, and the creation of singlet oxygen.

Figure 2.2

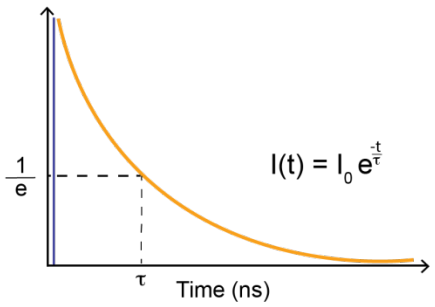

Figure 2.2. Fluorescence-lifetime decay curve of a fluorescent molecule. Decay curve (orange) representing the fluorescence-lifetime distribution histogram of a fluorophore after excitation (blue) at time 0. The fluorescence lifetime (τ) is equal to the time elapsed from t = 0, when the intensity of the fluorophore population has decreased by 1/e, as indicated by I(t) where I_0 is the intensity at time = 0, t is the time after the absorption, and τ is the fluorescence lifetime.

Figure 2.3

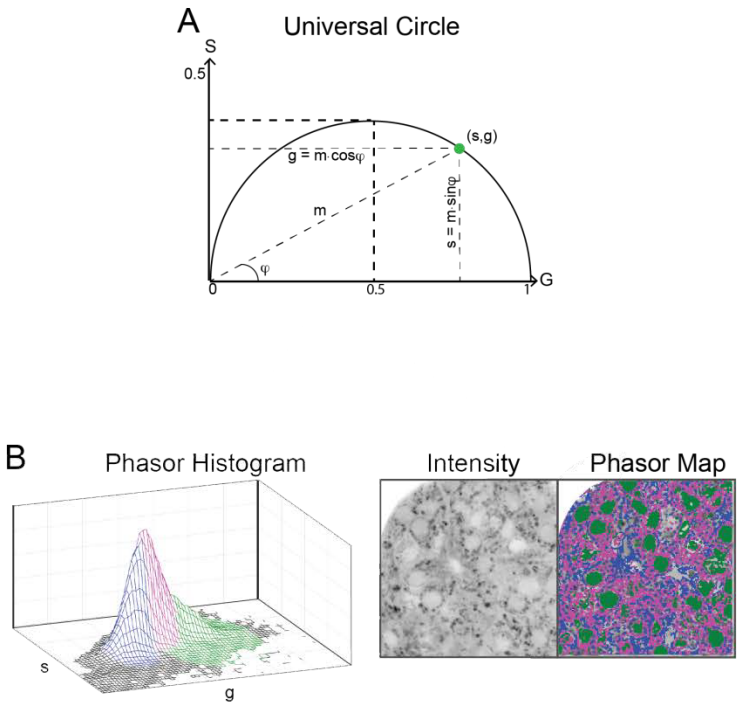

Figure 2.3. Phasor analysis of FLIM data. (**A**) Schematic of phasor properties on the universal circle, showing fluorescence lifetime (τ) at polar coordinates (s,g) as calculated by phase shift (φ) and demodulation (m). (**B**) Representative 3D phasor histogram of a B6 *ob/ob* islet at 10mM glucose. Regions of the phasor histogram are highlighted and mapped back onto the intensity image in corresponding colors.

Figure 2.4

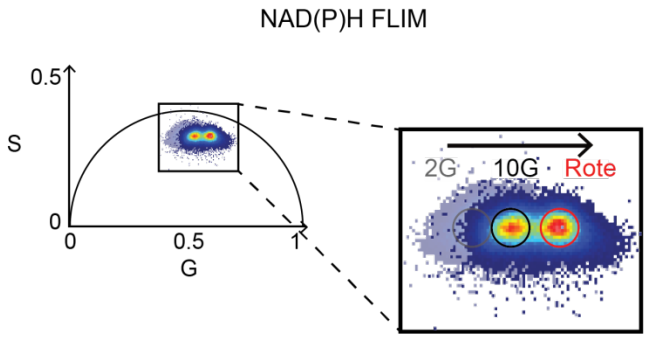

Figure 2.4. Linear trajectory of NAD(P)H fluorescence lifetime in phasor space. Fluorescence-lifetime phasor histogram of B6 lean islets (n = 10) at 2mM, 10mM, and 10mM glucose + 5μM Rotenone. Straight-line horizontal movement of histogram peak (red) indicates the presence of a single dominant lifetime contributing to the location of the phasor distribution.

Figure 2.5

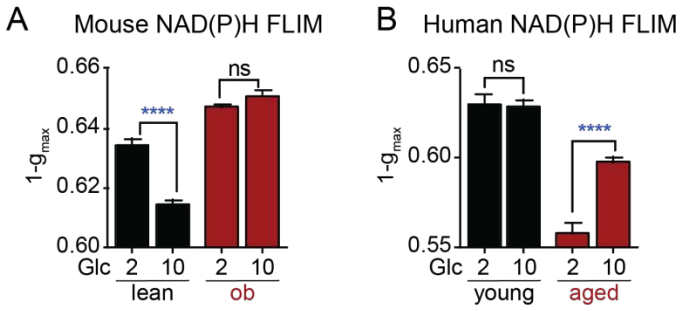

Figure 2.5. Differential effect of basal and stimulatory glucose affected by age and obesity. NAD(P)H fluorescence lifetime at 2 and 10 mM glucose (Glc) in lean and *ob/ob* mice (n = 2 mice with 10 islets each) and young and aged human islets (n = 4 humans with 20 islets each). Data are mean ± SEM and were compared using one-way ANOVA with Sidak's post-test. **** $P < 0.0001$. Human donor information in Table 3.1.

REFERENCES

1. Chen Y, Periasamy A. Characterization of two-photon excitation fluorescence lifetime imaging microscopy for protein localization. Microsc Res Tech. 2004 Jan 1;63(1):72–80.

2. Lakowicz JR, editor. Fluorophores. In: Principles of Fluorescence Spectroscopy [Internet]. Springer US; 2006 [cited 2017 Jun 3]. p. 63–95. Available from: http://link.springer.com/chapter/10.1007/978-0-387-46312-4_3

3. Berezin MY, Achilefu S. Fluorescence Lifetime Measurements and Biological Imaging. Chem Rev. 2010 May 12;110(5):2641–84.

4. Lakowicz JR, editor. Time-Domain Lifetime Measurements. In: Principles of Fluorescence Spectroscopy [Internet]. Springer US; 2006 [cited 2017 Jun 3]. p. 97–155. Available from: http://link.springer.com/chapter/10.1007/978-0-387-46312-4_4

5. Lakowicz JR, editor. Frequency-Domain Lifetime Measurements. In: Principles of Fluorescence Spectroscopy [Internet]. Springer US; 2006 [cited 2017 Jun 3]. p. 157–204. Available from: http://link.springer.com/chapter/10.1007/978-0-387-46312-4_5

6. Ballew RM, Demas JN. An error analysis of the rapid lifetime determination method for the evaluation of single exponential decays. Anal Chem. 1989 Jan 1;61(1):30–3.

7. Gratton E, Breusegem S, Sutin J, Ruan Q, Barry N. Fluorescence lifetime imaging for the two-photon microscope: time-domain and frequency-domain methods. J Biomed Opt. 2003;8(3):381–90.

8. Köllner M, Wolfrum J. How many photons are necessary for fluorescence-lifetime measurements? Chem Phys Lett. 1992 Nov 27;200(1):199–204.

9. Digman MA, Caiolfa VR, Zamai M, Gratton E. The Phasor Approach to Fluorescence Lifetime Imaging Analysis. Biophys J. 2008 Jan 15;94(2):L14–6.

10. Blinova K, Carroll S, Bose S, Smirnov AV, Harvey JJ, Knutson JR, et al. Distribution of Mitochondrial NADH Fluorescence Lifetimes: Steady-State Kinetics of Matrix NADH Interactions. Biochemistry (Mosc). 2005 Feb 1;44(7):2585–94.

11. Lakowicz JR, Szmacinski H, Nowaczyk K, Johnson ML. Fluorescence lifetime imaging of free and protein-bound NADH. Proc Natl Acad Sci. 1992 Feb 15;89(4):1271–5.

12. Gafni A, Steinberg IZ. Optical Activity and Lifetime Measurements of Tris-(2,2'-Bipyridine) Ruthenium (II) Bromide: Evidence for some Singlet-Singlet Emission. Isr J Chem. 1976 Jan 1;15(1–2):102–5.

13. Stringari C, Cinquin A, Cinquin O, Digman MA, Donovan PJ, Gratton E. Phasor approach to fluorescence lifetime microscopy distinguishes different metabolic states of germ cells in a live tissue. Proc Natl Acad Sci. 2011 Aug 16;108(33):13582–7.

14. Stringari C, Nourse JL, Flanagan LA, Gratton E. Phasor Fluorescence Lifetime Microscopy of Free and Protein-Bound NADH Reveals Neural Stem Cell Differentiation Potential. PLOS ONE. 2012 Nov 5;7(11):e48014.

15. Niewisch MR, Kuçi Z, Wolburg H, Sautter M, Krampen L, Deubzer B, et al. Influence of dichloroacetate (DCA) on lactate production and oxygen consumption in neuroblastoma cells: is DCA a suitable drug for neuroblastoma therapy? Cell Physiol Biochem Int J Exp Cell Physiol Biochem Pharmacol. 2012;29(3–4):373–80.

16. Datta R, Heylman C, George SC, Gratton E. Label-free imaging of metabolism and oxidative stress in human induced pluripotent stem cell-derived cardiomyocytes. Biomed Opt Express. 2016 Apr 5;7(5):1690–701.

17. Sekine N, Cirulli V, Regazzi R, Brown LJ, Gine E, Tamarit-Rodriguez J, et al. Low lactate dehydrogenase and high mitochondrial glycerol phosphate dehydrogenase in pancreatic beta-cells. Potential role in nutrient sensing. J Biol Chem. 1994 Feb 18;269(7):4895–902.

18. Patterson GH, Knobel SM, Arkhammar P, Thastrup O, Piston DW. Separation of the glucose-stimulated cytoplasmic and mitochondrial NAD(P)H responses in pancreatic islet β cells. Proc Natl Acad Sci U S A. 2000 May 9;97(10):5203–7.

19. Blinova K, Levine RL, Boja ES, Griffiths GL, Shi Z-D, Ruddy B, et al. Mitochondrial NADH Fluorescence Is Enhanced by Complex I Binding. Biochemistry (Mosc). 2008 Sep 9;47(36):9636–45.

20. Malmgren S, Nicholls DG, Taneera J, Bacos K, Koeck T, Tamaddon A, et al. Tight Coupling between Glucose and Mitochondrial Metabolism in Clonal β-Cells Is Required for Robust Insulin Secretion. J Biol Chem. 2009 Nov 20;284(47):32395–404.

Chapter 3

Pancreatic β Cells from Mice Offset Age-Associated Mitochondrial Deficiency with Reduced K_{ATP} Channel Activity

This chapter was published as:

Gregg T, Poudel C, Schmidt BA, Dhillon RS, Sdao SM, Truchan NA, et al. Pancreatic β-Cells From Mice Offset Age-Associated Mitochondrial Deficiency With Reduced KATP Channel Activity. Diabetes. 2016 Sep 1;65(9):2700–10.

ABSTRACT

Aging is accompanied by impaired glucose homeostasis and an increased risk of type 2 diabetes, culminating in the failure of insulin secretion from pancreatic β cells. To investigate the effects of age on β cell metabolism, we established a novel assay to directly image islet metabolism using NAD(P)H fluorescence lifetime imaging (FLIM). We determined that impaired mitochondrial activity underlies an age-dependent loss of insulin secretion in human islets. NAD(P)H FLIM revealed a comparable decline in mitochondrial function in the pancreatic islets of aged mice (≥ 24 months), resulting from 52% and 57% defects in flux through complex I and II of the electron transport chain. However, insulin secretion and glucose tolerance are preserved in aged mouse islets by the heightened metabolic sensitivity of the β cell triggering pathway, an adaptation clearly encoded in the metabolic and Ca^{2+} oscillations that trigger insulin release (Ca^{2+} plateau fraction: young, 0.380 ± 0.007; aged, 0.211 ± 0.006, $P < 0.0001$). This enhanced sensitivity is driven by a reduction in K_{ATP} channel conductance (diazoxide: young, 5.1 ± 0.2 nS; aged, 3.5 ± 0.5 nS, $P < 0.01$), resulting in a ~2.8 mM left shift in the β cell glucose threshold. Our results demonstrate how mice, but not humans, are able to successfully compensate for age-associated metabolic dysfunction by adjusting their β cell glucose sensitivity, and highlight an essential mechanism for ensuring the maintenance of insulin secretion.

INTRODUCTION

The incidence of type 2 diabetes is disproportionally high in the elderly, over 25%, by comparison to 4.1% in younger adults and 16.2% in the middle-aged (1). Although insulin resistance and β cell mass have been heavily studied as contributors to impaired glucose tolerance and diabetes

in the elderly (2–4), it remains uncertain whether β cell function contributes to this effect. Confounding our understanding is the misalignment of studies on humans and laboratory mice. A number of recent reports indicate that aging mice are resistant to a decline in glucose tolerance and β cell function (5–8), factors which reportedly decline in humans (2–4,9,10). One potential explanation is that differences in mitochondrial function, which are proposed to underlie the age-related decline of numerous tissues (11), exist between mouse and human β cells. If β cells are susceptible to age-related mitochondrial defects, one expects glucose-stimulated insulin secretion to significantly decline, considering that β cells use metabolism as a signaling pathway not only to trigger oscillations of insulin secretion, but also to augment the magnitude of the secretory response through metabolic amplifying pathways (12). Indeed, age-associated factors intrinsic to the β cell, including defects in NAD^+ synthesis (13), reduced mitochondrial copy number (14), and epigenomic changes affecting the expression of metabolic genes (7) have been reported, but the extent to which they affect metabolic function in mouse and human β cells remains unclear.

In this work, we explored the species differences between aging mouse and human β cells *ex vivo*, allowing us to define the effect of age on the intrinsic ability of the β cell to respond to glucose independently from other age-related physiological changes. We also used this opportunity to develop NAD(P)H fluorescence lifetime imaging (FLIM) as a novel approach to image islet metabolism. This method is more easily interpreted than intensity-based NAD(P)H imaging (15–18), which cannot distinguish increases in NADH production, for example, from the binding of NADH to proteins (which can multiply the fluorescence (19)). Using NAD(P)H FLIM, we report here that aged human and mouse β cells exhibit similar defects in mitochondrial glucose sensing. Yet, mouse β cells are uniquely resistant to age-associated defects in insulin secretion, which is maintained in aged mice by the heightened metabolic sensitivity of the β cell plasma membrane – an effect driven by the reduction of K_{ATP} channel activity.

RESEARCH DESIGN AND METHODS

Human Islets

An exemption was granted for all protocols by the Institutional Review Board at the University of Wisconsin-Madison under Protocol Number 2015-0356. Human islets were obtained from the Integrated Islet Distribution Program (IIDP), including the Center at University of Wisconsin. The IIDP published isolation protocols and insulin secretion quality control assays can be found at https://iidp.coh.org/investigator_sops.aspx. Following shipment, the islets were cultured overnight in RPMI1640/10% FBS and used within 24 hours for insulin secretion measurements.

Mice

All animal studies were approved by the Institutional Animal Care and Use Committees of the University of Wisconsin-Madison and the William S. Middleton Memorial Veterans Hospital. Aged (18, 24, and 30 month) and young (4-6 month) C57BL/6J male mice used for the insulin secretion and mitochondrial assays were from the NIA Aging Rodent Colony. Additional 4-6 month old C57BL/6J male mice used for the calcium and electrophysiology experiments were purchased from The Jackson Laboratory. The median life expectancy of C57BL/6J male mice from these sources is approximately 28 months ((20) and phenome.jax.org).

In Vivo Studies

Glucose tolerance tests were performed by fasting the mice overnight for 16 hours and then injecting 1 g/kg glucose intraperitoneally; glucose measurements were then performed at the indicated times using a Bayer Contour blood glucose meter and test strips. *In vivo* glucose-stimulated insulin secretion and fasting insulin levels were determined by fasting the mice overnight for 16 hours, measuring blood glucose and collecting tail blood (using Sarstedt heparinized tubes)

immediately prior to and 15 minutes after injecting 1 g/kg glucose. Insulin levels in heparinized plasma were determined using Mouse Insulin ELISA kits (Crystal Chem).

Islet Isolation and Adenoviral Infection

The mouse pancreas was inflated through the common bile duct with 3-5 mL of 0.5 mg/mL collagenase (Sigma C5138) and 0.2 mg/mL BSA (Sigma A8806) in HBSS (Invitrogen), excised, and incubated in a glass vial at 37°C in 5 mL HBSS/BSA/collagenase solution for 5 minutes on an orbital shaking water bath (Thermo SHKA7000) at 250 rpm. Beginning 6-minutes post-incubation, the digest was agitated for 20 seconds at 375 rpm every 2 minutes until minute 28, and washed three times with 30 mL ice-cold HBSS/BSA solution, and pelleted at 50*g* for 2 min. The pellets were resuspended by vortex at medium speed in 1-2 mL solution, and hand-picked in 60 mL ice-cold HBSS/BSA solution. After isolation the islets were maintained in RPMI1640 supplemented with 10% (v/v) fetal bovine serum, 100 units/ml penicillin and 100 μg/ml streptomycin (Invitrogen). Adenoviruses were used to express Perceval-HR ATP/ADP sensors (Addgene 49082) in islet β cells under control of the rat insulin promoter as in Merrins et al. (21). Groups of 25 freshly-isolated islets were immediately infected with 2000 MOI of each adenoviral construct for 2 h in a 95/5% air/CO_2 incubator at 37˚C, followed by removal to fresh culture media lacking virus. Islets were imaged after 1-3 days in culture. We confirmed that the presence of the Perceval-HR sensors, which were expressed in only a small fraction of β cells, had no effect on downstream Ca^{2+} oscillations.

Respirometry

Following overnight incubation, 150 islets/condition/mouse (6 mice/condition) were transferred to a 35 mm petri dish containing 2 ml of MiR05 (in mM: 0.5 EGTA, 3 $MgCl_2$, 60 lactobionic acid, 20 taurine, 10 KH_2PO_4, 20 HEPES, 110 sucrose, 1% BSA; pH 7.1, adjusted with 5 M KOH) (22) and 5 mg/ml saponin; preliminary experiments showed that permeabilized islets demonstrated higher coupled respiration rates. Islets were gently rocked in the permeabilization medium for 20 min. After

20 min, the islets were rinsed with fresh MiR05 in the absence of saponin, and then pipetted into an Oxygraph-2k chamber (Oroboros) containing 2 ml of MiR05 at 37ºC. Oxygen electrodes were calibrated to air-saturated MiR05 buffer at 37°C using published oxygen solubilities (23) corrected for local atmospheric pressure. Oxygen concentration and oxygen flux were recorded using DatLab software (Oroboros). A modified substrate-uncoupler-inhibitor titration (SUIT) protocol based on Votion et al. (24) was applied. Respiratory flux through complex I was measured by adding 5 mM glutamate and 1 mM malate, followed by 1.25 mM ADP to induce oxidative phosphorylation. To assess the integrity of the outer mitochondrial membrane, cytochrome c was added to the chamber (8 μM) (25), and no significant increases in respiration were observed. Damage to the outer mitochondrial membrane during permeabilization would result in a loss of cytochrome c, and a large increase in respiration upon the addition of exogenous cytochrome c to the respiration chamber. Convergent electron flow through complexes I and II was measured with the addition of 10 mM succinate, allowing the electron transport system to achieve maximal coupled respiration. Next, a step-wise addition of carbonyl cyanide p-trifluoro-methoxyphenyl hydrazone (FCCP) was used to completely uncouple mitochondria (0.250 μM initial + 0.250 μM additions). To assess oxygen flux through complex II, 0.5 μM rotenone was added to inhibit complex I. Finally, electron transfer was blocked at complex III with the addition of 5 μM antimycin A and allowed to run long enough to obtain a residual oxygen consumption. Oxygen flux was expressed per mg of total protein (Pierce 660 nm protein assay, ThermoFisher).

Fluorescence Lifetime Imaging (FLIM) of NAD(P)H

Islets were imaged in glass-bottom dishes on a custom built multiphoton laser scanning system based around a Nikon TE-300 inverted microscope equipped with a Plan Apo 60X/1.4NA Oil immersion objective (Nikon Instruments) in a standard external solution containing, in mM: 135 NaCl, 4.8 KCl, 5 $CaCl_2$, 1.2 $MgCl_2$, 20 HEPES, 10 glucose; pH 7.35. Temperature was maintained at

35°C using a LiveCell incubator (Pathology Devices). NAD(P)H was excited with Mai Tai DeepSee Ti:Sapphire laser (Spectra-Physics) at 740 nm with a 450/70m bandpass emission filter (Chroma) before being collected by a Hamamatsu H7422P-40 GaAsP photomultiplier tube. FLIM images were collected at 256x256 resolution with 120 s (1/s) collection using SPC-830 Photon Counting Electronics (Becker & Hickl GbmH). In each experiment, urea crystals were used to define the instrument response function with a 370/10 bandpass emission filter (Chroma), and coumarin was used as a reference for lifetime (2.5 ns) using a 450/70m bandpass emission filter (Chroma). For analysis, raw SDT files were imported into MATLAB (MathWorks), and a custom script was used to generate a phasor histogram for each treatment using the equations in (26). To avoid contamination from lipofuscin fluorescence in the aged cells (27), which forms a short-lifetime tail in the phasor plot, all data were reported as the phasor histogram peak ($1\text{-}g_{max}, s_{max}$).

Timelapse Imaging of NAD(P)H, ATP/ADP, and Ca^{2+}

For measurements of cytosolic Ca^{2+}, islets were preincubated in 2.5 μM FuraRed (Molecular Probes, Eugene, OR) for 45 min at 37°C. Islets were then placed in an RC-24N glass-bottomed chamber (54 μL volume) (Warner Instruments) on a Nikon Ti-Eclipse inverted microscope equipped with 10X/0.5NA and 20X/0.75NA SuperFluor objectives (Nikon Instruments). The chamber was perfused with standard external solution (above). The flow rate was 0.3 ml/min and temperature was maintained at 33°C using inline solution and chamber heaters (Warner Instruments). Excitation was provided by a SOLA SEII 365 (Lumencor) set to 10% output. Excitation (x) or emission (m) filters (ET type, Chroma Technology Corporation) were used in combination with an FF444/521/608-Di01 dichroic (Semrock) as follows: FuraRed, 430/20x and 500/20x, 630/70m (R430/500); NAD(P)H, 365/20x, 470/24m; Perceval-HR, 430/20x and 500/20x, 535/35m (R500/430). Fluorescence emission was collected with a Hamamatsu ORCA-Flash4.0 V2 Digital

CMOS camera at 0.125-0.2 Hz. A single region of interest was used to quantify the average response of each islet using Nikon Elements and MathWorks MATLAB software.

Electrophysiology

β cell membrane potential and K_{ATP} conductance were measured as in (28). Briefly, a Sutter MP-225 micromanipulator was used together with a HEKA EPC10 patch-clamp amplifier in the perforated patch-clamp configuration to record membrane potential from intact islets perfused with standard external solution (above). Pipette tips were filled with an internal solution (in mM: 28.4 K_2SO_4, 63.7 KCl, 11.8 NaCl, 1 $MgCl_2$, 20.8 HEPES, 0.5 EGTA; 40 sucrose; pH 7.2) containing 0.36 mg/ml amphotericin B. Islet β cells were identified by the presence of slow oscillations in 10 mM glucose. The amplifier was then switched into voltage clamp mode. Conductance changes were determined from the current-voltage relation (I-V) using 2 s voltage ramps from -120 to -50 mV every 20 seconds during the silent phase of bursting and following application of 200 μm diazoxide. Assuming that diazoxide acts by maximizing steady-state K_{ATP} open probability, changes in conductance primarily reflect changes in the number of open K_{ATP} channels.

***Ex Vivo* Insulin Release**

The glucose-stimulated insulin secretion assay was performed on human and mouse islets using a high-throughput multiple-well plate technique (29) in which islets were individually incubated in a tissue culture-treated 96-well V-bottom plate, allowed to adhere for 24 h, and incubated with Krebs-Ringer bicarbonate buffer at 1.7 mM glucose (preincubation) followed by a stimulatory 16.7 mM glucose incubation for 45 min each. Secretory medium was then collected, and the islets were lysed utilizing a cell lysis buffer (Cell Signaling Technology 9803). Insulin secretion as a percentage of total islet insulin content was measured by ELISA.

Statistics

Data are expressed as means ± SE. Statistical significance was determined using one- or two-way ANOVA with Sidak multiple-comparisons test post hoc or Student's t-test as appropriate. Differences were considered to be statistically significant at $P < 0.05$. Statistical calculations were performed with GraphPad Prism.

RESULTS

Human aging is associated with defects in GSIS and islet metabolism

Insulin secretion measured in islets isolated from 31 human donors ranging from 19-64 years of age (Table S1) revealed a significant decline in β cell function with age that was prominent at high glucose levels ($R^2 = 0.51$, $P < 0.0001$) (Figure 3.1A). The stimulation index, defined as the fold-change in glucose-stimulated insulin secretion (GSIS), points the same age-related deficiency ($R^2 = 0.26$, $P = 0.0046$) (Figure 3.1B). There was no change in insulin content with age (Figure 3.1C), or a trend in BMI across the donor population (Figure 3.1D). Neither the insulin secretion in high glucose nor the stimulation index were correlated with BMI (Figures 3.1E and 3.1F).

To ascertain the relationship between insulin secretion and glucose metabolism in these islets, we used multiphoton fluorescence lifetime imaging (FLIM) of NADH and NADPH to directly image human islet metabolism. Rather than reporting NAD(P)H fluorescence intensity (Figure 3.2A, *left*) (16), FLIM measures the duration that NAD(P)H remains in the excited state – its fluorescence lifetime – which increases ~6-fold when the coenzymes are bound to protein (19,30). The discrete lifetimes imparted on NADH and NADPH by each of their binding proteins were plotted as phasor histograms (26) so that each distinct mixture of lifetimes occupies a unique position on the plot (Figure 3.2A, *right*). Note that the images of aged islets, especially, contain

lipofuscin puncta (arrows), a cellular waste product identifiable by its broad spectrum excitation (31) that accumulates with age independently of obesity or diabetes phenotypes (27); based on its very short lifetime, lipofuscin was excluded from our analysis of the phasor histogram peak. Relative to islets from an older donor (58 years old, ACKH054A), the application of 17 mM glucose to islets from a young donor (24 years old, ACJ3270) shifted the phasor peak significantly further along the abscissa, reflecting an increase in bound NAD(P)H, which has a long lifetime (32). The difference in islet metabolism between aged and young islets was even more pronounced at 2 mM glucose (Figures 3.2B, 3.2C). A shift in the histogram peaks toward free NADH was induced by rotenone, which blocks NADH utilization at complex I and served as a positive control to calibrate the FLIM; changes in the islet phasor histogram peak along the *1-gmax* axis reflect the metabolic consequences of activating/inactivating the electron transport chain, consistent with NAD(P)H FLIM studies that used alternative electron transport chain inhibitors (e.g. KCN (32,33)). Importantly, donor age was correlated with the progressive loss of glucose-dependent NADH utilization ($R^2 = 0.63$, $P = 0.006$, Figure 3.2D), indicating that a reduction in mitochondrial metabolism contributes to the loss of insulin secretion with age.

Despite mitochondrial decline, insulin secretion and glucose tolerance are preserved in aged mice

Given the strong relationship between β cell secretory dysfunction and human aging, we investigated organismal glucose homeostasis in young (4-6 months), middle-aged (18 months), and aged (≥ 24 months) C57BL/6J mice from the NIA (National Institute on Aging) Aged Rodent Colony. Glucose tolerance, measured in fasted animals, was equivalent between the young and aged mice (Figures 3.3A and 3.3B) as reported previously (5,8). However, middle-aged and aged animals trended toward increased fasting insulin levels, and aged animals exhibited an augmented insulin

secretory response following intraperitoneal glucose injection (Figures 3.3C and 3.3D). To determine whether this effect can be explained by a β cell autonomous mechanism, pancreatic islets isolated from young and aged mice were subjected to an *ex vivo* GSIS assay. Islets from the aged mice secreted significantly more insulin than young islets at both basal and stimulatory glucose concentrations (Figure 3.3E); no difference in insulin content was observed (not shown). These data, which are in alignment with recent reports (7,34), imply that β cell compensation is necessary to maintain euglycemia in the aged mice, which could reflect increased β cell mass – islet area was 43% larger in the aged mice relative to controls (Figure 3.3F) – but also functional compensation.

As a means to compare metabolic function in young and old mice with the human islet phenotype, multiphoton NAD(P)H FLIM was again used to directly image mitochondrial metabolism (Figure 3.4). While glucose induced an increase in free NAD(P)H in both groups, quantification of the phasor histogram peaks shows that the NAD(P)H response is depressed in the aged islets in response to glucose (Figures 3.4A and 3.4B). NADH consumption by the mitochondrial respiratory chain was assessed by acute application of rotenone (5 μM, Complex I inhibitor) and oligomycin (5 μM, Complex V inhibitor). In all four treatments, a decline in mitochondrial function – reflected by the decline in bound NAD(P)H – was evident in aged islets relative to young controls (Figure 3.4C). The relative difference in the cellular response to oligomycin and rotenone, which reveals the proton leak (35), was not altered.

As a second approach, we measured mitochondrial oxygen consumption in permeabilized islets stimulated with glutamate, malate, succinate, and ADP. In excellent agreement with the NAD(P)H FLIM, mitochondrial respiration was strongly decreased in the aged islets (Figure 3.4D). Flux through Complex I and II were similarly reduced (by 52% and 57%, respectively), indicating that defects in aged cells manifest within the electron transport chain. As age-associated

mitochondrial dysfunction afflicts both human and mouse islets, these findings prompted us to seek an explanation for the augmented insulin secretion we observed in aged mice.

Hyper-sensitivity of the β cell plasma membrane, driven by a reduction in K_{ATP} conductance, compensates for mitochondrial dysfunction in aged mice

Downstream of the mitochondria, ATP/ADP, K_{ATP} channels, and Ca^{2+} control the triggering pathway of insulin secretion. Oscillations in these parameters between active and silent phases occur within an intermediate range of glucose levels (Figure 3.5A). Within this range, an analysis of the oscillatory plateau fraction – the fraction of the time the islet spends in the active state (21,36,37) – can provide direct information on the β cell glucose threshold, without the need for a full glucose dose-response curve. This is because of the direct relationship between β cell glucose metabolism and plateau fraction, which can be calculated from ATP/ADP or Ca^{2+} oscillations (Figure 3.5B). Note that increased ATP/ADP plateau fraction ≠ increased ATP level; the plateau fraction of ATP/ADP follows activity of membrane potential oscillations strictly (21), while the plateau fraction of Ca^{2+} oscillations (in the same islet) is slightly longer due to extended Ca^{2+} release from the ER during the silent phase (38).

When measured simultaneously, Ca^{2+} and ATP/ADP oscillations in mouse islets (Figure 3.5C) are out of phase due to ATP consumption by Ca^{2+}-ATPases located in the ER and plasma membrane (39,40). By comparison with young islets, aged islets displayed an increased oscillatory plateau fraction, reflecting increased sensitivity to glucose (Figure 3.5D); based on Figure 5B, we estimate this effect corresponds to a ~2.8 mM left shift in the plasma membrane glucose threshold. While enhanced insulin secretion is consistent with enhanced Ca^{2+} activity in aged β cells (Figure 3.3), this observation remains surprising because of the respiratory chain failure we observed in the aged mouse islets (Figure 3.4), which would be expected to restrict K_{ATP} channel inhibition and Ca^{2+}

channel activation. These findings suggest that the β cell plasma membrane in aged cells is hyper-sensitive to glucose metabolism.

As K_{ATP} channels serve as the primary metabolic sensor for the β cell plasma membrane (41,42), we hypothesized that the loss of K_{ATP} channel conductance (G_{KATP}) could account for the enhanced Ca^{2+} oscillations we observed in aged islets. G_{KATP} was calculated from voltage ramps (28) during islet bursting and in the presence of the K_{ATP} channel opener diazoxide (200 μM) (Figure 3.5E). The more K_{ATP} channels present in the plasma membrane, the larger the change in G_{KATP} seen in response to diazoxide; by this measure, G_{KATP} was reduced by 31% in aged relative to young β cells (Figure 3.5F, *left*). There was no difference in cell size between groups (not shown). We also confirmed that these results were not due to differences in leak resistance between individual islets by subtracting the conductances measured during the silent phase of bursting from the same β cell during diazoxide application, which yielded the same fundamental conclusion (Figure 3.5F, *right*). The age-dependent loss of K_{ATP} channels would be expected to reduce the ATP/ADP ratio required to initiate membrane depolarization, and account for the enhanced plateau fraction of calcium oscillations and elevated insulin release we observed in aged islets.

DISCUSSION

The focus of this work was to compare the effects of age on β cell metabolism and insulin secretion in mouse and human islets. To do so we developed a novel assay for metabolic fingerprinting of the pancreatic islet, NAD(P)H FLIM. We demonstrated that both human and mouse islets exhibited an age-associated decline in mitochondrial NADH utilization due to defects in the electron transport chain. Significantly, we found that islets from aged mice compensated for this defect with restricted β cell K_{ATP} channel conductance, which in turn increased the glucose

sensitivity of plasma membrane Ca^{2+} triggering and insulin secretion. While our results help to explain the resistance of mice to age-induced defects in insulin secretion, human islets apparently lack this compensation.

Human aging is accompanied by declining glucose tolerance (2–4), and we detected a corresponding defect in insulin secretion in pancreatic islets isolated from aged human subjects. Surprisingly, our measurements revealed an age-dependent defect in *stimulated* insulin secretion (R^2 = 0.51, P < 0.0001), with a much weaker effect on the stimulation index (R^2 = 0.26, P = 0.0046). A decline in the stimulation index based instead on an age-dependent increase in *basal* insulin secretion has also been reported (9,10), while another study found no age-related defects (5). While we find no fault with these studies, or a satisfactory explanation for the discrepancy between them, our results are qualitatively similar to unpublished study by Benninger and colleagues (Personal communication) showing a significant age-dependent decline in both stimulated and basal insulin secretion (n = 21 preparations); in our study basal secretion trended lower with age but was not significant (P = 0.08, n = 31 preparations).

Recent studies of glucose homeostasis in aged mice are more consistent. The widely studied C57BL/6 inbred mouse strain exhibits normal glucose tolerance with age (Figure 3.3 and (5,43,44); but see (6)), and in addition to the present study, three recent reports utilizing mice from the NIA Aging Rodent Colony found that insulin secretion increases with age (Figure 3.3 and (5,7,8)). What, then, explains the discrepant phenotype of human and mouse islets? We considered the possibility that mitochondrial health, which declines with age in human β cells (14), might be unaffected in mouse islets. However, using NAD(P)H FLIM, we showed that mitochondrial NADH utilization declines with age in both species (Figures 3.2 and 3.4). Using respirometry we directly identified defects in complexes I and II of the electron transport chain, which likely underlies the impairment in glucose-dependent hyperpolarization of the mitochondrial membrane potential in aged C57BL/6J

mouse islets (6). However, by quantifying the dynamics of glucose-dependent β cell oscillations in metabolism and Ca^{2+}, we discovered that these age-associated defects in metabolism are compensated by hypersensitivity of the mouse β cell plasma membrane. The mechanism of this effect was due specifically to a reduction in K_{ATP} channel conductance, which was accompanied by increased insulin secretion.

The appeal of an age-dependent shift in the β cell glucose threshold is that insulin secretion can increase despite defects in mitochondrial respiration. Two lines of evidence might explain how regulation of K_{ATP} occurs. The first is based on experiments demonstrating that exposure of islets to hyperglycemic conditions can reduce β cell K_{ATP} conductance by adjusting K_{ATP} channel trafficking to the plasma membrane (45,46). Interestingly, this trafficking mechanism requires autocrine feedback of insulin (46), which is reminiscent of a second potential mechanism involving insulin-dependent transcriptional regulation of K_{ATP}. In this case, insulin receptor signaling activates cyclin-dependent kinase 4 (Cdk4), which phosphorylates Rb to activate the E2F transcription factors required for Kir6.2 (KCNJ11) promoter activity (47). By activating Kir6.2, which comprises the pore forming subunits of K_{ATP}, the insulin receptor signaling pathway acts to limit β cell excitability. Importantly, several groups have demonstrated that β cells exhibit increased expression of cell cycle inhibitors with age (reviewed in (3)), most prominently the Cdk4 inhibitor p16/Ink4a (34,48), which would be expected to restrict E2F activation and Kir6.2 transcription. In this second model, the reduced K_{ATP} channel activity we observed in mouse islets is an inevitable but welcome adaptation to β cell senescence. Ultimately however, distinguishing between these two alternative models will require additional experimentation in genetically modified aged mice, for example mice lacking Cdk4.

In addition to advancing our understanding of β cell aging, we have made a significant technical leap by utilizing FLIM of NADH and NADPH to quantify the metabolic health of islet

cells. Although we do not currently possess a way to distinguish between the endocrine cell types, NAD(P)H FLIM addressed a number of issues inherent to the intensity-based NAD(P)H measurements used in our prior studies (49,50). First, the autofluorescence signal in aged islets is dominated by lipofuscin, which accumulates with age (27). We were able to exclude lipofuscin from our analysis by its short lifetime using the phasor approach to FLIM (26,32); as lipofuscin is accumulated by many cell types in aging rodents and humans, we expect this approach to be broadly applicable to the study of metabolism in other tissues. Second, we noted that NAD(P)H fluorescence intensity, when determined using epifluorescence, is strongly dependent on islet size. Size-matching would have skewed our comparison of young and old islets, which were 42% larger, and would be impossible when studying islets isolated from some genetic models of obesity such *ob/ob* mice. Islet size is normalized when using multiphoton microscopy, which ensures a uniform volume is measured from each islet.

As the population grays, it seems likely that the already high prevalence of diabetes among the aged will continue to rise. In the present work, we determined that a reduction in the β cell glucose threshold allows mice, but apparently not humans of the studied age group, to circumvent age-associated mitochondrial decline and maintain insulin secretion. This left shift in the glucose threshold for Ca^{2+} activation may also be found in studies of genetic (*db/db*), pharmacologic (streptozotocin), and diet-induced diabetes models (51,52), hinting that threshold shifting is an important mechanism of β cell compensation for all ages.

Figure 3.1

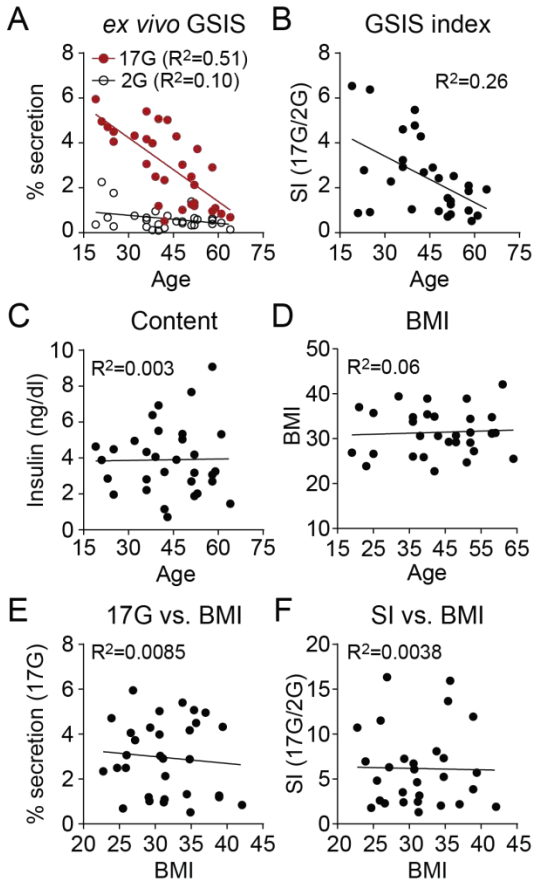

Figure 3.1. Insulin secretion declines with age in human islets. Insulin secretion (2 and 17 mM glucose) (**A**) stimulation index (i.e. stimulated/basal secretion) (**B**), insulin content (**C**), and BMI (**D**) as a function of donor age (*n = 31*). (**E and F**) Insulin secretion (17 mM glucose) and stimulation index as a function of BMI (*n = 31*). Donor information is listed in Table S1.

Figure 3.2

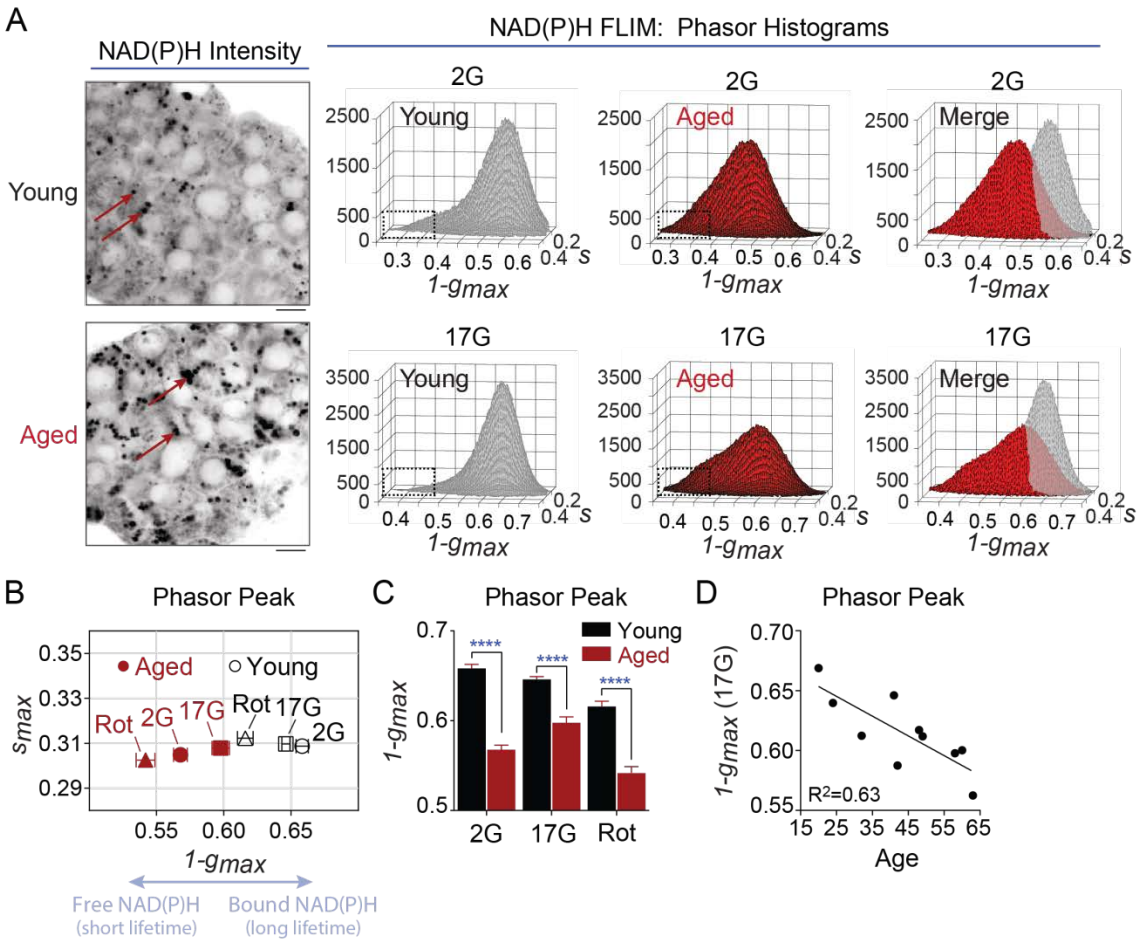

Figure 3.2. NAD(P)H FLIM of human islet metabolism. (**A**) Multiphoton FLIM of NAD(P)H in human islets from representative young (24 year old, ACJ3270) and aged donors (58 year old, ACKH054A). Phasor histograms show the frequency distribution of NAD(P)H lifetimes in young and aged islets (n = 20 islets each). Lipofuscin (red arrows) was excluded from the FLIM analysis based on its very short lifetime, which forms a tail at the right of the phasor plots (dashed boxes). Image scale bar = 5 µm. (**B, C**) Translation of the phasor histogram peaks ($1\text{-}g_{max}$,s_{max}) along the $1\text{-}g$ axis were used to quantify changes in Bound:Free NAD(P)H in response to 2 mM glucose (2G), 17 mM glucose (17G), and 17 mM glucose plus 5 µM rotenone (Complex I inhibitor). $1\text{-}g_{max}$ is plotted to give the same directionality as mitochondrial oxygen consumption. Data are mean ± SEM and were compared by 2-way ANOVA with Sidak's post-test. **** $P < 0.0001$. (**D**) Islet mitochondrial response to glucose (17 mM) declines with age. Data reflect 20 islets from each of 10 human islet donors (ACJV399A, ACJY368C, ACJ3270, ACKB319, ACKB044, ACKB010B, ACKH054A, ADAH342, ADAN146A, ADAT167). Donor information is listed in Table S1.

Figure 3.3

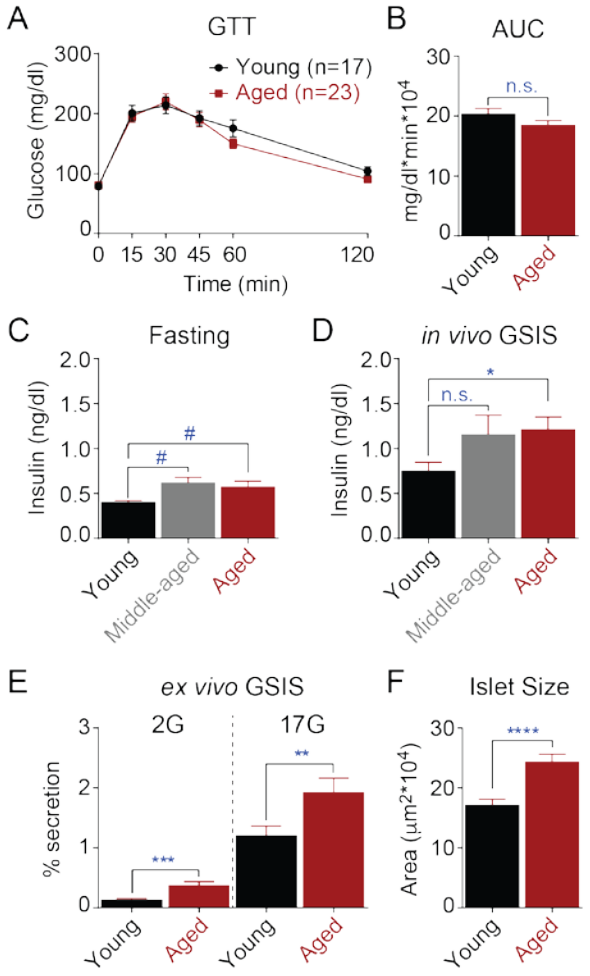

Figure 3.3. Insulin secretion is increased in aged mice. *In vivo* glucose tolerance (**A and B**) in young (6 month old) and aged (>= 24 month old) C57BL/6J mice. (**C and D**) Plasma insulin levels in young (6 month old, n = 5), middle-aged (18 month old n = 5), and aged (>= 24 month old, n = 10) mice after an overnight fast, prior to (**C**) and 15 minutes after (**D**) intraperitoneal glucose injection. (**E**) Insulin secretion measured *ex vivo* using islets from young (n = 2) and aged (n = 2) mice. (**F**) Islet size was estimated from the cross-sectional area. Young, n = 103 islets from 2 mice; Aged, n = 122 islets from 5 mice. Data are mean ± SEM and were compared by t test (A-D, F) or ANOVA with Sidak's post-test (E). $^{\#}$ P = 0.07, * P < 0.05, ** P < 0.01, *** P < 0.001, **** P < 0.0001.

Figure 3.4

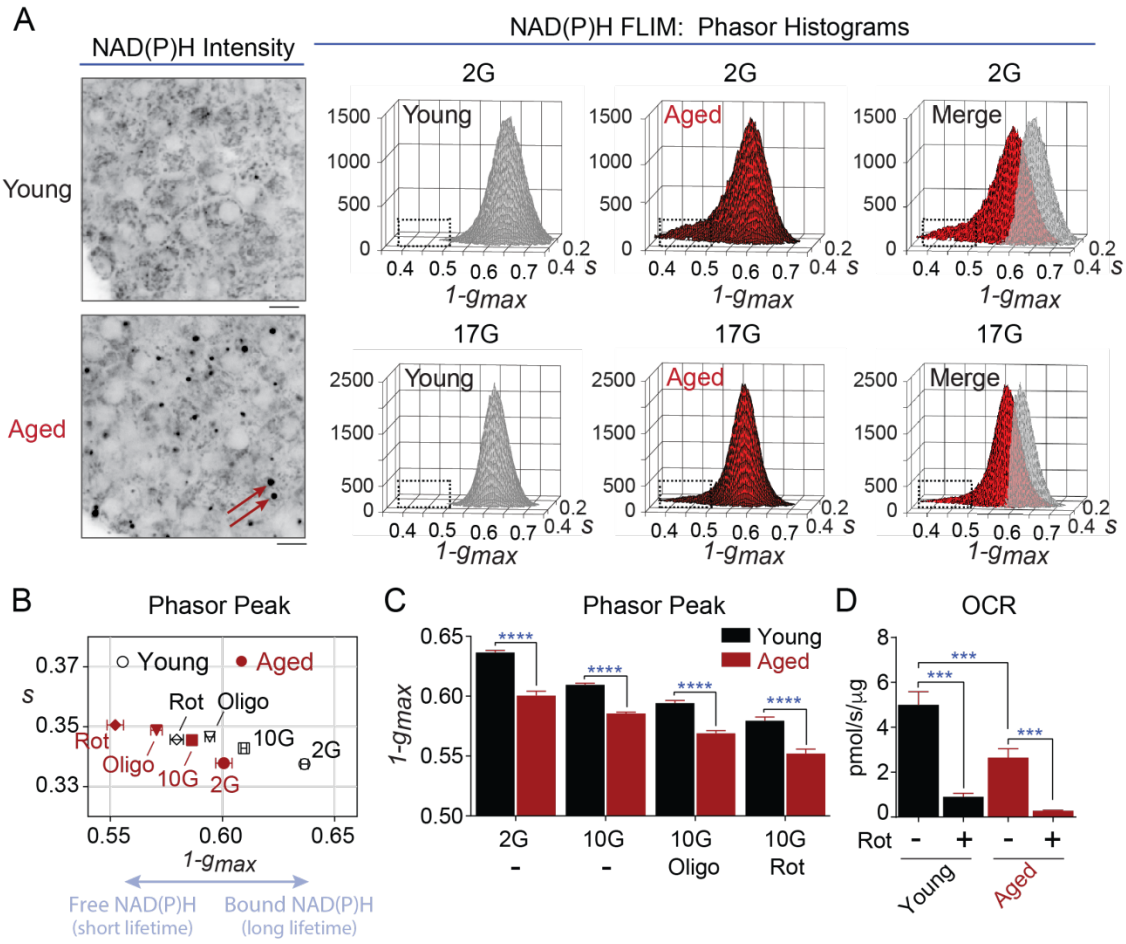

Figure 3.4. NAD(P)H FLIM of mouse islet metabolism. (A) Multiphoton FLIM of NAD(P)H in islets isolated from young (6 months) and aged C57BL/6J mice (30 months). Arrows in the NAD(P)H intensity images indicate contaminating lipofuscin fluorescence. Scale bar = 5 µm. Phasor histograms show the frequency distribution of NAD(P)H lifetimes in young and aged islets in the presence of 2 and 10 mM glucose (n = 10 islets per condition). (**B,C**) Translation of the phasor histogram peaks ($1\text{-}g_{max}$,s_{max}) along the abscissa were used to quantify changes in Bound:Free NAD(P)H in response to 2 mM glucose, 10 mM glucose, and 10 mM glucose plus 5 µM oligomycin (Complex V inhibitor) or 5 µM rotenone (Complex I inhibitor) as indicated. **(D)** Oxygen consumption rate (OCR) measured from 5 mice per condition (150 islets per mouse) shows that stimulated mitochondrial respiration is deficient in aged islets. Rotenone (5 µM) was present as indicated. Data are mean ± SEM and were compared by ANOVA with Sidak's post-test. *** P < 0.001, **** P < 0.0001.

Figure 3.5

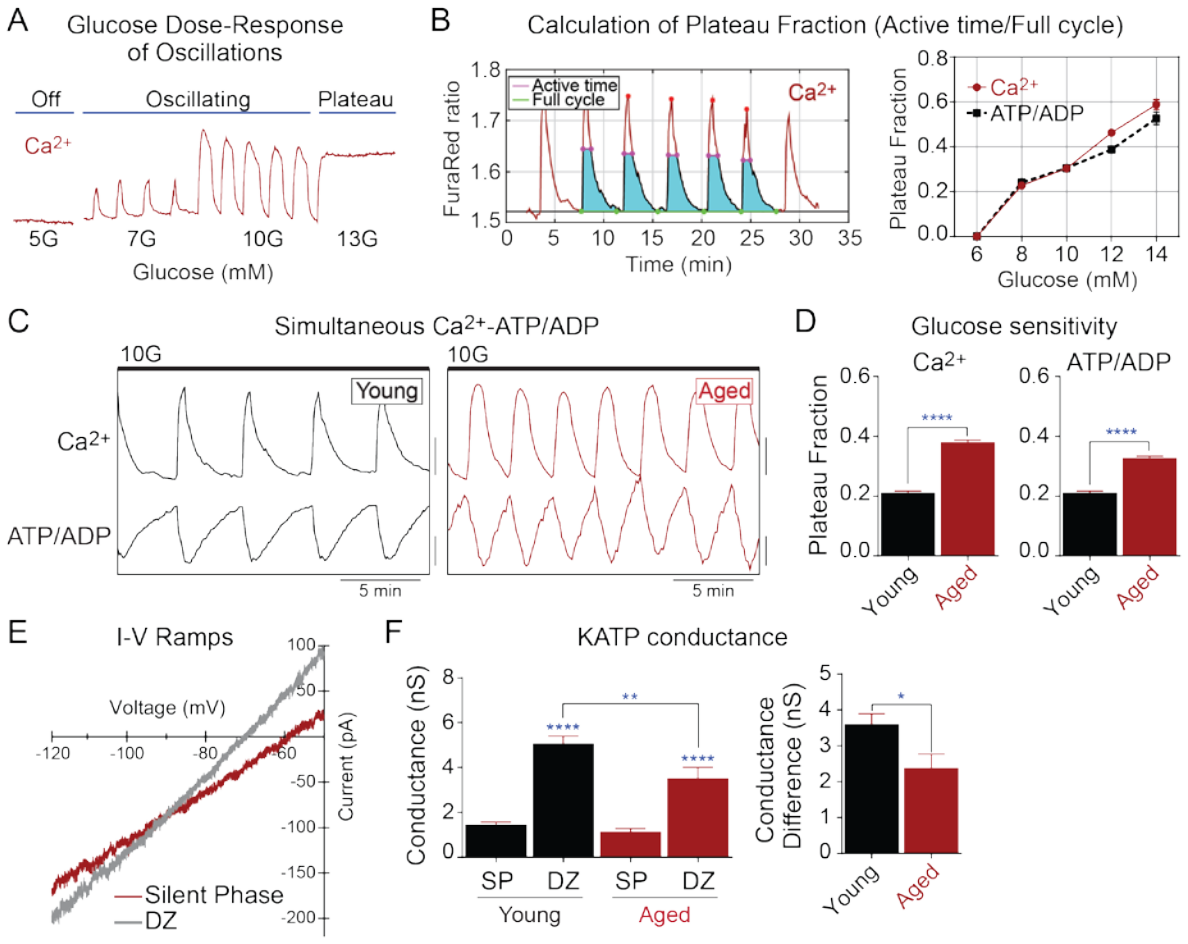

Figure 3.5. Loss of K_{ATP} channel conductance underlies a left shift in the glucose threshold of aged mouse β cells. (**A**) Recording of islet Ca^{2+} in response to increase glucose levels. (**B**) Glucose-dependence of plateau fraction, calculated from simultaneous recordings of Ca^{2+} (FuraRed) and ATP/ADP (Perceval-HR) oscillations using MATLAB. (**C**) Ca^{2+} and ATP/ADP oscillations in young (6 month) and aged (24 month) C57BL/6J mouse islet β cells in the presence of 10 mM glucose. (**D**) The oscillatory plateau fraction, reflecting the plasma membrane glucose sensitivity, was calculated as the fraction of time spent in the active state of each oscillation. Young, n = 124 islets from 4 mice; aged, n = 210 islets from 5 mice. (**E and F**) Representative I-V curves showing slope conductance changes in islet β cells during the silent phase (SP) of bursting (10 mM glucose) and 5 min after treatment with 200 μM diazoxide (DZ). Average KATP conductance, as well as conductance difference (DZ – Silent Phase), is reduced in aged β cells (n = 8 cells from 3 mice) relative to young controls (n = 19 cells from 4 mice). Data are mean ± SEM and were compared by 2-way ANOVA with Sidak's post-test. ** $P < 0.01$, **** $P < 0.0001$.

Donor	Age (years)	Sex	BMI	HbA1c % (mmol/mol)
AABW178	42	M	34.9	
AACC270	64	M	25.5	
AADU498	21	M	37	
AAEG306	36	F	34.8	
AAE2431	25	M	26.6	
AAFD181	52	M	34.4	5.7 (39)
AAGW388	43	M	30.6	5.8 (40)
AAG5351	23	M	23.9	5.3 (34)
AAHE140	25	M	35.7	
AAHP353	19	M	26.9	
AAIQ245	51	M	38.9	
AAI4274	42	M	22.76	
AAI1303	53	M	27.2	5.1 (32)
AAJF122	52	M	29.1	5.4 (36)
AAJY035	40	M	38.91	
AAKE155	36	M	33.8	5.4 (36)
AAK4206	48	F	29.2	
ABAW280	40	M	35.4	
ABCJ117	46	M	29.3	
ABCM211	58	F	31.1	
ABDG032	61	M	42.1	

ABDG134	36	M	26	
ABDN160	38	F	30.6	
ABEI387	58	M	34.8	
ABIT067	32	F	39.4	
ABJA126	59	F	31.3	
ABJN226	39	F	25.9	5 (31)
ABJU206	52	F	31.4	5 (31)
ABJ5204	51	M	24.7	
ABKH361	48	M	30.7	5.8 (40)
ABLM090	58	M	31.2	
ACJV399A	41	F	43.1	6.5 (48)
ACJY368C	42	F	23.1	5.4 (36)
ACJ3270	24	M	50.4	5.6 (38)
ACKB319	49	F	31.6	5.2 (33)
ACKB044	32	F	31.3	5.1 (32)
ACKB010B	20	M	30.9	5.6 (38)
ACKH054A	58	F	35.1	4.8 (29)
ADAH342	48	M	43.7	6.6 (49)
ADAN146A	63	M	31.8	5.8 (40)
ADAT167	60	M	23.7	5.7 (39)
AVG±SEM	43.54±2.0		32.17±0.96	5.52±0.07 (36.89±0.84)

Table S1. Human Islet Donors from the Integrated Islet Distribution Program (IIDP).
Summary characteristics of donors studied by Unos ID. BMI – Body Mass Index, HbA1c – glycated hemoglobin.

REFERENCES

1. 2014 National Diabetes Statistics Report [Internet]. Center for Disease Control; 2014. Available from: http://www.cdc.gov/diabetes/data/statistics/2014StatisticsReport.html

2. Chang AM, Halter JB. Aging and insulin secretion. Am J Physiol Endocrinol Metab. 2003 Jan;284(1):E7-12.

3. Gunasekaran U, Gannon M. Type 2 diabetes and the aging pancreatic beta cell. Aging (Albany NY). 2011 Jun;3(6):565–75.

4. Kushner JA. The role of aging upon β cell turnover. J Clin Invest. 2013 Mar;123(3):990–5.

5. Almaça J, Molina J, Arrojo E Drigo R, Abdulreda MH, Jeon WB, Berggren P-O, et al. Young capillary vessels rejuvenate aged pancreatic islets. Proc Natl Acad Sci USA. 2014 Dec 9;111(49):17612–7.

6. Li L, Trifunovic A, Köhler M, Wang Y, Petrovic Berglund J, Illies C, et al. Defects in β-cell Ca2+ dynamics in age-induced diabetes. Diabetes. 2014 Dec;63(12):4100–14.

7. Avrahami D, Li C, Zhang J, Schug J, Avrahami R, Rao S, et al. Aging-Dependent Demethylation of Regulatory Elements Correlates with Chromatin State and Improved β Cell Function. Cell Metab. 2015 Oct 6;22(4):619–32.

8. Naidoo N, Davis JG, Zhu J, Yabumoto M, Singletary K, Brown M, et al. Aging and sleep deprivation induce the unfolded protein response in the pancreas: implications for metabolism. Aging Cell. 2014 Feb;13(1):131–41.

9. Iozzo P, Beck-Nielsen H, Laakso M, Smith U, Yki-Järvinen H, Ferrannini E. Independent influence of age on basal insulin secretion in nondiabetic humans. European Group for the Study of Insulin Resistance. J Clin Endocrinol Metab. 1999 Mar;84(3):863–8.

10. Ihm S-H, Matsumoto I, Sawada T, Nakano M, Zhang HJ, Ansite JD, et al. Effect of donor age on function of isolated human islets. Diabetes. 2006 May;55(5):1361–8.

11. Khrapko K, Vijg J. Mitochondrial DNA mutations and aging: devils in the details? Trends Genet. 2009 Feb;25(2):91–8.

12. Henquin J-C. The dual control of insulin secretion by glucose involves triggering and amplifying pathways in β-cells. Diabetes Res Clin Pract. 2011 Aug;93 Suppl 1:S27-31.

13. Yoshino J, Mills KF, Yoon MJ, Imai S. Nicotinamide mononucleotide, a key NAD(+) intermediate, treats the pathophysiology of diet- and age-induced diabetes in mice. Cell Metab. 2011 Oct 5;14(4):528–36.

14. Cree LM, Patel SK, Pyle A, Lynn S, Turnbull DM, Chinnery PF, et al. Age-related decline in mitochondrial DNA copy number in isolated human pancreatic islets. Diabetologia. 2008 Aug;51(8):1440–3.

15. Patterson GH, Knobel SM, Arkhammar P, Thastrup O, Piston DW. Separation of the glucose-stimulated cytoplasmic and mitochondrial NAD(P)H responses in pancreatic islet beta cells. Proc Natl Acad Sci USA. 2000 May 9;97(10):5203–7.

16. Rocheleau JV, Head WS, Piston DW. Quantitative NAD(P)H/flavoprotein autofluorescence imaging reveals metabolic mechanisms of pancreatic islet pyruvate response. J Biol Chem. 2004 Jul 23;279(30):31780–7.

17. Luciani DS, Misler S, Polonsky KS. Ca2+ controls slow NAD(P)H oscillations in glucose-stimulated mouse pancreatic islets. J Physiol (Lond). 2006 Apr 15;572(Pt 2):379–92.

18. Quesada I, Todorova MG, Soria B. Different metabolic responses in alpha-, beta-, and delta-cells of the islet of Langerhans monitored by redox confocal microscopy. Biophys J. 2006 Apr 1;90(7):2641–50.

19. Lakowicz JR, Szmacinski H, Nowaczyk K, Johnson ML. Fluorescence lifetime imaging of free and protein-bound NADH. Proc Natl Acad Sci USA. 1992 Feb 15;89(4):1271–5.

20. Turturro A, Witt WW, Lewis S, Hass BS, Lipman RD, Hart RW. Growth curves and survival characteristics of the animals used in the Biomarkers of Aging Program. J Gerontol A Biol Sci Med Sci. 1999 Nov;54(11):B492-501.

21. Merrins MJ, Poudel C, McKenna JP, Ha J, Sherman A, Bertram R, et al. Phase Analysis of Metabolic Oscillations and Membrane Potential in Pancreatic Islet β-Cells. Biophys J. 2016 Feb 2;110(3):691–9.

22. Gnaiger E, Kuznetsov AV. Mitochondrial respiration at low levels of oxygen and cytochrome c. Biochem Soc Trans. 2002 Apr;30(2):252–8.

23. Forstner H, Gnaiger E. Calculation of Equilibrium Oxygen Concentration. In: Polarographic Oxygen Sensors. Springer; 1983. p. 321–33.

24. Votion D-M, Gnaiger E, Lemieux H, Mouithys-Mickalad A, Serteyn D. Physical fitness and mitochondrial respiratory capacity in horse skeletal muscle. PLoS ONE. 2012;7(4):e34890.

25. Kuznetsov AV, Schneeberger S, Seiler R, Brandacher G, Mark W, Steurer W, et al. Mitochondrial defects and heterogeneous cytochrome c release after cardiac cold ischemia and reperfusion. Am J Physiol Heart Circ Physiol. 2004 May;286(5):H1633-1641.

26. Digman MA, Caiolfa VR, Zamai M, Gratton E. The phasor approach to fluorescence lifetime imaging analysis. Biophys J. 2008 Jan 15;94(2):L14-16.

27. Cnop M, Hughes SJ, Igoillo-Esteve M, Hoppa MB, Sayyed F, van de Laar L, et al. The long lifespan and low turnover of human islet beta cells estimated by mathematical modelling of lipofuscin accumulation. Diabetologia. 2010 Feb;53(2):321–30.

28. Ren J, Sherman A, Bertram R, Goforth PB, Nunemaker CS, Waters CD, et al. Slow oscillations of KATP conductance in mouse pancreatic islets provide support for electrical bursting driven by metabolic oscillations. Am J Physiol Endocrinol Metab. 2013 Oct 1;305(7):E805-817.

29. Truchan NA, Brar HK, Gallagher SJ, Neuman JC, Kimple ME. A single-islet microplate assay to measure mouse and human islet insulin secretion. Islets. 2015 Oct 9;0.

30. Blinova K, Levine RL, Boja ES, Griffiths GL, Shi Z-D, Ruddy B, et al. Mitochondrial NADH fluorescence is enhanced by complex I binding. Biochemistry. 2008 Sep 9;47(36):9636–45.

31. Marmorstein AD, Marmorstein LY, Sakaguchi H, Hollyfield JG. Spectral profiling of autofluorescence associated with lipofuscin, Bruch's Membrane, and sub-RPE deposits in normal and AMD eyes. Invest Ophthalmol Vis Sci. 2002 Jul;43(7):2435–41.

32. Wright BK, Andrews LM, Markham J, Jones MR, Stringari C, Digman MA, et al. NADH distribution in live progenitor stem cells by phasor-fluorescence lifetime image microscopy. Biophys J. 2012 Jul 3;103(1):L7-9.

33. Pate KT, Stringari C, Sprowl-Tanio S, Wang K, TeSlaa T, Hoverter NP, et al. Wnt signaling directs a metabolic program of glycolysis and angiogenesis in colon cancer. EMBO J. 2014 Jul 1;33(13):1454–73.

34. Helman A, Klochendler A, Azazmeh N, Gabai Y, Horwitz E, Anzi S, et al. p16(Ink4a)-induced senescence of pancreatic beta cells enhances insulin secretion. Nat Med. 2016 Mar 7;

35. Wikstrom JD, Sereda SB, Stiles L, Elorza A, Allister EM, Neilson A, et al. A novel high-throughput assay for islet respiration reveals uncoupling of rodent and human islets. PLoS ONE. 2012;7(5):e33023.

36. Nunemaker CS, Bertram R, Sherman A, Tsaneva-Atanasova K, Daniel CR, Satin LS. Glucose modulates [Ca2+]i oscillations in pancreatic islets via ionic and glycolytic mechanisms. Biophys J. 2006 Sep 15;91(6):2082–96.

37. Henquin JC. Regulation of insulin secretion: a matter of phase control and amplitude modulation. Diabetologia. 2009 May;52(5):739–51.

38. Ravier MA, Daro D, Roma LP, Jonas J-C, Cheng-Xue R, Schuit FC, et al. Mechanisms of control of the free Ca2+ concentration in the endoplasmic reticulum of mouse pancreatic β-cells: interplay with cell metabolism and [Ca2+]c and role of SERCA2b and SERCA3. Diabetes. 2011 Oct;60(10):2533–45.

39. Detimary P, Gilon P, Henquin JC. Interplay between cytoplasmic Ca2+ and the ATP/ADP ratio: a feedback control mechanism in mouse pancreatic islets. Biochem J. 1998 Jul 15;333 (Pt 2):269–74.

40. Li J, Shuai HY, Gylfe E, Tengholm A. Oscillations of sub-membrane ATP in glucose-stimulated beta cells depend on negative feedback from Ca(2+). Diabetologia. 2013 Jul;56(7):1577–86.

41. Henquin JC. ATP-sensitive K+ channels may control glucose-induced electrical activity in pancreatic B-cells. Biochem Biophys Res Commun. 1988 Oct 31;156(2):769–75.

42. Nichols CG. KATP channels as molecular sensors of cellular metabolism. Nature. 2006 Mar 23;440(7083):470–6.

43. Leiter EH, Premdas F, Harrison DE, Lipson LG. Aging and glucose homeostasis in C57BL/6J male mice. FASEB J. 1988 Sep;2(12):2807–11.

44. Lamming DW, Mihaylova MM, Katajisto P, Baar EL, Yilmaz OH, Hutchins A, et al. Depletion of Rictor, an essential protein component of mTORC2, decreases male lifespan. Aging Cell. 2014 Oct;13(5):911–7.

45. Ma Z, Portwood N, Brodin D, Grill V, Björklund A. Effects of diazoxide on gene expression in rat pancreatic islets are largely linked to elevated glucose and potentially serve to enhance beta-cell sensitivity. Diabetes. 2007 Apr;56(4):1095–106.

46. Glynn E, Thompson B, Vadrevu S, Lu S, Kennedy RT, Ha J, et al. Chronic glucose exposure systematically shifts the oscillatory threshold of mouse islets: Experimental evidence for an early intrinsic mechanism of compensation for hyperglycemia. Endocrinology. 2015 Dec 23;en20151563.

47. Annicotte J-S, Blanchet E, Chavey C, Iankova I, Costes S, Assou S, et al. The CDK4-pRB-E2F1 pathway controls insulin secretion. Nat Cell Biol. 2009 Aug;11(8):1017–23.

48. Krishnamurthy J, Ramsey MR, Ligon KL, Torrice C, Koh A, Bonner-Weir S, et al. p16INK4a induces an age-dependent decline in islet regenerative potential. Nature. 2006 Sep 28;443(7110):453–7.

49. Merrins MJ, Fendler B, Zhang M, Sherman A, Bertram R, Satin LS. Metabolic oscillations in pancreatic islets depend on the intracellular Ca2+ level but not Ca2+ oscillations. Biophys J. 2010 Jul 7;99(1):76–84.

50. Merrins MJ, Van Dyke AR, Mapp AK, Rizzo MA, Satin LS. Direct measurements of oscillatory glycolysis in pancreatic islet β-cells using novel fluorescence resonance energy transfer (FRET) biosensors for pyruvate kinase M2 activity. J Biol Chem. 2013 Nov 15;288(46):33312–22.

51. Soria B, Martín F, Andreu E, Sanchez-Andrés JV, Nacher V, Montana E. Diminished fraction of blockable ATP-sensitive K+ channels in islets transplanted into diabetic mice. Diabetes. 1996 Dec;45(12):1755–60.

52. Erion KA, Berdan CA, Burritt NE, Corkey BE, Deeney JT. Chronic Exposure to Excess Nutrients Left-shifts the Concentration Dependence of Glucose-stimulated Insulin Secretion in Pancreatic β-Cells. J Biol Chem. 2015 Jun 26;290(26):16191–201.

Chapter 4

Cdk1, by Stimulating Mitochondrial Respiration, Restricts the Metabolic Amplifying Pathways of Insulin Secretion

ABSTRACT

Type 2 diabetes is linked genetically to Cyclin-dependent kinase (Cdk) signaling. However, the significance of Cdk1/Cyclin B1 signaling in adult β-cells remains largely unknown. Here, we show that one of the key mitotic functions of Cdk1/Cyclin B1 – the activation of mitochondrial respiratory Complex I – is active in adult β-cells and hyperactive in β-cells from obese (*ob/ob*) mice. In wild-type islets, an analysis of TCA cycle and electron transport chain (ETC) fluxes with NAD(P)H FLIM and respirometry revealed that 65 ± 13% ($P = 0.0106$) of Complex I flux and 49 ± 12% ($P < 0.05$) of State 3 respiration is sensitive to Cdk1 inhibition. Islets from *ob/ob* mice express more Cyclin B1 and exhibit an even higher sensitivity to Cdk1 blockade, which reduced Complex I flux by 76 ± 11% ($P < 0.001$) and State 3 respiration by 79 ± 6% ($P < 0.001$). While Cdk1 signaling and ETC flux were correlated with the activity of glucose-stimulated Ca^{2+} oscillations, insulin secretion increased following Cdk1 inhibition as carbon shifted to the K_{ATP}-independent metabolic amplifying pathways. These results reveal that ETC activity is inversely proportional to insulin secretion. Our results further demonstrate that Cdk1 and Complex I are control points for β-cell metabolism which, in the setting of obesity, rebalance the insulin secretory pathway.

INTRODUCTION

Obesity is characterized by insulin resistance, and in the islet, adaptive compensation by pancreatic β-cells. Leptin-deficient (*ob/ob*) mice are a well-studied model for β-cell compensation arising from hyperphagia and obesity in which numerous adaptations to the insulin secretory pathway facilitate insulin hypersecretion, β-cell growth, and proliferation (1–4). In 2008, Attie and colleagues (5) took advantage of the phenotypic differences between *ob/ob* mice on two different backgrounds – diabetes-resistant C57Bl/6J *ob/ob*, and diabetic BTBR *ob/ob* – to model the β-cell

compensation and decompensation that accompanies human type 2 diabetes (6). A strong genetic linkage was observed between the cell cycle regulators and diabetes susceptibility (5). Here, we focus on the significance of Cyclin-dependent kinase 1 (Cdk1), and its activator Cyclin B1, for the β-cell secretory pathway.

There is little doubt that the raison d'etre of Cdk1/Cyclin B1 signaling is the control of proliferative signaling (7), and it was recently discovered that Cdk1 is a critical mediator of adaptive proliferation in β-cells (8). However, Cdk1 signaling may be controlled in quiescent β-cells, at least in part, by autocrine insulin signaling (9–11). Not only is Cdk1 expression lost in β-cells derived from β-cell-specific insulin receptor knockout (i.e. βIRKO) mice, but more physiologically, short-term blockade of insulin secretion with diazoxide is sufficient to restrict glucose-induced Cdk1 signaling in wild-type β-cells (8). These *in vitro* experiments are paralleled by prior studies showing that diazoxide blocks glucose-induced β-cell proliferation *in vivo* (12). An important question, then, is whether the insulin secretory pathway is impacted by Cdk1 signaling, both in quiescent β-cells and during the adaptive response to obesity, when Cdk1 signaling is upregulated and insulin demand is high.

Here, we show that one of the key mitotic functions of Cdk1/Cyclin B1 – the activation of mitochondrial respiratory Complex I – is active in adult β-cells and hyperactive in β-cells from obese (*ob/ob*) mice. Although the best-studied functions of Cdk1 are cytosolic and nuclear (7), our studies focused on the mitochondrial pool of Cdk1/Cyclin B1 (13–16). Cdk1 phosphorylates an estimated 52 mitochondrial substrates at consensus sites (S/T*P-x-K/R or S/T*-P), including eight subunits within Complex I of the electron transport chain (ETC) (13,14). Complex I occupies a key postion in the β-cell secretory pathway. Not only does it link TCA cycle-dependent NADH turnover to the ATP/ADP ratio, a key component of the β-cell triggering pathway, but the tight coupling of the TCA cycle to the ETC indirectly links Complex I to a number of mitochondrial cycles that amplify

insulin secretion (i.e. the pyruvate and phosphoenolpyruvate (PEP) cycles) (17,18). Our studies demonstrate that Cdk1 signaling acts at Complex I to enhance oxygen consumption, while simultaneously depleting the metabolic amplifying pathways. We propose that this reciprocal relationship between ETC flux and the TCA cycle-derived amplifying pathways is a general property of β-cell metabolism, imbalanced in the setting of obesity.

RESEARCH DESIGN AND METHODS

Mice

All animal studies were approved by the Institutional Animal Care and Use Committees of the University of Wisconsin-Madison and the William S. Middleton Memorial Veterans Hospital. C57Bl6/J wild-type and leptin-deficient (*ob/ob*) mice were obtained from The Jackson Laboratory (stocks 000664 and 000632). Male mice were analyzed between 10-16 weeks of age.

In Vivo Studies

Glucose tolerance tests were performed on mice fasted overnight for 16 hours. Following intraperitoneal injection of 1 g/kg glucose in sterile saline, glucose measurements were taken at 0, 15, 30, 60 and 120 minutes via tail nick using a Bayer Contour glucometer.

Islet Isolation and Cdk1 inhibitor treatment

Mice were sacrificed via cervical dislocation and islet isolations were carried out as previously described (19). Islets were cultured overnight in RPMI1640 supplemented with 10% (v/v) fetal bovine serum (Invitrogen A31605), 100 units/ml penicillin and 100 μg/ml streptomycin (Invitrogen) containing Cdk1 selective inhibitor, 5 μM RO-3306 (Enzo ALX-270-463) (20), or vehicle (0.1% DMSO).

Immunoblotting

Islets were lysed in buffer containing 20 mM Tris, 100 mM NaCl, 1 mM EDTA and 0.5% Triton-X. Protein concentrations were determined using Pierce 660 nm protein assay (Thermo Fisher). All antibodies except Cdk4 (Santa Cruz sc260) were purchased from Cell Signaling (Cyclin B1, 4138; Cdk1, 77055; Hsp90, 4877; Lamin, A/C; Cox IV, 11967).

Ca^{2+} Imaging

Islets treated with vehicle or Cdk1 inhibitor were imaged simultaneously; one treatment group was pre-labeled with 0.5 μg/mL DiR (Molecular Probes, Eugene, OR) for 10 minutes. DiR labeling had no effect on islet metabolic or Ca^{2+} oscillations (data not shown). For measurements of cytosolic Ca^{2+}, islets were pre-incubated in 2.5 μM FuraRed (Molecular Probes F3020) in islet media for 45 min at 37°C before they were placed in a glass-bottomed QE1/RC-37W imaging chamber (Warner Instruments) mounted on a Nikon Ti-Eclipse inverted microscope equipped with a 20X/0.75NA SuperFluor air objective (Nikon Instruments). The chamber was perfused with a standard external solution containing 135 mM NaCl, 4.8 mM KCl, 5 mM $CaCl_2$, 1.2 mM $MgCl_2$, 20 mM HEPES (pH 7.35). The flow rate was 0.4 mL/min and temperature was maintained at 33°C using inline solution and chamber heaters (Warner Instruments). Excitation was provided by a SOLA SEII 365 (Lumencor) set to 10% output. Excitation (430/20x and 500/20x) and emission (630/70m) filters (ET type, Chroma Technology Corporation) were used in combination with an FF444/521/608-Di01 dichroic (Semrock) and reported as an excitation ratio (R430/500). Single DiR images utilized a Chroma Cy7 cube (710/75x, T760lpxr, 810/90m). Fluorescence emission was collected with a Hamamatsu ORCA-Flash4.0 V2 Digital CMOS camera at 0.125 Hz. A single region of interest was used to quantify the average response of each islet using Nikon Elements and custom MATLAB software (MathWorks).

NAD(P)H Fluorescence Lifetime Imaging (FLIM)

Islets were imaged in #1.5 glass-bottom dishes on a custom-built multiphoton laser scanning system based around a Nikon TE-300 inverted microscope equipped with a Plan Apo 60X/1.4NA Oil immersion objective (Nikon Instruments) in a standard external solution (above). Temperature was maintained at 35°C using a LiveCell incubator (Pathology Devices). NAD(P)H was excited with Mai Tai DeepSee Ti:Sapphire laser (Spectra-Physics) at 740 nm with a 450/70m bandpass emission filter (Chroma) before collection by a Hamamatsu H7422P-40 GaAsP photomultiplier tube. FLIM images were collected at 256x256 resolution with 120 s collection at 1 Hz using SPC-830 Time-Correlated Single Photon Counting (TCSPC) electronics (Becker & Hickl GbmH). In each experiment, urea crystals were used to define the instrument response function with a 370/10 bandpass emission filter (Chroma), and coumarin was used as a reference for lifetime (2.5 ns) using a 450/70m bandpass emission filter (Chroma). For analysis, raw SDT files were imported into MATLAB (MathWorks), and a custom script was used to generate phasor histograms for each treatment using the equations in (21). All data were reported as the phasor histogram peak ($1\text{-}g_{max}, s_{max}$).

Islet Respirometry

Following overnight incubation in either islet media or islet media containing 5 μM Cdk1i, 150 islets/condition/mouse (5 mice/condition) were transferred to a 35 mm petri dish containing 2 ml of MiR05 (in mM: 0.5 EGTA, 3 $MgCl_2$, 60 lactobionic acid, 20 taurine, 10 KH_2PO_4, 20 HEPES, 110 sucrose, 1% BSA; pH 7.1, adjusted with 5 M KOH) (22) and 5 mg/ml saponin; preliminary experiments showed that permeabilized islets demonstrated higher coupled respiration rates. Islets were gently rocked in the permeabilization medium for 20 min. After 20 min, the islets were rinsed with fresh MiR05 in the absence of saponin, and then pipetted into an Oxygraph-2k chamber (Oroboros) containing 2 ml of air-equilibrated MiR05 at 37°C. Oxygen electrodes were calibrated to air-saturated MiR05 buffer at 37°C using published oxygen solubilities (23) corrected for local

atmospheric pressure, and zero oxygen calibrations were performed at regular intervals throughout the study. Oxygen concentration and oxygen flux were recorded using DatLab software (Oroboros). A modified substrate-uncoupler-inhibitor titration (SUIT) protocol based on Votion et al. (24) was applied. Respiratory flux through complex I was measured by adding 5 mM glutamate and 1 mM malate, followed by 1.25 mM ADP to induce oxidative phosphorylation. To assess the integrity of the outer mitochondrial membrane, cytochrome c was added to the chamber (8 μM) (25), and no significant increases in respiration were observed. Damage to the outer mitochondrial membrane during permeabilization would result in a loss of cytochrome c, and a large increase in respiration upon the addition of exogenous cytochrome c to the respiration chamber. Convergent electron flow through complexes I and II was measured with the addition of 10 mM succinate, allowing the electron transport system to achieve maximal coupled respiration. Next, a step-wise addition of carbonyl cyanide p-trifluoro-methoxyphenyl hydrazone (FCCP) was used to completely uncouple mitochondria (0.250 μM initial + 0.250 μM additions). To assess oxygen flux through complex II, 0.5 μM rotenone was added to inhibit complex I. Finally, electron transfer was blocked at complex III with the addition of 5 μM antimycin A and allowed to run long enough to obtain a residual oxygen consumption rate. Oxygen flux was expressed per mg of total protein (Pierce 660 nm protein assay, ThermoFisher 22660).

Ex Vivo Insulin Release

The glucose-stimulated insulin secretion assay was performed on mouse islets treated overnight with vehicle or Cdk1i, which were present throughout the assay. All experiments were carried out at 37°C in a 5% CO_2 incubator using DMEM (Sigma D-5030) supplemented with 4 mM L-glutamine, 44 mM sodium bicarbonate, 10 mM HEPES and 0.2% BSA. 60 islets per treatment were pre-incubated for 45 minutes in DMEM/1.7 mM glucose, which was discarded. Six groups of 10 islets were then moved to 12-well plates (Falcon 353225) containing 1 mL of DMEM/1.7 mM glucose for 45 min.

The islets were transferred to a new 12-well plate, each well containing 1 mL of DMEM/16.7 mM glucose for an additional 45-minute incubation. The incubation media was collected and the islets were lysed in cell lysis buffer containing 20 mM Tris-HCl (pH 7.5), 150mM NaCl, and 1% Triton-X.

Insulin ELISA

Insulin secretion as a percentage of total islet insulin content was measured by ELISA in 96-well high-binding plates (Corning 3096) coated overnight with 3 μg/mL (50 μL/well) of anti-insulin primary antibody (Research Diagnostics, RDI-TRK2IP10- D6C4) diluted 1:2500 in PBS. Plates were blocked with PBS containing 4% BSA (Sigma A-7888) for 1 h (100 μL/well). Following blocking, plates were emptied and incubated for 1 h with either insulin standards (Millipore 24304391/8013-k, 0.1–10 ng/mL), secretion media, or islet lysate (25 μL/well). Secondary antibody (Research Diagnostics, RDI-TRK2IP10-D3E7- BT) (25 μL/well) diluted 1:1000 in PBS with 1% BSA was added to each well, gently mixed, and incubated for an additional hour. Wells were then washed three times (50 mM Tris, 0.2% Tween-20, pH 8.0), and 1 μg/mL of streptavidin-HRP (Pierce 21126) in PBS with 0.1% BSA was added (50 μL/well) and incubated for 30 min. Plates were then washed three times. 16 μmol/mL of *o*-phenylenediamine (Sigma P-5412), dissolved in citrate buffer (0.1 M citrate-phosphate, 0.03% H_2O_2 at pH 5.0), was then added (50 μL/well). After 3-5 minutes of development, 0.18 M sulfuric acid (50 μL/well) was added to quench the reaction. Absorbance at 492 nm was determined by a plate reader (TECAN Infinite M1000 Pro). Insulin contents in plasma were calculated by comparison to known standards.

Human Islets

An exemption was granted for all protocols by the Institutional Review Board at the University of Wisconsin-Madison under Protocol Number 2015-0356. Human islets were obtained from the Integrated Islet Distribution Program (IIDP). Donor information is listed in Table S1. The IIDP published isolation protocols and insulin secretion quality control assays can be found

at https://iidp.coh.org/investigator_sops.aspx. Following shipment, the islets were cultured overnight in islet media prior to imaging.

Islet Mitochondrial Content

Islets were isolated and washed with PBS. DNA was isolated with a Mini Genomic DNA kit (IBI Scientific). qPCR was performed in triplicate using primers MT9 (GAGCATCTTATCCACGCTTCC) and MT11 (GGTGGTACTCCCGCTGTAAA), normalized to reference gene Ndufv1: F (TTCCTCTGGATTCACCCTCA), R (CATGAGGAGCGCGAGTATTT) with FastStart Universal SYBR Green Master (Rox) (Roche). 30 ng of DNA was used per reaction with a final primer concentration of 2 μM. Reactions were run on a StepOne Plus Real-Time PCR system (Applied Biosystems). PCR product specificity was determined by melt-curve analysis and data was reported as ΔΔCt.

Statistics

Data are expressed as means ± SE. Statistical significance was determined using one- or two-way ANOVA with Sidak multiple-comparisons test post hoc or Student's t-test as appropriate. Differences were considered to be statistically significant at $P < 0.05$. Statistical calculations were performed with GraphPad Prism.

RESULTS

Cdk1 Signaling is Upregulated in Pancreatic Islets from Obese (*ob/ob*) Mice

Leptin-deficient (*ob/ob*) mice were used as a model of adaptive β-cell compensation (1–4). At 10 weeks of age, *ob/ob* mice weighed significantly more than their lean (i.e. wild-type) counterparts, and exhibited elevated fasting blood glucose and impaired glucose tolerance (Figures 1A, 1B, 1C). We compared islet mRNA expression levels between lean and *ob/ob* mice using the database

provided by Attie and colleagues (http://diabetes.wisc.edu), who previously described a confluence of gene expression changes surrounding the cell cycle regulators (5). Among these, the mRNA levels of the Cdk1 and its activators Cyclin B1 and Cdc25c were increased in *ob/ob* mice relative to their lean counterparts (Figure 4.1C). At the protein level, Cdk1 was unchanged, while Cyclin B1 was significantly increased in *ob/ob* islets relative to lean controls (Figure 4.1D).

Cdk1 is present in multiple cellular compartments, including a mitochondrial pool (13–16,26) and a cytosolic/nuclear pool (7,27). In Min6 cells, 29.6 ± 0.6% (n = 2) of Cdk1 was found in the mitochondrial fraction, while Cdk2 and Cdk4 (i.e. the Cdks associated with G1) were more prominent in the nuclear fractions (Figure 4.1E). Notably, the majority of Cdk1 immunofluorescence in adult β-cells is perinuclear (28), suggesting that the mitochondrial localization is favored in quiescent cells. Our subsequent studies focused on determining whether Cdk1 has a role in controlling β-cell mitochondrial function.

Cdk1 Activates Mitochondrial Respiration at Complex I

Considering that the reported functions of mitochondrial Cdk1 include the activation of Complex I (13–16), we hypothesized that the consequences of increased Cyclin B1 in *ob/ob* islets (Figure 4.1D) would be to enhance Cdk1 signaling and mitochondrial bioenergetics. We took advantage of the small-molecule Cdk1 inhibitor RO-3306 (20), which was chosen based on its low non-specificity for endogenous kinases other than Cdk1, and because its effectiveness to block Cdk1/Cyclin B1-dependent Complex I activation was previously validated with genetic mutants of Cdk1, Cyclin B1, and Complex I (14).

To compare metabolic function in wild-type and *ob/ob* islets, we performed multiphoton NAD(P)H fluorescence lifetime imaging (FLIM) using the assay we developed to assess NADH utilization by the ETC in intact islets (19). Figure 4.2A shows representative NAD(P)H lifetime images of wild-type and *ob/ob* islets. These images are spatial maps of islet redox metabolism

reflecting the glucose-dependent changes in NAD(P)H lifetime that accompanies each coenzyme-protein interaction (19,29); advantageously, much of the assay's resolution comes from NADH binding to Complex I (30,31). For quantification, each image pixel was plotted on a phasor histogram (21) so that each distinct mixture of lifetimes occupies a unique position on the plot (Figure 4.2B). Relative to wild-type islets incubated in 10 mM glucose, the *ob/ob* islet phasor was shifted further along the 1-*gmax* axis (Figure 4.2C), reflecting an increase in bound NAD(P)H lifetime that occurs with increasing Complex I flux (19). Overnight incubation with 5 μM Cdk1 inhibitor RO-3306 reduced *1-gmax* in both wild-type and *ob/ob* islets, but to a lesser extent than direct Complex I inhibition with 5 μM rotenone. In *ob/ob* islets, the simultaneous application of these inhibitors had no further effect, implying that the ETC is more highly dependent on Cdk1 signaling in *ob/ob* islets relative to controls. The similar directionality of Cdk1 and Complex I inhibition in phasor space is consistent with them working in the same pathway. Comparable effects were observed on NAD(P)H lifetime in human islets treated overnight with Cdk1 inhibitor (Figure 4.S1).

To directly test the effect of Cdk1 inhibition on individual ETC fluxes, we measured mitochondrial oxygen consumption in permeabilized mouse islets stimulated with glutamate, malate, succinate, and ADP. In excellent agreement with NAD(P)H FLIM assay, *ob/ob* islets exhibited increased State 3 respiration relative to lean controls, and Complex I flux was blocked by overnight application of Cdk1 inhibitor RO-3306 (Figure 4.2D). No further effect of Cdk1 inhibition was seen when Complex I was directly inhibited with rotenone. Compared with wild-type islets, the elevated Cyclin B1 levels observed in *ob/ob* islets (Figure 4.1) would be predicted to activate Cdk1 signaling, and Complex I in turn. As expected, respiration in *ob/ob* islets exhibited a higher rotenone sensitivity than lean controls (84 ± 6% reduction in *ob/ob* vs. 61 ± 11% in wild-type, $P < 0.0001$). Importantly, RO-3306 had no acute effects on NADH or Ca^{2+} oscillations, ruling out off-target inhibition of

Complex I (data not shown). Complex II activity, which was equivalent between wild-type and *ob/ob* islets, was unaffected by treatment with Cdk1 inhibitor (Figure 4.2E). No difference in mitochondrial mass was observed between wild-type and *ob/ob* islets (Figure 4.2F). These results directly identify Complex I as a target of Cdk1 signaling, which is highly active in *ob/ob* relative to wild-type islets.

Activation of Cdk1 and Complex I Correlates with Ca^{2+} Influx

Because of the important linkage between the metabolic generation of ATP/ADP and plasma membrane depolarization in β-cells, we predicted that glucose-stimulated Ca^{2+} influx should be higher in *ob/ob* islets, and more sensitive to Cdk1 inhibition. A recent study by Quesada and colleagues (4) had already established that Ca^{2+} influx in *ob/ob* islets is triggered at a lower glucose concentration than in wild-type islets (Km ~5.6 vs 7 mM). The data in Figure 4.3 confirms this result; when exposed to a typical subthreshold glucose level (6 mM), 94% of *ob/ob* islets (n = 49) displayed Ca^{2+} oscillations compared to only 9% of lean controls (n = 47) (Figure 4.3C, 4.3F). The same conclusion can be drawn by examining the oscillatory plateau fraction – also known as the pulse-width or activity fraction – which is the fraction of time the islet spends in the active state during each Ca^{2+} oscillation. This parameter is useful because it directly relates the sensitivity of β-cell Ca^{2+} to glucose metabolism (17,19,32). *Ob/ob* islets stimulated by 8 mM glucose exhibited significantly a higher plateau fraction (0.50 ± 0.09, n = 38) than wild-type islets stimulated by 10 mM glucose (0.35 ± 0.07, n = 47) (Figure 4.3B, 4.3E). As predicted, overnight treatment with Cdk1 inhibitor reduced the plateau fraction by 9 ± 3% in wild-type islets ($P < 0.0001$) compared with 15 ± 1% in *ob/ob* islets ($P < 0.0001$). The alternative Cdk1/2 inhibitor SU9516 (33), which was otherwise omitted from this study because its effects on insulin secretion are dominated by Cdk2 inhibition (34), nonetheless had a similar effect to reduce Ca^{2+} plateau fraction when applied overnight (0.1% DMSO, 0.54 ± .01, n = 30; 5 μM SU9516, 0.39 ± .006, n = 66, $P < 0.0001$); no acute effects of

either inhibitor were observed (data not shown). Collectively, the data in Figures 2-3 indicate that Cdk1, acting via Complex I, is coupled to downstream oscillations in Ca^{2+}, the direct trigger for insulin release.

Cdk1, by Stimulating Mitochondrial Respiration, Restricts the Metabolic Amplifying Pathways of Insulin Secretion

We next tested the effects of Cdk1 inhibition on glucose-stimulated insulin secretion using islets isolated from wild-type and *ob/ob* mice (Figures 4A and 4B). Insulin secretion and content were higher overall in the *ob/ob* islets, although secretion appears lower when normalized to insulin content. Interestingly, insulin secretion stimulated by 16.7 mM glucose was increased by Cdk1 blockade with RO-3306, by 151 ± 13% in wild-type islets and 266 ± 32% in *ob/ob* islets (Figure 4.4A). Insulin content was unaffected by Cdk1 inhibition in wild-type islets and reduced in *ob/ob* islets (Figure 4.4B), not by enough to account for the increased insulin secretion. These results, taken together with Figures 2-3, reveal a reciprocal relationship between Complex I flux and insulin secretion.

Since Ca^{2+} influx was reduced by Cdk1 inhibition (Figure 4.3), we hypothesized that glucose-derived carbon was diverted to the metabolic amplifying pathways that emanate from the mitochondrial TCA cycle (18). To test this idea, "K_{ATP}-independent" insulin secretion was measured from islets exposed to 1.7 mM or 16.7 mM glucose in the continuous presence of 200 μM diazoxide (to open K_{ATP} channels) and 30 mM KCl (to depolarize the plasma membrane) (Figure 4.4C). In wild-type islets, KCl-induced insulin secretion increased in response to glucose elevation, reflecting metabolic amplification, while KCl-induced secretion from *ob/ob* islets started higher and was fully saturated in low glucose. Treatment with Cdk1 inhibitor approximately doubled the K_{ATP}-independent secretory capacity in all treatments. In this case, insulin content was unaffected by Cdk1 inhibition (Figure 4.4D). These data indicate that Cdk1, acting though Complex I, sets the dynamic

range of the metabolic amplifying pathway, and imply that activation of the triggering pathway inductively removes carbon from the metabolic amplifying pathway. A model is shown in Figure 4.5.

DISCUSSION

Here, we demonstrate that Cdk1 signaling is active in quiescent β-cells, and upregulated in β-cells from obese (*ob/ob*) mice, a model of proliferative signaling and adaptive β-cell mass expansion. While the mechanism of this effect appears to be the stabilization of Cyclin B1 mRNA and protein, the bulk of our experiments were focused on understanding the dominant effects of Cdk1 on islet function and insulin secretion. Using NAD(P)H FLIM and respirometry in combination with the small-molecule Cdk1 inhibitor RO-3306 (20), we demonstrate that both mouse and human islets exhibit Cdk1-dependent activation of mitochondrial Complex I. Intriguingly, activation of the β-cell ETC reduces insulin secretion by limiting the metabolic amplifying pathways.

Prior studies show that mitochondrial Cdk1 phosphorylates Complex I, and that phosphorylation-insensitive mutants of Complex I block the effects of Cdk1/Cyclin B1 on oxidative phosphorylation and ATP production (13–16). As our islet respirometry experiments directly implicate Complex I as the target of Cdk1 in β-cells, this mechanism seems an obvious explanation. However, we make no claim to have proven that the global application of Cdk1 inhibitor affects the mitochondria directly, as the observed reduction in Complex I flux could in principle reflect non-mitochondrial Cdk1-dependent signaling pathways, such as the recently discovered FoxM1/Plk1/CENP-A pathway (8). Notably, Plk1 is known to activate Cdk1 through a positive feedback loop involving the Cdc25 proteins (7), and we show that Cdc25c mRNA is increased in *ob/ob* islets relative to controls (Figure 4.1 and (5)). RO-3306 had no acute effects on metabolic or Ca^{2+} oscillations (data not shown), arguing against dynamic regulation of Complex I by rapidly-

reversible phosphorylation, and placing the inhibitor's effects on a similar timescale to the restriction of Cdk1 signaling observed following overnight inhibition of autocrine insulin signaling (8).

Given that Cdk2 is also activated by insulin receptor signaling (8,35), one potential confounder is that RO-3306 is reported to inhibit Cdk1 with only 10-fold selectivity over Cdk2 (Ki, 35 vs. 340 nM) (20). Importantly, though, RO-3306 arrests proliferating cells at G2 rather than G1, suggesting that it does not inhibit Cdk2 or Cdk4 *in vivo* (20,36). The available data suggests furthermore that Cdk1 and Cdk2/4 control different pathways. Not only is the subcellular distribution of Cdk1 distinct from Cdk2 and Cdk4 (Figure 4.1 and (28)), but our recent collaborative study showed that both whole-animal and pancreas-specific $Cdk2^{-/-}$ mice exhibit reduced insulin secretion (34), whereas Cdk1 restriction increased glucose and KCl-stimulated insulin secretion. Likely, the timing of proliferative signaling carried out in the mitochondrial and cytosolic/nuclear compartments by Cdk1 and Cdk2 are coordinated by insulin receptor signaling (8), to different ends.

We also established a novel role of Cdk1/Complex I to counterbalance ETC function and the metabolic amplifying pathway of insulin secretion. Notably, the inhibition of carnitine acyl-carnitine translocase (*Slc25a20*), which fuels the TCA cycle by transporting fatty acids into the mitochondria, increases insulin secretion (37). Likewise, inhibition of Complex I by rotenone in permeabilized islets stimulated with ADP and PEP was found to increase K_{ATP}-independent insulin secretion (38), and here we show using NAD(P)H FLIM and respirometry that Cdk1/Complex I inhibition enhances K_{ATP}-independent insulin secretion in intact islets (Figures 2 and 4). Finally, data provided by our collaborator Richard Kibbey (personal communication) shows that accelerating the TCA cycle via double knockout of pyruvate dehydrogenase kinases 2/4 ($Pdk2^{-/-}$ $Pdk4^{-/-}$), both inhibitors of pyruvate dehydrogenase (PDH), reduced second-phase insulin secretion by 50% in an islet perifusion assay ($n = 4$, $P < 0.0001$). Collectively, these data mitigate doubts about the pharmacologic approach employed here, and show that the balance between oxidative

phosphorylation and the metabolic amplifying pathways is determined by the flux through the TCA cycle and Complex I of the ETC.

As the consensus model of the β-cell secretory pathway continues to be revised, an important discovery is that Complex I activation is antagonistic to one or more of the metabolic amplifying pathways of insulin secretion (see the model in Figure 4.5). As Complex I activation would not be expected to restrict glucokinase, which admits glucose to glycolysis (39), we expect little effect on the glycolytic amplifying pathways that provide glucose-6-phosphate for adenylosuccinate (S-AMP) signaling (40), and glycerol-3-phosphate for the glycerolipid/free fatty acid cycle (41). Pyruvate and PEP cycling, on the other hand, is almost certainly affected by ETC inhibition. Pyruvate entering the TCA cycle through PDH raises the levels of citrate and isocitrate, which can exit the mitochondria and through cytosolic malic enzyme (ME1) or isocitrate dehydrogenase (IDH1) raise the cytosolic levels of NADPH, a critical amplifying factor that feeds the free radical scavenging SENP1 pathway (42). Accelerating NADH consumption by Complex I could limit citrate-isocitrate departure, depleting cytosolic NADPH, or if the cytosolic aconitase (ACO1) and IDH1 reactions run in reverse to accommodate the cytosolic α-ketoglutarate deposited by the oxoglutarate carrier, then cytosolic NADPH would be consumed. Either possibility is consistent with the observed reduction in NAD(P)H lifetime when the Complex I flux is slowed by Cdk1 blockade. Finally, increased TCA cycle/ETC activity could disturb pyruvate carboxylase (PC)-dependent (anaplerotic) fluxes by depleting allosteric activation of PC by acetyl-CoA and limiting PEP production by mitochondrial PEPCKm, which is required for insulin secretion (43). Thus, Cdk1 signaling – or indeed any mechanism that increases flux through the TCA cycle and ETC without also increasing glucose uptake – would be predicted to restrict insulin secretion through the metabolic amplifying pathways. By further constraining the β-cell consensus model, our data enables testable predictions surrounding the mitochondrial amplifying pathways.

In conclusion, our findings have important and broad conceptual implications for type 2 diabetes therapies. We demonstrate that for a given level of glucose, the secretory pathway can be internally remodeled to tune the glucose responsiveness of the β-cell. Notably, currently available drugs that increase insulin secretion by stimulating glucose uptake (e.g. non-liver specific glucokinase activators) increase the metabolic workload on each β-cell (12), leading to glucotoxic-like damage (44). Drugs that increase insulin secretion by directly triggering membrane depolarization such as sulfonylureas, while invaluable for treating some forms of maturity-onset diabetes of the young (MODY) (45), decouple β-cell nutrient sensing with insulin secretion. Further studies aimed at remodeling the β-cell metabolic pathways could lead to a treatment for diabetes that avoids these pitfalls.

Figure 4.1

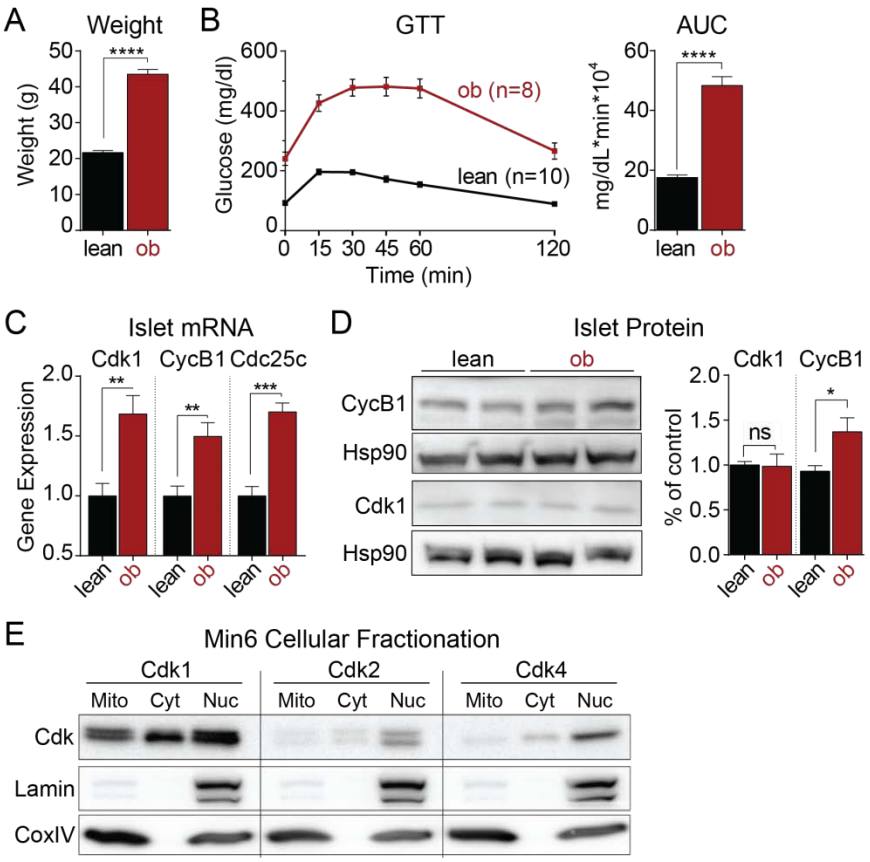

Figure 4.1. Cdk1 signaling is upregulated in islets from obese (*ob/ob*) mice. Body weight **(A)** and glucose tolerance test (GTT) **(B)** of lean (i.e. wild-type) and (n = 8) and *ob/ob* (n = 8) mice aged 8-14 weeks. GTT data is reported as area under the curve (AUC) **(C)**. **(D)** Normalized islet gene expression in lean and *ob/ob* mice aged 10 weeks mined from Keller et al. (5) (diabetes.wisc.edu) for Cdk1, Cyclin B1 (cycB1), and Cdc25c (n = 5 mice per condition). **(E)** Representative Western blot of Cyclin B1 and Cdk1 in lean and *ob/ob* islets. Protein levels were quantified after normalizing to Hsp90 loading controls (n = 5-9 islet preparations per condition). **(F)** Western blot showing Cdk1, Cdk2, Cdk4 expression and together with mitochondrial (Cox IV) and nuclear (Lamin A/C) markers and following Min6 cellular fractionation. Representative of 2 independent experiments. Data are mean ± SEM and were compared by t test (A-B) or ANOVA with Sidak's post-test (C-D). * P < 0.05, ** P < 0.01, *** P < 0.001, **** P < 0.0001.

Figure 4.2

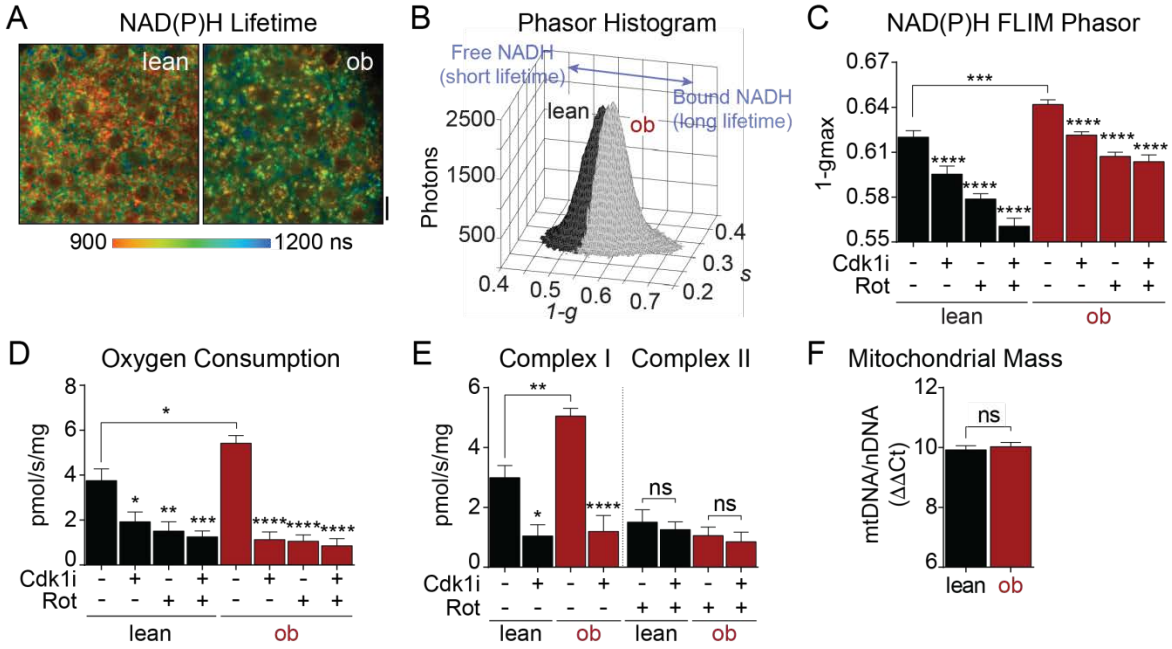

Figure 4.2. Cdk1 increases mitochondrial NADH utilization by activating flux through Complex I. (A) Representative multiphoton images showing the intensity-weighted mean NAD(P)H lifetime of lean and *ob/ob* islets. n = 20-22 islets per condition from 2 mice each. Scale bar = 5 μm. **(B)** Representative phasor histograms showing the frequency distribution of NAD(P)H lifetimes (*1-g*, *s*) in lean (n = 10) and *ob/ob* (n = 10) islets imaged in 10 mM glucose. Projection of the phasor histogram peak along the abscissa **(C)** was used to quantify bound:free NAD(P)H in lean and *ob/ob* islets in the presence of 10 mM glucose, Cdk1 inhibitor (Cdk1i) (5 μM RO-3306, 12 hr), and Complex I inhibitor (Rot) (5 μM rotenone, 15 min) as indicated. n = 20-22 islets per condition. **(D-E)** Oxygen consumption rate (OCR) of lean and *ob/ob* islets measured from 5 mice per condition (150 islets per mouse) with inhibitor treatments equivalent to (A-C). Complex I and Complex II flux calculated from state 3 respiration (D) are shown in (E). **(F)** Mitochondrial mass in lean and *ob/ob* islets was proxied by the ratio of mitochondrial DNA (mtDNA) to nuclear DNA (nDNA) (n = 3 mice per condition). Data are mean ± SEM and were compared by t test (F) or ANOVA with Sidak's post-test (C-E). * $P < 0.05$, ** $P < 0.01$, *** $P < 0.001$, **** $P < 0.0001$.

Figure 4.3

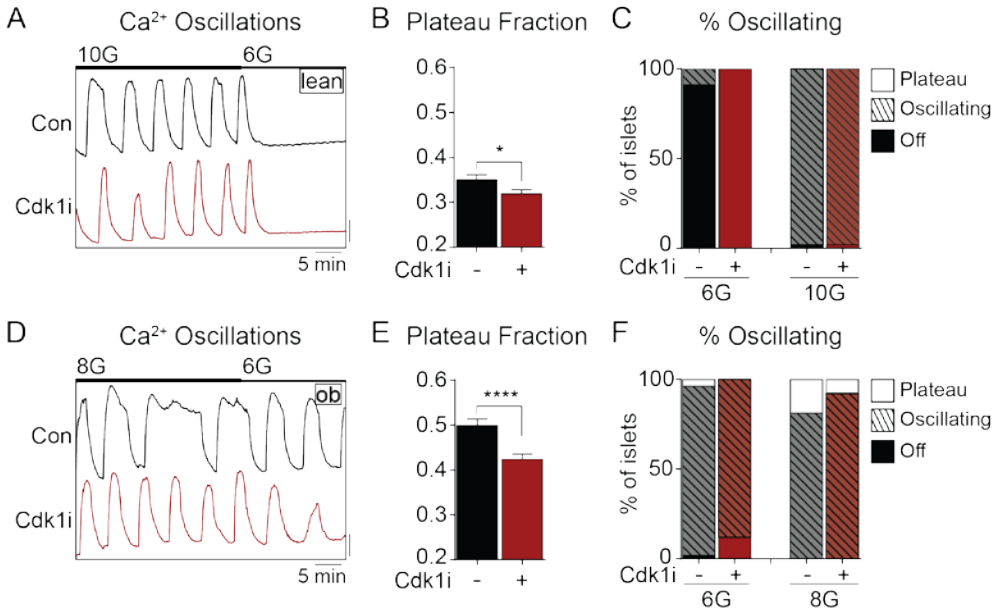

Figure 4.3. Ca^{2+} influx is correlated with Cdk1/Complex I activity. Ca^{2+} oscillations in lean **(A-C)** and *ob/ob* **(D-F)** islets in the presence of 6-10 mM glucose. The islets were pre-treated with 0.1% DMSO (Con) or Cdk1i (5 μM, 12 hr) as indicated. The plateau fraction at 10 mM glucose (lean, B) and 8 mM glucose (*ob/ob*, E) was calculated as the fraction of time spent in the active state of each oscillation. The active state was defined as >50% oscillation amplitude. At each glucose concentration, the percent of islets in the plateau, oscillating, or off state is shown for lean (C) and *ob/ob* (F) islets. Lean, $n = 100$ islets from 3 mice; ob/ob, $n = 100$ islets from 3 mice. Data are mean ± SEM and were compared by t test. * $P < 0.05$, **** $P < 0.0001$.

Figure 4.4

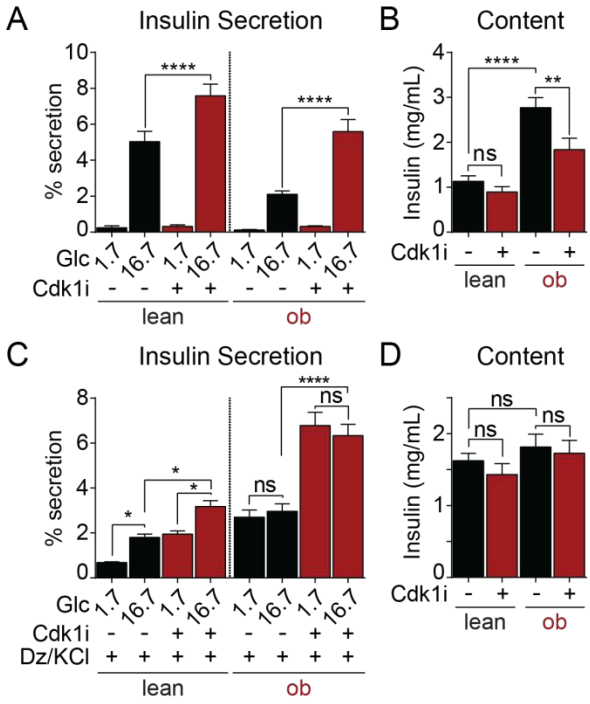

Figure 4.4. Cdk1 signaling limits the metabolic amplifying pathways of insulin secretion. (A-B) *Ex vivo* glucose-stimulated insulin secretion (A) and content (B) in islets isolated from lean (n = 3) and *ob/ob* (n = 3) mice. Islets were pre-treated with vehicle (0.1% DMSO) or Cdk1i (5 μM, 12 hr). **(C-D)** K_{ATP} channel-independent insulin secretion (C) and content (D) measured in islets isolated from from lean (n = 3) and *ob/ob* (n = 3) mice in the presence of 30 mM KCl and 200 μM diazoxide (Dz/KCl). Islets were pre-treated with vehicle or Cdk1i as in A-B. Data are mean ± SEM and were compared by ANOVA with Sidak's post-test. * $P < 0.05$, ** $P < 0.01$, **** $P < 0.0001$.

Figure 4.5

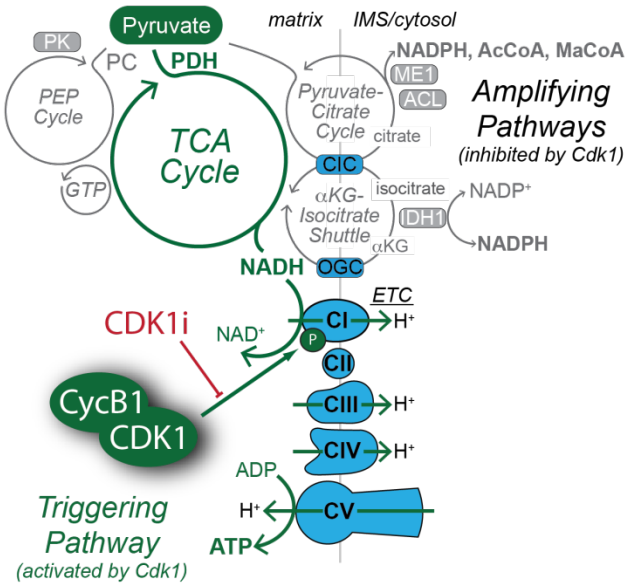

Figure 4.5. Proposed regulation of β-cell mitochondrial fluxes by Cdk1-dependent activation of Complex I. Model showing the inverse relationship between TCA cycle/ETC activation and insulin secretion through the metabolic amplifying pathways. Activation mitochondrial Cdk1 by Cyclin B1 (CycB1) increases Complex I (CI) flux, which increases NADH turnover and consumption of TCA cycle intermediates, reducing metabolic flux through one or more cycles (e.g. the PEP or pyruvate-citrate cycles) or shuttles (e.g. α-ketoglutarate-isocitrate) that produce metabolic coupling factors (NADPH, AcCoA, MaCoA) known to amplify insulin secretion. Abbreviations: PDH, pyruvate dehydrogenase; PC, pyruvate carboxylase; OGC, oxoglutarate carrier; CIC, citrate-isocitrate carrier; IDH1, isocitrate dehydrogenase; ACL, ATP citrate lyase; ME1, malic enzyme; PEP, phosphoenolpyruvate; AcCoA, acetyl-CoA; MaCoA, malonyl-CoA; PK, pyruvate kinase; αKG, α-ketoglutarate.

Figure 4.S1

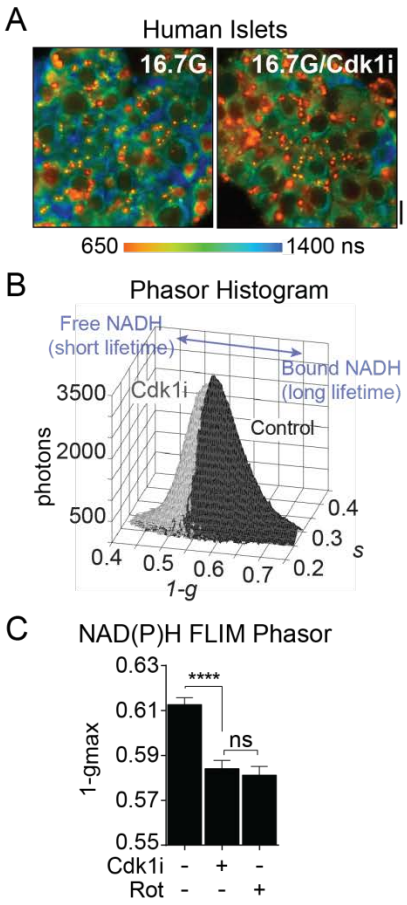

Figure 4.S1. Inhibition of Cdk1 reduces mitochondrial NAD(P)H utilization in human islets. Representative NAD(P)H mean lifetime images **(A)** and corresponding phasor histograms **(B)** in human islets stimulated with 16.7 mM glucose. Islets were pre-treated for 12 hr with vehicle (0.1% DMSO) or Cdk1i (5 μM) in the presence of 10 mM glucose. Scale bar = 5 μm. **(C)** Quantification of the phasor histogram peak along the abscissa (*1-g* axis). Vehicle (0.1% DMSO, 12 hr), n = 152 islets; Cdki (5 μM RO-3306, 12 hr), n = 151 islets; Rot (5 μM rotenone, 15 min), n = 146 islets. Data reflect islets from 9 human islet donors. Donor information is listed in Table S1. Data are mean ± SEM and were compared by ANOVA with Sidak's post-test. **** $P < 0.0001$.

Donor	Age (years)	Sex	BMI	HbA1c % (mmol/mol)
ACJV399A	41	F	43.1	6.5 (48)
ACJY368C	42	F	23.1	5.4 (36)
ACJ3270	24	M	50.4	5.6 (38)
ACKB319	49	F	31.6	5.2 (33)
ACKB044	32	F	31.3	5.1 (32)
ACKB010B	20	M	30.9	5.6 (38)
ACKH054A	58	F	35.1	4.8 (29)
ADAN146A	63	M	31.8	5.8 (40)
ADAT167	60	M	23.7	5.7 (39)

Table S1. Human Islet Donors from the Integrated Islet Distribution Program (IIDP).
Summary characteristics of donors studied by Unos ID. BMI – Body Mass Index, HbA1c – glycated hemoglobin.

REFERENCES

1. Bock T, Pakkenberg B, Buschard K. Increased islet volume but unchanged islet number in ob/ob mice. Diabetes. 2003 Jul;52(7):1716–22.

2. Golson ML, Misfeldt AA, Kopsombut UG, Petersen CP, Gannon M. High Fat Diet Regulation of β-Cell Proliferation and β-Cell Mass. Open Endocrinol J. 2010;4.

3. Park S-H, Ryu S-Y, Yu W-J, Han YE, Ji Y-S, Oh K, et al. Leptin promotes K(ATP) channel trafficking by AMPK signaling in pancreatic β-cells. Proc Natl Acad Sci USA. 2013 Jul 30;110(31):12673–8.

4. Irles E, Ñeco P, Lluesma M, Villar-Pazos S, Santos-Silva JC, Vettorazzi JF, et al. Enhanced glucose-induced intracellular signaling promotes insulin hypersecretion: pancreatic beta-cell functional adaptations in a model of genetic obesity and prediabetes. Mol Cell Endocrinol. 2015 Mar 15;404:46–55.

5. Keller MP, Choi Y, Wang P, Davis DB, Rabaglia ME, Oler AT, et al. A gene expression network model of type 2 diabetes links cell cycle regulation in islets with diabetes susceptibility. Genome Res. 2008 May;18(5):706–16.

6. DeFronzo RA. Lilly lecture 1987. The triumvirate: beta-cell, muscle, liver. A collusion responsible for NIDDM. Diabetes. 1988 Jun;37(6):667–87.

7. Wieser S, Pines J. The biochemistry of mitosis. Cold Spring Harb Perspect Biol. 2015 Feb 6;7(3):a015776.

8. Shirakawa J, Fernandez M, Takatani T, El Ouaamari A, Jungtrakoon P, Okawa ER, et al. Insulin Signaling Regulates the FoxM1/PLK1/CENP-A Pathway to Promote Adaptive Pancreatic β Cell Proliferation. Cell Metab. 2017 Apr 4;25(4):868–882.e5.

9. Kulkarni RN, Brüning JC, Winnay JN, Postic C, Magnuson MA, Kahn CR. Tissue-specific knockout of the insulin receptor in pancreatic beta cells creates an insulin secretory defect similar to that in type 2 diabetes. Cell. 1999 Feb 5;96(3):329–39.

10. Leibiger IB, Leibiger B, Berggren P-O. Insulin signaling in the pancreatic beta-cell. Annu Rev Nutr. 2008;28:233–51.

11. Wang M, Li J, Lim GE, Johnson JD. Is dynamic autocrine insulin signaling possible? A mathematical model predicts picomolar concentrations of extracellular monomeric insulin within human pancreatic islets. PLoS ONE. 2013;8(6):e64860.

12. Porat S, Weinberg-Corem N, Tornovsky-Babaey S, Schyr-Ben-Haroush R, Hija A, Stolovich-Rain M, et al. Control of pancreatic β cell regeneration by glucose metabolism. Cell Metab. 2011 Apr 6;13(4):440–9.

13. Dephoure N, Zhou C, Villén J, Beausoleil SA, Bakalarski CE, Elledge SJ, et al. A quantitative atlas of mitotic phosphorylation. Proc Natl Acad Sci USA. 2008 Aug 5;105(31):10762–7.

14. Wang Z, Fan M, Candas D, Zhang T-Q, Qin L, Eldridge A, et al. Cyclin B1/Cdk1 coordinates mitochondrial respiration for cell-cycle G2/M progression. Dev Cell. 2014 Apr 28;29(2):217–32.

15. Qin L, Fan M, Candas D, Jiang G, Papadopoulos S, Tian L, et al. CDK1 Enhances Mitochondrial Bioenergetics for Radiation-Induced DNA Repair. Cell Rep. 2015 Dec 15;13(10):2056–63.

16. Veas-Pérez de Tudela M, Delgado-Esteban M, Maestre C, Bobo-Jiménez V, Jiménez-Blasco D, Vecino R, et al. Regulation of Bcl-xL-ATP Synthase Interaction by Mitochondrial Cyclin B1-Cyclin-Dependent Kinase-1 Determines Neuronal Survival. J Neurosci. 2015 Jun 24;35(25):9287–301.

17. Henquin JC. Regulation of insulin secretion: a matter of phase control and amplitude modulation. Diabetologia. 2009 May;52(5):739–51.

18. Prentki M, Matschinsky FM, Madiraju SRM. Metabolic signaling in fuel-induced insulin secretion. Cell Metab. 2013 Aug 6;18(2):162–85.

19. Gregg T, Poudel C, Schmidt BA, Dhillon RS, Sdao SM, Truchan NA, et al. Pancreatic β-Cells From Mice Offset Age-Associated Mitochondrial Deficiency With Reduced KATP Channel Activity. Diabetes. 2016 Sep;65(9):2700–10.

20. Vassilev LT, Tovar C, Chen S, Knezevic D, Zhao X, Sun H, et al. Selective small-molecule inhibitor reveals critical mitotic functions of human CDK1. Proc Natl Acad Sci USA. 2006 Jul 11;103(28):10660–5.

21. Digman MA, Caiolfa VR, Zamai M, Gratton E. The phasor approach to fluorescence lifetime imaging analysis. Biophys J. 2008 Jan 15;94(2):L14-16.

22. Gnaiger E, Kuznetsov AV. Mitochondrial respiration at low levels of oxygen and cytochrome c. Biochem Soc Trans. 2002 Apr;30(2):252–8.

23. Forstner H, Gnaiger E. Calculation of Equilibrium Oxygen Concentration. In: Polarographic Oxygen Sensors. Springer; 1983. p. 321–33.

24. Votion D-M, Gnaiger E, Lemieux H, Mouithys-Mickalad A, Serteyn D. Physical fitness and mitochondrial respiratory capacity in horse skeletal muscle. PLoS ONE. 2012;7(4):e34890.

25. Kuznetsov AV, Schneeberger S, Seiler R, Brandacher G, Mark W, Steurer W, et al. Mitochondrial defects and heterogeneous cytochrome c release after cardiac cold ischemia and reperfusion. Am J Physiol Heart Circ Physiol. 2004 May;286(5):H1633-1641.

26. Li H-B, Wang R-X, Jiang H-B, Zhang E-D, Tan J-Q, Xu H-Z, et al. Mitochondrial Ribosomal Protein L10 Associates with Cyclin B1/Cdk1 Activity and Mitochondrial Function. DNA Cell Biol. 2016 Nov;35(11):680–90.

27. Gavet O, Pines J. Activation of cyclin B1-Cdk1 synchronizes events in the nucleus and the cytoplasm at mitosis. J Cell Biol. 2010 Apr 19;189(2):247–59.

28. Fiaschi-Taesch NM, Kleinberger JW, Salim FG, Troxell R, Wills R, Tanwir M, et al. Human pancreatic β-cell G1/S molecule cell cycle atlas. Diabetes. 2013 Jul;62(7):2450–9.

29. Lakowicz JR, Szmacinski H, Nowaczyk K, Johnson ML. Fluorescence lifetime imaging of free and protein-bound NADH. Proc Natl Acad Sci USA. 1992 Feb 15;89(4):1271–5.

30. Blinova K, Carroll S, Bose S, Smirnov AV, Harvey JJ, Knutson JR, et al. Distribution of mitochondrial NADH fluorescence lifetimes: steady-state kinetics of matrix NADH interactions. Biochemistry. 2005 Feb 22;44(7):2585–94.

31. Blinova K, Levine RL, Boja ES, Griffiths GL, Shi Z-D, Ruddy B, et al. Mitochondrial NADH fluorescence is enhanced by complex I binding. Biochemistry. 2008 Sep 9;47(36):9636–45.

32. Nunemaker CS, Bertram R, Sherman A, Tsaneva-Atanasova K, Daniel CR, Satin LS. Glucose modulates [Ca2+]i oscillations in pancreatic islets via ionic and glycolytic mechanisms. Biophys J. 2006 Sep 15;91(6):2082–96.

33. Lane ME, Yu B, Rice A, Lipson KE, Liang C, Sun L, et al. A novel cdk2-selective inhibitor, SU9516, induces apoptosis in colon carcinoma cells. Cancer Res. 2001 Aug 15;61(16):6170–7.

34. Kim SY, Lee J-H, Merrins MJ, Gavrilova O, Bisteau X, Kaldis P, et al. Loss of Cyclin-dependent Kinase 2 in the Pancreas Links Primary β-Cell Dysfunction to Progressive Depletion of β-Cell Mass and Diabetes. J Biol Chem. 2017 Mar 3;292(9):3841–53.

35. Folli F, Okada T, Perego C, Gunton J, Liew CW, Akiyama M, et al. Altered Insulin Receptor Signalling and β-Cell Cycle Dynamics in Type 2 Diabetes Mellitus. PLoS One [Internet]. 2011 Nov 30 [cited 2017 May 16];6(11). Available from: http://www.ncbi.nlm.nih.gov/pmc/articles/PMC3227614/

36. Lapenna S, Giordano A. Cell cycle kinases as therapeutic targets for cancer. Nat Rev Drug Discov. 2009 Jul;8(7):547–66.

37. Soni MS, Rabaglia ME, Bhatnagar S, Shang J, Ilkayeva O, Mynatt R, et al. Downregulation of carnitine acyl-carnitine translocase by miRNAs 132 and 212 amplifies glucose-stimulated insulin secretion. Diabetes. 2014 Nov;63(11):3805–14.

38. Pizarro-Delgado J, Deeney JT, Corkey BE, Tamarit-Rodriguez J. Direct Stimulation of Islet Insulin Secretion by Glycolytic and Mitochondrial Metabolites in KCl-Depolarized Islets. PLoS ONE. 2016;11(11):e0166111.

39. Doliba NM, Qin W, Najafi H, Liu C, Buettger CW, Sotiris J, et al. Glucokinase activation repairs defective bioenergetics of islets of Langerhans isolated from type 2 diabetics. Am J Physiol Endocrinol Metab. 2012 Jan 1;302(1):E87–102.

40. Gooding JR, Jensen MV, Dai X, Wenner BR, Lu D, Arumugam R, et al. Adenylosuccinate Is an Insulin Secretagogue Derived from Glucose-Induced Purine Metabolism. Cell Rep. 2015 Oct 6;13(1):157–67.

41. Zhao S, Mugabo Y, Iglesias J, Xie L, Delghingaro-Augusto V, Lussier R, et al. α/β-Hydrolase domain-6-accessible monoacylglycerol controls glucose-stimulated insulin secretion. Cell Metab. 2014 Jun 3;19(6):993–1007.

42. Ferdaoussi M, Dai X, Jensen MV, Wang R, Peterson BS, Huang C, et al. Isocitrate-to-SENP1 signaling amplifies insulin secretion and rescues dysfunctional β cells. J Clin Invest. 2015 Oct 1;125(10):3847–60.

43. Stark R, Pasquel F, Turcu A, Pongratz RL, Roden M, Cline GW, et al. Phosphoenolpyruvate cycling via mitochondrial phosphoenolpyruvate carboxykinase links anaplerosis and mitochondrial GTP with insulin secretion. J Biol Chem. 2009 Sep 25;284(39):26578–90.

44. Nakamura A, Terauchi Y. Present status of clinical deployment of glucokinase activators. J Diabetes Investig. 2015 Mar;6(2):124–32.

45. Kim S-H. Maturity-Onset Diabetes of the Young: What Do Clinicians Need to Know? Diabetes Metab J. 2015 Dec;39(6):468–77.

Chapter 5

Discussion

Summary

Aging and obesity are major risk factors for T2D. In the pancreatic islet, both induce adaptive compensation by pancreatic β cells. In the work presented here, we defined strong linkages between changes in mitochondrial respiration and insulin secretion in response to these stressors.

Work presented in Chapter 3 of this dissertation tested the hypothesis that impaired β-cell respiration underlies the age-associated phenotype of compromised insulin secretion in both mouse and human islets. This was the case in human islets. However, we also demonstrated that aged mouse islets maintain adequate insulin secretion through compensation linked to K_{ATP} ion channel function.

Chapter 4 examined changes in mitochondrial metabolism associated with obesity, focusing on the induction of Cdk1 signaling and its consequences for insulin secretion. We showed that the obesity-associated increase in Cdk1 signaling enhances mitochondrial respiration, but, surprisingly, this negatively impacted the secretory pathway in β-cells. This suggests that increased β-cell mass may come at the expense of the secretory capacity of the β cell, limiting functional compensation.

As a central part of these studies, we introduced Fluorescence Lifetime Imaging of NAD(P)H to the islet field, a technique especially useful for examining β-cell TCA cycle and ETC function. Significant work remains to take full advantage of the capabilities of NAD(P)H FLIM, some of which will be addressed later in this chapter. Nonetheless, the work described in this dissertation also represents some of the first steps toward discovering what NAD(P)H FLIM can tell us about islet metabolism.

Future Work in Aging Islets

Comparison of the species-specific effects of aging on β-cell metabolism revealed important differences in human and mouse islet biology. Human islet insulin secretion measurements also revealed an age-dependent defect in stimulated insulin secretion ($R^2 = 0.51$, $P < 0.0001$). Mouse islets, by contrast, showed improved insulin secretion with age. We found that islets from aged mice compensated for mitochondria defects with restricted β-cell K_{ATP} channel conductance, which in turn increased the glucose sensitivity of the plasma membrane. In this research, it was not possible to establish the origin of the K_{ATP} channel conductance differences based on perforated patch clamp electrophysiology measurements alone. Perforated patch clamp analysis is not capable of distinguishing between changes in the K_{ATP} channel number versus changes in individual channel competence. Several additional experiments will be necessary in order to make this distinction. Individual channel flux rates should be directly assessed using either a cell-attached patch clamp or excised patch clamp techniques. If the individual channel conductance rates prove similar between young and aged mouse islets, the observed difference is K_{ATP} channel conductance is like due to changes in K_{ATP} channel expression on the plasma membrane. Variation in K_{ATP} channel number could potentially derive from defects in channel trafficking to the plasma membrane, but a more likely cause would be the decreased proliferative signaling associated with aging. As expression levels of K_{ATP} channel subunit Kir6.2 are directly impacted by Cdk2/4-E2F signaling pathways, decreased proliferative signaling—specifically decreased Cdk2/4 activity—associated with age likely also reduces Kir6.2 expression in aged islets. Comparing islet Kir6.2 protein and mRNA levels between young and aged mouse islets will provide insight into this hypothesis.

The source of age-related mitochondrial dysfunction in both mouse and human islets remains unresolved. The observed decrease in flux through both Complex I and Complex II in mice—by 52% and 57%, respectively—could result from a number of phenomena. The most

straightforward possibility is that the decrease in ETC flux is due to decreased mitochondrial mass in aged islets, a phenomenon observed in several other tissue types (1). Quantifying mitochondrial mass or mitochondrial DNA copy number—techniques used in Chapter 4—would be a simple follow-up experiment to address this possibility. However, if mitochondrial number is not significantly impacted by age in islets, the observed decrease in flux could then result from one of two processes: either a decrease in production of ETC fuel (i.e. a defect in glucose oxidation), or decreased consumption due to dysfunction of the ETC itself. A metabolic control analysis (2), which provides a bioenergetics description of ETC function by quantitatively relating mitochondrial membrane potential to respiration, would begin to address this question.

Future Work on Cdk Signaling in Aging Islets

As mentioned in Chapter 1, Helman et al. identified a link between the age-related increase in β-cell senescence and increased insulin secretion (3). This finding was related to increased expression of the Cdk4 inhibitor p16INK4a, which also indirectly inhibits Cdk2, and was proposed to increase mitochondrial biogenesis due to increased mTOR and PGC-1α signaling. The authors also observed increased oxygen consumption rates in islets over-expressing p16INK4a. These findings raise the question: would the effects of aging, namely decreased mitochondrial respiration, be exacerbated if not for the accompanying decrease in proliferative signaling due to senescence? This possibility raises important and unanswered questions about the relationship between Cdk1 activity and senescing islets. Based on the data presented herein, one hypothesis is that decreased Cdk1 activity would enhance the amplifying pathway in aged islets, facilitating increased compensatory insulin secretion. Unfortunately, due to small sample size, we observed no correlation between age and the effect of Cdk1 inhibitor on mitochondrial TCA cycle/ETC function in human islets, which we examined with NAD(P)H FLIM (R^2 = 0.25) (Figure 5.1). Additional research is

needed to understand the link between age-associated decreases in proliferative signaling and mitochondrial function.

Future Work on the Impact of Proliferative Signaling on β-Cell Function

Islet mitochondrial function in the context of obesity and increased proliferative signaling was also examined. We reported that in *ob/ob* islets, increased Cdk1 activity enhanced mitochondrial oxidative flux through Complex I of the electron transport chain by 41% ±11%. As expected due to the tight linkage between ETC flux and Ca^{2+} signaling in pancreatic islets, increased Complex I flux increased in proportion to Ca^{2+} influx. Surprisingly, we found that increased Ca^{2+} and mitochondrial activity correlated with a reduction in the amplification pathways of glucose-stimulated insulin secretion, ultimately decreasing the overall magnitude of insulin secretion in *ob/ob* islets.

These experiments were carried out using the small-molecule inhibitor RO-3306. Although considerable work has been done to demonstrate the specificity and efficacy of this inhibitor, concerns with inhibitor-based studies remain. RO-3306 is a competitive inhibitor for the ATP-binding pocket of Cdk1 with a Ki of 35 nM. Work by Vassilev et al. revealed a 10-fold specificity for Cdk1 over Cdk2 and a still greater 50-fold selectivity over Cdk4 (4–8). The authors also found at least a 15-fold difference in Ki between Cdk1 and a suite of other cellular kinases, including a nearly 60-fold difference in specificity over PKA, AKT, and ERK. Despite these validations, ATP-binding pocket-specific kinase inhibitors are notoriously non-specific (9–11). The International Center for Kinase Profiling, however, has tested other ATP-pocket Cdk inhibitors such as Roscovitine and has concluded that, at minimum, they meet acceptable standards for use as a pan-Cdk inhibitor. They have also suggested a minimum set of requirements for a kinase inhibitor to pass muster, and RO-3306 satisfies these requirements (12). Nonetheless, the validity of the results presented in Chapter 4 would be significantly enhanced by genetic-based verification, such as siRNA knock down of Cdk1

in either Min6 cells or dispersed islets, or through the expression of dominant-negative Cdk1 constructs. These approaches could be used to confirm the specific role of Cdk1 in modulating Complex I activity, and that flux through the TCA cycle and Complex I of the ETC determines the balance between ATP/ADP generation by oxidative phosphorylation and the metabolic amplifying pathway.

Future Work on the Balance Between ETC Flux and Amplifying Pathways

We have discovered an inverse relationship between the ETC/TCA flux and metabolic amplification of insulin secretion. We propose this to be a general feature of β-cell metabolism that merits further investigation. Well-known mitochondrially derived amplifying factors that play a role in the balance between triggering and amplifying pathways are PEP, cytosolic NADPH, Acetyl-CoA (AcCoA), and Malonyl-CoA (MalCoA). These amplifying factors are generated through the efflux of TCA-cycle intermediates into the cytosol, a process called cataplerosis (13). These cataplerotic shuttles/cycles include the pyruvate/citrate cycle, the pyruvate/malate cycle, the PEP cycle, and the α-ketoglutarate shuttle (Figure 5.2). Replenishment of TCA cycle intermediates, or anaplerosis, is fueled via pyruvate carboxylation to form oxaloacetate by pyruvate carboxylase (PC) and the irreversible consumption of pyruvate by pyruvate dehydrogenase (PDH) to create AcCoA (14). For every turn of the TCA cycle, cataplerotic flux in the form of citrate, isocitrate, α-ketoglutarate, or PEP reduces mitochondrial matrix levels of NADH and succinate. We propose that the cataplerotic shuttles then produce amplifying factors in the cytosol at the expense of ETC flux. In addition to describing glucose carbon utilization, this model can be understood through redox coenzymes, specifically, the balance between mitochondrial NADH generation and cytosolic NADPH production. Mitochondrial citrate-isocitrate carrier (CIC) is capable of running in reverse, importing cytosolic citrate into the mitochondrial matrix (15). If NADH demand is high enough, the TCA

cycle may act like a vortex, pulling cytosolic citrate into the mitochondrial matrix to feed oxidative phosphorylation.

To test this hypothesis, future development of several experimental tools will be instrumental for furthering our understanding of the relationship between ETC flux and the amplification of insulin secretion. Assay development and β-cell specific characterization of two fluorescence-based biosensors will be a critical first step. One of these sensors is the cytosolic citrate biosensor, Cit96μ. Cit96μ is a Venus/CFP (yellow/cerulean)-based FRET biosensor centered around the citrate binding domain of histidine sensor kinase CitA (16). Application of this biosensor in the cytosol of β cells would allow us to examine the level of cytosolic citrate and its relationship to islet metabolic and Ca^{2+} oscillations. In accordance with the idea that increased TCA flux would result in mitochondrial import of cytosolic citrate, preliminary experiments in our lab indicate that cytosolic citrate levels decrease upon glucose stimulation (Figure 5.3A). Oscillations in cytosolic citrate levels were also observed (Figure 5.3B). Further analysis of changes in citrate oscillation plateau fraction, as well as amplitude, would provide insight into the dynamics of citrate production. Experimentally, it is also worth considering the addition of a mitochondrial targeting sequence to the Cit96μ probe, modified with lower affinity to accommodate elevated mitochondrial citrate levels. Comparison of mitochondrial and cytosolic citrate level fluctuations in response to stimulatory glucose, or the application of electron transport chain inhibitors, would provide direct evidence of the balance between cataplerotic shutting and ETC flux.

Additionally, it would be worth developing the NADPH fluorescent biosensor Apollo-$NADP^+$ in intact islets. Apollo-$NADP^+$ is a homo-FRET anisotropy based sensor that relies on the homodimerization of a catalytically inactive mutant of NADPH-dependent glucose-6-phosphate dehydrogenase (17). Apollo-$NADP^+$ is theoretically capable of reporting fluctuations in cytosolic $NADP^+$/NADPH levels in islets in real time. In conjunction with cytosolic and mitochondria

Cit96μ measurements, Apollo-$NADP^+$ would provide a more complete picture of NADPH generation, a well-established amplifying factor in glucose-stimulated insulin secretion.

Based on our current understanding of the oscillatory characteristics of several metabolic and secretory factors in islets, such as Ca^{2+}, mitochondrial NADH, ATP, and mitochondrial membrane potential (MMP), it is possible to predict the phase relationships expected for cytosolic NADPH and mitochondrial citrate (18) (Figure 5.4). Similar to the out-of-phase relationship observed between MMP and mitochondrial NADH, mitochondrial citrate is likely out of phase with cytosolic citrate. As cytosolic citrate is used in the generation of cytosolic NADPH, NADPH oscillations would be predicted to oscillate in phase or at a slight lag relative to those of cytosolic citrate. Of course, experiments with the two biosensors detailed above will be integral to validating these hypothesizes.

Generation of several mouse lines would also be valuable for verifying this hypothesis. Inducible β-cell specific knock-ins of several pyruvate carboxylase and pyruvate dehydrogenase mutants would be priority models for development. Specifically, pyruvate dehydrogenase phospho-mimetic and phospho-resistant mutants S293D and S293A would provide critical insight into the role of PDH flux in metabolic amplification (19). PDH S293D has been shown to reduce mitochondrial ATP generation by ~50% in mouse oocytes compared to a non-statistically significant 10% increase conferred by the S293A mutant PDH. Tuning PDH flux would provide a more physiologically relevant picture compared to complete knock-out models. Similarly, the PC mutant A610T does not affect the enzyme's K_m for pyruvate, but rather results in a ~50% reduction in mitochondria import (20,21). Islets isolated from these mouse models should then be assayed for citrate and NADPH oscillations in addition to NAD(P)H-FLIM, oxygen consumption, and Ca^{2+} measurements.

Future Proteins of Interest

An additional protein of interest that fits nicely into this model is the mitochondrial protein nicotinamide nucleotide transhydrogenase (NNT). NNT is a mitochondrial inner membrane protein that takes advantage of the mitochondrial proton gradient to facilitate hydride transfer from NADH to NADPH in the mitochondrial matrix. Mitochondrial NADPH can then be used either by glutathione reductase/thioredoxin reductase to combat reactive oxygen species or by IDH2 running in reverse to make isocitrate (Figure 5.2) (22,23).

The role of NNT in insulin secretion is controversial in the field of islet biology. Some studies, some of which of which have been called into question, reveal that NNT plays a critical role in mitochondrial ROS detoxification and insulin secretion (24,25). Other studies have found no impact of NNT deletion on β-cell function (26). NNT has, however, also been shown to play an important role in β-cell compensation for diet-induced obesity (DOI), with NNT mutant mice gaining significantly more weight and exhibiting increased plasma glucose levels as a result of high-fat diet (27). Study of NNT are also particularly relevant because a large fraction of the islet biology field employs C57Bl6/J as their experimental model. In 2005, Toye et al. discovered, C57Bl6/J mice carry a series of mutations in the NNT gene that result in nonfunctional NNT protein in these mice (28). Discovery of a critically important role for NNT in insulin secretion or T2D progression would undeniably disrupt the field.

While our research into the effects of increased Cdk1 activity in the context of obesity were performed in NNT null C57Bl6/J mice, the impact of NNT phosphorylation on this phenomenon is yet to be examined. Regardless of the controversy surrounding NNT, it is perfectly poised as the next avenue of study to follow the work described in this dissertation. Not only does NNT appear to play a key role in cataplerotic shuttling and amplification of insulin secretion, but human NNT is also phosphorylated by mitochondrial Cdk1 at S^{400} and T^{467} (29).

Further Development of NAD(P)H FLIM

Considerable work also remains for improving our understanding of NAD(P)H FLIM results, which in turn will assist with the experiments proposed for further research. Ideally, the next step in developing FLIM for more detailed metabolic analysis would be to establish a database of NAD(P)H lifetimes bound to a suite of binding partners. This can be accomplished using free—i.e., in-solution—NADH/NADPH in conjunction with purified individual NAD(P)H binding proteins such as pyruvate dehydrogenase, isocitrate dehydrogenate 1/2/3, malic enzyme, malate dehydrogenase, and α-ketoglutarate dehydrogenase, to name a few. These *in vitro* experiments should then be repeated using a combination of inhibitors or knockdown/knockout models to validate that *ex vivo* changes in NAD(P)H lifetime values reflect the *in vitro* measurements. Then, by applying vector math and the FLIM analysis techniques described in Chapter 2, we can attempt to place individual NAD(P)H binding proteins on the universal circle. This is a daunting task, but if a database can be successfully established, one could use FLIM to probe specific biological questions and extrapolate metabolic changes based on shifts in phasor space and NAD(P)H binding partner. Similar work, focusing on a variety of intrinsic fluorophores in germ cells, was carried out by Stringari et al. and would serve as an experimental blueprint (30).

Even if resolving numerous NAD(P)H-dependent pathways proves unsuccessful, our work strongly suggests that NADPH FLIM can be used in islets as a specific assay for TCA cycle and ETC flux. This observation could be further validated with experiments examining the impact of alternate metabolic fuels and a suite of ETC inhibitors. One specific experimental example would be stimulating mitochondrial metabolism with leucine and a-ketoisocaproic acid (KIC), or glutamine plus BCH (a non-metabolizable activator of glutamate dehydrogenase), either of which bypass PDH,

feeding the TCA cycle. Effects of anaplerotic fuels could then be cross-examined with a suite of ETC inhibitors and parallel measurements of oxygen consumption.

Additionally, while we have observed that the g-axis variable on the phasor plot correlated with TCA cycle/ETC activity and drives changes in mean lifetime, the significance of s-axis movement in phasor space remains a mystery. Changes in s could, in theory, reflect changes in the number of components contributing to the histogram mixture. What seems a more likely explanation, however, is that s is a complex variable affected by numerous parameters we are yet to identify. As such, perhaps the more valuable variable would be an s:g ratio, the meaning of which remains to be tested but that could potentially indicate a relationship between lifetime change and the profile of NAD(P)H binding partners. Regardless of these remaining black boxes, it is clear that NAD(P)H FLIM is a powerful technique, ideally suited to analysis of islet function and type 2 diabetes.

Final Considerations

Current mainstream pharmacological treatment for type 2 diabetes primarily consists of two different drug classes: Metformin and sulfonylureas. The mechanism of action of sulfonylureas is not ideal and these drugs are generally viewed as the second line of pharmacologic defense against glucose dysregulation (31). This is because sulfonylureas decouple insulin secretion from blood glucose concentration. These drugs are direct inhibitors of the K_{ATP} channel subunit SUR1. Binding of sulfonylureas closes K_{ATP} channels, depolarizing the cell and inducing granule fusion, decoupling β-cell nutrient sensing from insulin secretion (32).

Metformin on the other hand is effective in more settings and more widely prescribed, although its mode of action is still not fully understood. Metformin is primarily recognized as an inhibitor of hepatic gluconeogenesis (33). One of the mechanisms of inhibition is proposed to be

direct inhibition of Complex I of the ETC (34). The corresponding decrease in ATP/ADP ratio inhibits PEP formation, thus decreasing gluconeogenesis (35). Metformin has also been shown to enhance insulin secretion, but the exact mechanism remains to be discovered. Interestingly, the effects of Metformin on Complex I are remarkably similar to the effects of Cdk1 inhibition. Like Cdk1 inhibitor treatment, Metformin reduces Complex I flux by only 40%, compared to the 80% inhibition seen with rotenone treatment (35). The difference in the magnitude of effect on Complex I between Metformin and rotenone is most likely due to the two inhibitors acting on different subunits in the complex (34). It seems likely that Cdk1 also acts on a different subunit. This suggests that the improvement in GSIS after Metformin treatment may be similar to the effect of Cdk1 inhibition, namely, an increase in the metabolic amplifying pathways in the β cell. Experiments examining amplifying-pathway activity and K_{ATP} independent insulin secretion could provide some insight into Metformin's mode of action. Metformin also inhibits cellular proliferation (36). While an unlikely target, it may also be informative to examine the effects of Metformin treatment of Cdk1 activity.

A significant amount of work also focuses on enhanced β-cell proliferation as a treatment for T2D. Based on the data presented in this dissertation, as well as findings from several other papers (3,37), new research should consider coupling pro-proliferative treatments with metabolic-based insulin secretion enhancers.

β cells are, in essence, organismal metabolic sensors. Understanding the mechanistic details that regulate β-cell metabolism is of paramount importance if we are to appropriately treat metabolic disorders like type 2 diabetes.

Figure 5.1

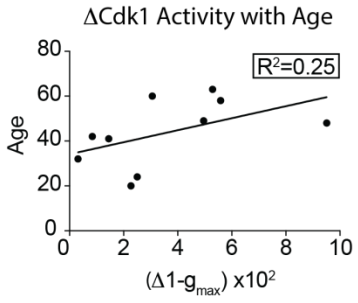

Figure 5.1. Cdk1 activity may be affected by age. In human islets, the change in NAD(P)H fluorescence lifetime ($\Delta 1\text{-}g_{max}$) between 10mM glucose and 10mM glucose after overnight treatment with 5μM Cdk1 inhibitor (RO-3306) as a function of donor age. (n = 9 human donors with 20 islets each). $R^2 = 0.25$. Donor information in Table 3.1.

Figure 5.2

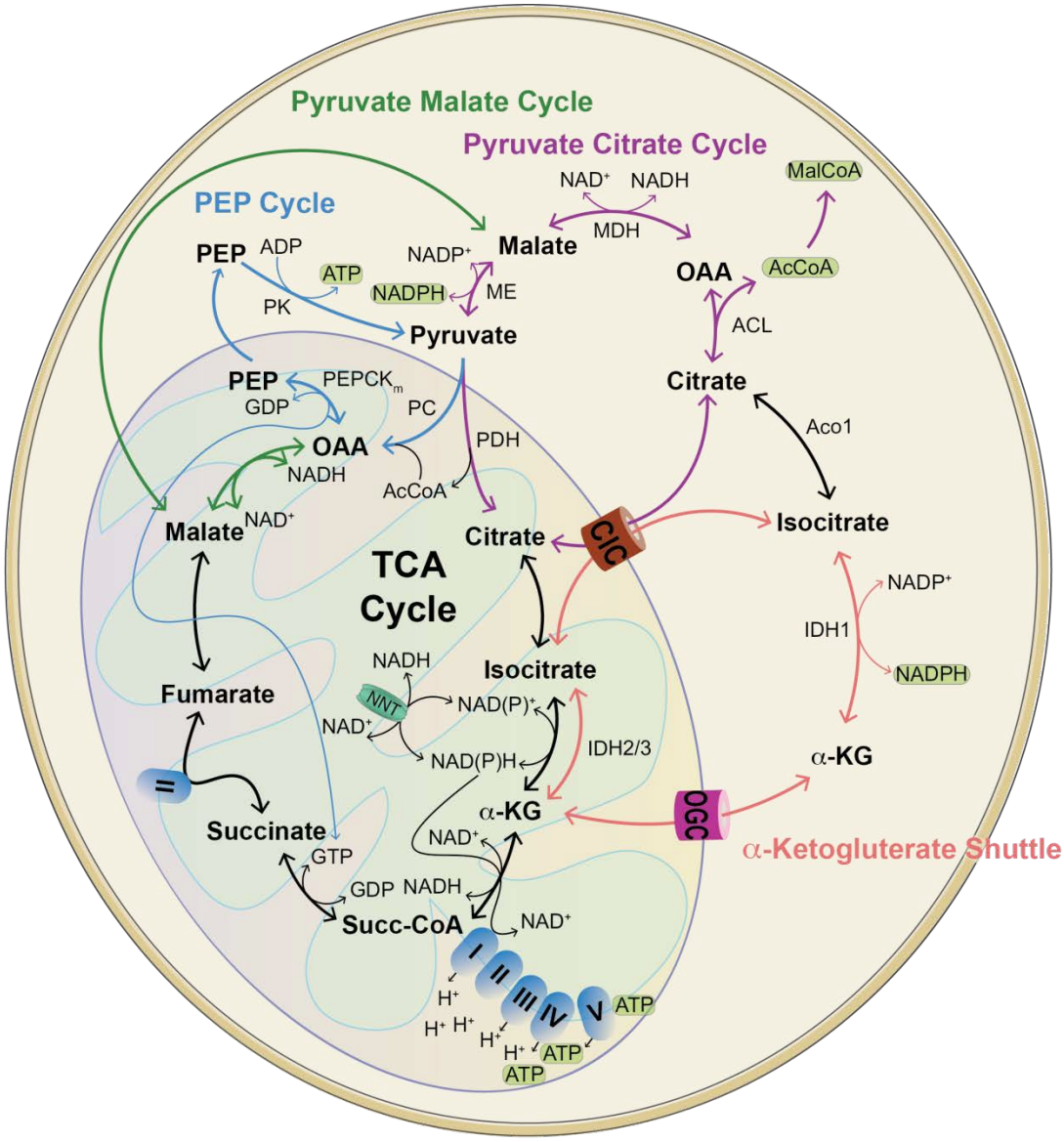

Figure 5.2. Mitochondrial shuttles contributing to metabolic amplification of insulin secretion. Pyruvate derived from glycolysis enters the mitochondria through the mitochondrial pyruvate carrier where it is used to generate energy in the form of ATP. Cataplerotic shuttling also uses pyruvate-derived intermediates to generate metabolic amplifying factors such as NADPH and MalonylCoA. In the Phosphoenolpyruvate cycle (blue), cytosolic ATP is generated through the dephosphorylation of PEP by Pyruvate kinase to form pyruvate which can reenter the mitochondria.

Once inside the mitochondria, two molecules of pyruvate—one in the form of AcCoA—can be converted into oxaloacetate via pyruvate carboxylase. Oxaloacetate (OAA) can then be converted back into PEP by mitochondrial PEPCK, a reaction which requires GTP generated by Succinyl-CoA sythetase. This completes the cycle. The pyruvate citrate cycle (purple) generates cytosolic NADPH and acetyl/malonylCoA by exporting citrate or isocitrate through the Citrate Isocitrate Carrier (CIC) into the cytosol. Once in the cytosol, isocitrate can be converted into citrate via Aconotase 1 (Aco1). Citrate in turn converts to OAA via ATP citrate lyase (ACL). Conversion of citrate to OAA produces AcCoA, which can then carboxylated by AcCoA carboxylate to form MalCoA. OAA is converted to pyruvate by malate dehydrogenase (MDH) and malic Enzyme (ME), which produces cytosolic NADPH. The α-Ketoglutarate (α-KG) cycle (salmon) produces cytosolic NADPH through cytosolic export of isocitrate through the CIC) followed by conversion to α-KG by isocitrate dehydrogenase 1 (IDH1). α-KG is then returned to the mitochondria through the oxoglutarate carrier (OGC). Mitochondria α-KG can be converted into isocitrate through NAD(P)H-dependent IDH2/3. The pyruvate malate cycle (green) uses ME to produce cytosolic NADPH in the conversion of exported malate into pyruvate. Finally, the TCA cycle (black) produces mitochondrial NADH, which is then consumed by the ETC to produce ATP. The TCA cycle also produces mitochondrial GTP in the conversion of Succinyl-CoA to succinate which is then used by the PEP cycle. The transhydrogenase NNT likely plays a role in regulating the balance between mitochondrial NADH and NADPH by exploiting mitochondrial membrane potential to drive the hydride transfer between the two coenzymes. Cartoon adapted from (Prentki, Matschinsky, and Madiraju 2013).

Figure 5.3

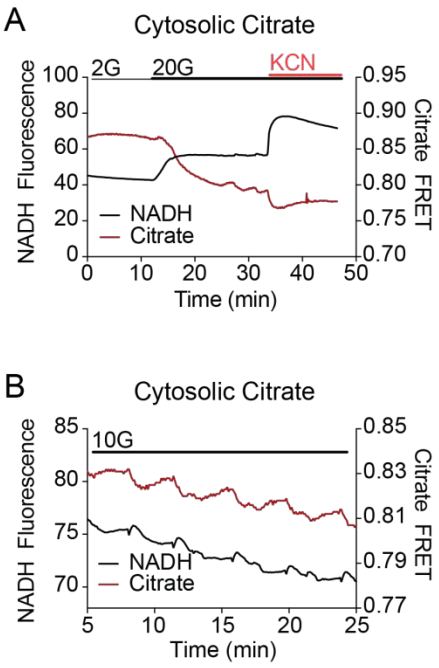

Figure 5.3. Changes in cytosolic citrate levels in response to glucose and ETC inhibitor. Representative NAD(P)H and FRET measurements taken from a B6J lean islet expressing cytosolic citrate biosensor Cit96μ. **A**) Islets were exposed to 2mM, then 20mM glucose, followed by 20mM glucose plus 5mM KCN to inhibit ETC activity and induce mitochondrial membrane depolarization. **B**) Representative oscillations of NAD(P)H and cytosolic citrate in islets exposed to 10mM glucose.

Figure 5.4

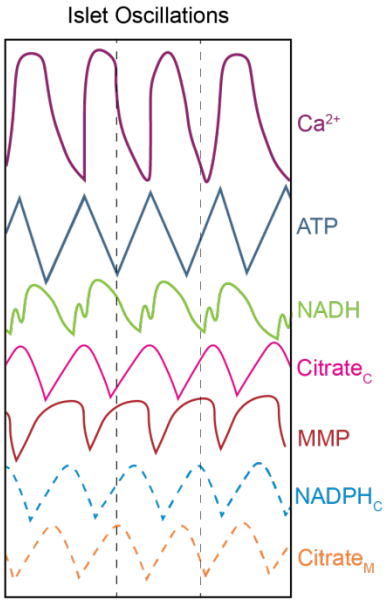

Figure 5.4 Schematic of Islet Metabolic Oscillations. Schematic representing the shape and phase relationship of several oscillating molecules, both known (solid lines) and unknown (dashed lines) in pancreatic islets. The phase relationship between Ca^{2+} (purple) and ATP (dark blue) is largely determined by the action of ER calcium pump activity and is predictably out of phase. Additionally, mitochondrial NADH (green) and mitochondrial membrane potential (red) are out of phase as Complex I flux increased mitochondrial proton gradient at the expense of NADH. Cytosolic citrate levels (pink) rise with the generation of ATP and are anti-correlated with NADH and predicted mitochondrial citrate oscillations (orange). Finally, the oscillatory behavior of cytosolic NADPH is predicted to be 90 degrees out of phase with mitochondrial NADH and related to cytosolic citrate oscillator behavior.

REFERENCES

1. Barazzoni R, Short KR, Nair KS. Effects of Aging on Mitochondrial DNA Copy Number and Cytochromec Oxidase Gene Expression in Rat Skeletal Muscle, Liver, and Heart. J Biol Chem. 2000 Feb 4;275(5):3343–7.

2. Gerencser AA, Mookerjee SA, Jastroch M, Brand MD. Positive Feedback Amplifies the Response of Mitochondrial Membrane Potential to Glucose Concentration in Clonal Pancreatic Beta Cells. Biochim Biophys Acta BBA - Mol Basis Dis. 2017 May;1863(5):1054–65.

3. Helman A, Klochendler A, Azazmeh N, Gabai Y, Horwitz E, Anzi S, et al. p16Ink4a-induced senescence of pancreatic beta cells enhances insulin secretion. Nat Med. 2016 Apr;22(4):412–20.

4. Vassilev LT. Cell cycle synchronization at the G2/M phase border by reversible inhibition of CDK1. Cell Cycle Georget Tex. 2006 Nov;5(22):2555–6.

5. Vassilev LT, Tovar C, Chen S, Knezevic D, Zhao X, Sun H, et al. Selective small-molecule inhibitor reveals critical mitotic functions of human CDK1. Proc Natl Acad Sci U S A. 2006 Jul 11;103(28):10660–5.

6. Petrone A, Adamo ME, Cheng C, Kettenbach AN. Identification of Candidate Cyclin-dependent kinase 1 (Cdk1) Substrates in Mitosis by Quantitative Phosphoproteomics. Mol Cell Proteomics MCP. 2016 Jul;15(7):2448–61.

7. Kojima K, Shimanuki M, Shikami M, Andreeff M, Nakakuma H. Cyclin-dependent kinase 1 inhibitor RO-3306 enhances p53-mediated Bax activation and mitochondrial apoptosis in AML. Cancer Sci. 2009 Jun;100(6):1128–36.

8. Voets E, Marsman J, Demmers J, Beijersbergen R, Wolthuis R. The lethal response to Cdk1 inhibition depends on sister chromatid alignment errors generated by KIF4 and isoform 1 of PRC1. Sci Rep. 2015 Oct 1;5:14798.

9. Davies SP, Reddy H, Caivano M, Cohen P. Specificity and mechanism of action of some commonly used protein kinase inhibitors. Biochem J. 2000 Oct 1;351(Pt 1):95–105.

10. Bain J, McLauchlan H, Elliott M, Cohen P. The specificities of protein kinase inhibitors: an update. Biochem J. 2003 Apr 1;371(Pt 1):199–204.

11. Bain J, Plater L, Elliott M, Shpiro N, Hastie CJ, Mclauchlan H, et al. The selectivity of protein kinase inhibitors: a further update. Biochem J. 2007 Dec 15;408(Pt 3):297–315.

12. Cohen P. Guidelines for the effective use of chemical inhibitors of protein function to understand their roles in cell regulation. Biochem J. 2010 Jan 1;425(1):53–4.

13. Farfari S, Schulz V, Corkey B, Prentki M. Glucose-regulated anaplerosis and cataplerosis in pancreatic beta-cells: possible implication of a pyruvate/citrate shuttle in insulin secretion. Diabetes. 2000 May 1;49(5):718–26.

14. Sugden MC, Holness MJ. The pyruvate carboxylase-pyruvate dehydrogenase axis in islet pyruvate metabolism. Islets. 2011 Nov 1;3(6):302–19.

15. Gnoni GV, Priore P, Geelen MJH, Siculella L. The mitochondrial citrate carrier: Metabolic role and regulation of its activity and expression. IUBMB Life. 2009 Oct 1;61(10):987–94.

16. Ewald JC, Reich S, Baumann S, Frommer WB, Zamboni N. Engineering Genetically Encoded Nanosensors for Real-Time In Vivo Measurements of Citrate Concentrations. PLOS ONE. 2011 Dec 2;6(12):e28245.

17. Cameron WD, Bui CV, Hutchinson A, Loppnau P, Gräslund S, Rocheleau JV. Apollo-NADP+: a spectrally tunable family of genetically encoded sensors for NADP+. Nat Methods. 2016 Apr;13(4):352–8.

18. Merrins MJ, Poudel C, McKenna JP, Ha J, Sherman A, Bertram R, et al. Phase Analysis of Metabolic Oscillations and Membrane Potential in Pancreatic Islet β-Cells. Biophys J. 2016 Feb 2;110(3):691–9.

19. Hou X, Zhang L, Han L, Ge J, Ma R, Zhang X, et al. Differing roles of pyruvate dehydrogenase kinases during mouse oocyte maturation. J Cell Sci. 2015 Jul 1;128(13):2319–29.

20. Jitrapakdee S, Maurice MS, Rayment I, Cleland WW, Wallace JC, Attwood PV. Structure, Mechanism and Regulation of Pyruvate Carboxylase. Biochem J. 2008 Aug 1;413(3):369–87.

21. Carbone MA, Robinson BH. Expression and characterization of a human pyruvate carboxylase variant by retroviral gene transfer. Biochem J. 2003 Feb 15;370(Pt 1):275–82.

22. Rydström J. Mitochondrial NADPH, transhydrogenase and disease. Biochim Biophys Acta BBA - Bioenerg. 2006 May;1757(5–6):721–6.

23. Guay C, Joly É, Pepin É, Barbeau A, Hentsch L, Pineda M, et al. A Role for Cytosolic Isocitrate Dehydrogenase as a Negative Regulator of Glucose Signaling for Insulin Secretion in Pancreatic ß-Cells. PLoS ONE [Internet]. 2013 Oct 10 [cited 2017 May 8];8(10). Available from: http://www.ncbi.nlm.nih.gov/pmc/articles/PMC3795013/

24. Aston-Mourney K, Wong N, Kebede M, Zraika S, Balmer L, McMahon JM, et al. Increased nicotinamide nucleotide transhydrogenase levels predispose to insulin hypersecretion in a mouse strain susceptible to diabetes. Diabetologia. 2007 Dec 1;50(12):2476–85.

25. Freeman H, Shimomura K, Horner E, Cox RD, Ashcroft FM. Nicotinamide nucleotide transhydrogenase: a key role in insulin secretion. Cell Metab. 2006 Jan;3(1):35–45.

26. Wong N, Blair AR, Morahan G, Andrikopoulos S. The deletion variant of nicotinamide nucleotide transhydrogenase (Nnt) does not affect insulin secretion or glucose tolerance. Endocrinology. 2010 Jan;151(1):96–102.

27. Nicholson A, Reifsnyder PC, Malcolm R, Lucas CA, MacGregor GR, Zhang W, et al. Diet induced obesity in two C57BL/6 substrains with intact or mutant Nicotinamide Nucleotide Transhydrogenase (Nnt) gene. Obes Silver Spring Md. 2010 Oct;18(10):1902–5.

28. Toye AA, Lippiat JD, Proks P, Shimomura K, Bentley L, Hugill A, et al. A genetic and physiological study of impaired glucose homeostasis control in C57BL/6J mice. Diabetologia. 2005 Apr 1;48(4):675–86.

29. Wang Z, Fan M, Candas D, Zhang T-Q, Qin L, Eldridge A, et al. Cyclin B1/Cdk1 Coordinates Mitochondrial Respiration for Cell-Cycle G2/M Progression. Dev Cell. 2014 Apr 28;29(2):217–32.

30. Stringari C, Cinquin A, Cinquin O, Digman MA, Donovan PJ, Gratton E. Phasor approach to fluorescence lifetime microscopy distinguishes different metabolic states of germ cells in a live tissue. Proc Natl Acad Sci. 2011 Aug 16;108(33):13582–7.

31. ADA Guidelines Type 2 Diabetes Pharmacologic Therapy | NDEI [Internet]. [cited 2017 May 30]. Available from: http://www.ndei.org/ADA-diabetes-management-guidelines-pharmacologic-therapy-for-type-2-diabetes.aspx.html

32. Aquilante CL. Sulfonylurea pharmacogenomics in Type 2 diabetes: the influence of drug target and diabetes risk polymorphisms. Expert Rev Cardiovasc Ther. 2010 Mar;8(3):359–72.

33. Cusi K, Consoli A, DeFronzo RA. Metabolic effects of metformin on glucose and lactate metabolism in noninsulin-dependent diabetes mellitus. J Clin Endocrinol Metab. 1996 Nov;81(11):4059–67.

34. Viollet B, Guigas B, Garcia NS, Leclerc J, Foretz M, Andreelli F. Cellular and molecular mechanisms of metformin: an overview. Clin Sci. 2012 Mar 1;122(6):253–70.

35. Owen MR, Doran E, Halestrap AP. Evidence that metformin exerts its anti-diabetic effects through inhibition of complex 1 of the mitochondrial respiratory chain. Biochem J. 2000 Jun 15;348(Pt 3):607–14.

36. Wheaton WW, Weinberg SE, Hamanaka RB, Soberanes S, Sullivan LB, Anso E, et al. Metformin inhibits mitochondrial complex I of cancer cells to reduce tumorigenesis. eLife. 2014 May 13;3:e02242.

37. Shirakawa J, Fernandez M, Takatani T, El Ouaamari A, Jungtrakoon P, Okawa ER, et al. Insulin Signaling Regulates the FoxM1/PLK1/CENP-A Pathway to Promote Adaptive Pancreatic β Cell Proliferation. Cell Metab. 2017 Apr 4;25(4):868–882.e5.